Catalytic asymmetric diarylphosphine addition to α-diazoesters for the synthesis of P-stereogenic phosphinates via P*-N bond formation

László B. Balázs,[†] Yinhua Huang,[‡] Jasmina B. Khalikuzzaman,[†] Yongxin Li,[†] Sumod A. Pullarkat*[†] and Pak-Hing Leung*[†]

[†]Division of Chemistry & Biological Chemistry, School of Physical and Mathematical Sciences, Nanyang Technological University, Singapore 637371

[‡]College of Material, Chemistry and Chemical Engineering, Hangzhou Normal University, Hangzhou 311121, China

*e-mail for Pullarkat, S.A.: sumod@ntu.edu.sg
*e-mail for Leung, P.-H.: pakhing@ntu.edu.sg

Supporting Information

Table of content

1. Optimization of the reaction conditions

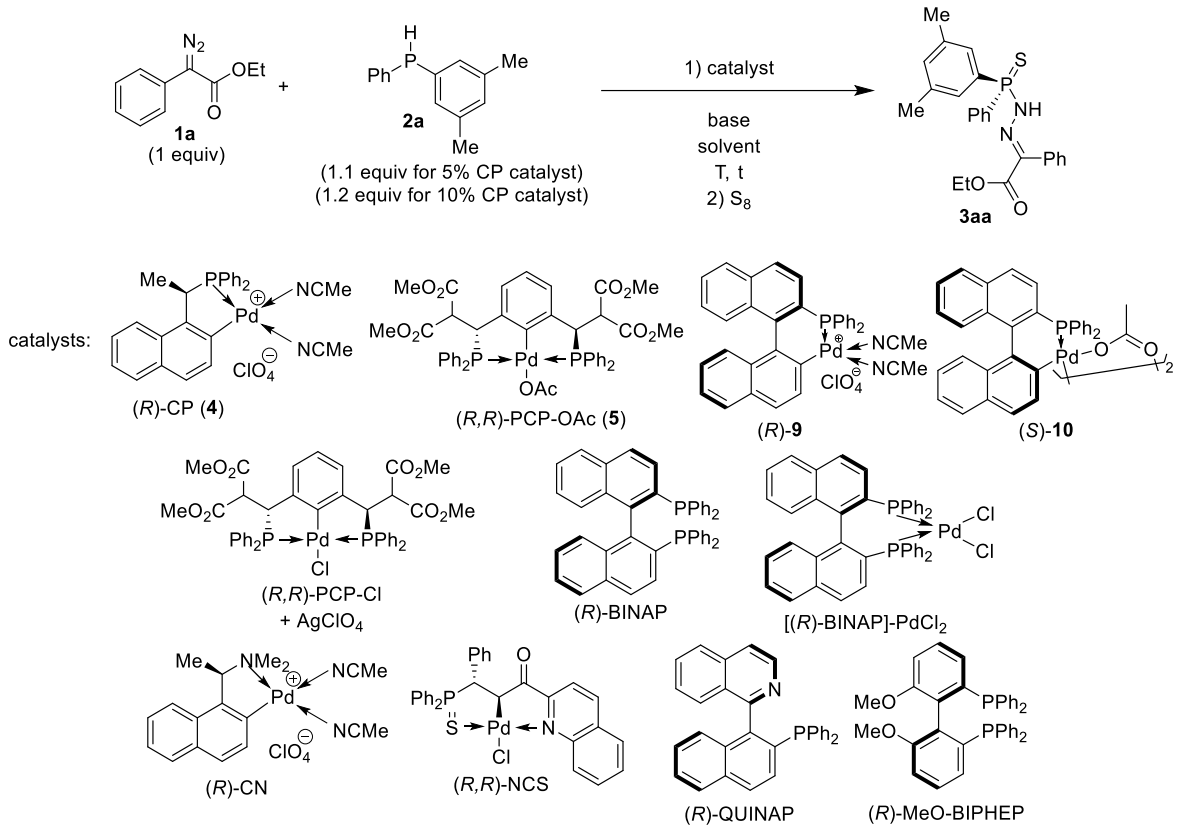

Table S1 Reaction condition optimization of asymmetric phosphination of α-diazoesters.

Entry	Catalyst [mol%]	Solvent	Base (1 equiv)	T [°C]	t	Conversion[a] [%]	*ee*[b] [%]
1	-	$CHCl_3$	-	-40	16 h	-	-
2	-	$CHCl_3$	Et_3N	-40	16 h	-	-
3	5% $Pd(OAc)_2$	$CHCl_3$	-	-40	16 h	-	-
4	5% $Pd(OAc)_2$	acetone	-	rt	22 h	19[c]	-
5	5% $Pd(MeCN)_2Cl_2$	$CHCl_3$	DBU	rt	24 h	26[c]	-
6	5% (*R*)-CP (**4**)	$CHCl_3$	Et_3N	-40	65 h	69	35
7	10% (*R*)-CP (**4**)	$CHCl_3$	Et_3N	-40	65 h	79	39
8	15% (*R*)-CP (**4**)	$CHCl_3$	Et_3N	-40	65 h	93	38
9	20% (*R*)-CP (**4**)	$CHCl_3$	Et_3N	-40	65 h	90	38
10	10% (*R,R*)-PCP-OAc (**5**)	$CHCl_3$	-	-40	72 h	3[c]	N.D.
11	10% (*R,R*)-PCP-OAc (**5**)	$CHCl_3$	-	rt	48 h	8[c]	16
12	5% (*R,R*)-PCP-Cl / 10% $AgClO_4$	$CHCl_3$/acetone (8:1)	DBU	-80	15 h	29[c]	8
13	2.5% Pd_2dba_3 / 6% (R)-BINAP	$CHCl_3$/acetone (8:1)	DBU	-80	15 h	16[c]	3
14	5% $Pd(OAc)_2$ / 6% (R)-BINAP	$CHCl_3$	DBU	-40	65 h	no reaction	N.D.
15	5% [(R)-BINAP]-$PdCl_2$ / 10% $AgClO_4$	$CHCl_3$	DBU	-40	65 h	no reaction	N.D.
16	5% (*R*)-CN	$CHCl_3$	DBU	-40	65 h	no reaction	N.D.
17	5% (*R,R*)-NCS	$CHCl_3$	DBU	-40	65 h	no reaction	N.D.
18	5% $Pd(OAc)_2$ / 6% (R)-QUINAP	$CHCl_3$	DBU	-40	65 h	no reaction	N.D.
19	5% $Pd(OAc)_2$ / 6% (R)-MeO-BIPHEP	$CHCl_3$	DBU	-40	65 h	no reaction	N.D.
20	5% (*R*)-**9**	$CHCl_3$/acetone (8:1)	DBU	-80	40 h	30[c]	0
21	5% (*S*)-**10**	$CHCl_3$/acetone (8:1)	DBU	-80	24 h	54[c]	-15
22	5% (*R*)-CP (**4**)	$CHCl_3$	DMA[d]	-40	24 h	no reaction	N.D.
23	5% (*R*)-CP (**4**)	$CHCl_3$	DMA[d]	rt	15 h	61	4

24	5% (*R*)-CP (**4**)	$CHCl_3$	DBU	-40	24 h	99	36
25	5% (*R*)-CP (**4**)	$CHCl_3$	TBD[e,h]	-40	3 h	99	34
26	5% (*R*)-CP (**4**)	$CHCl_3$	TMG[f,h]	-40	3 h	99	38
27	5% (*R*)-CP (**4**)	$CHCl_3$	DABCO	-40	65 h	30	39
28	5% (*R*)-CP (**4**)	MeCN	Et_3N	-40	65 h	99	29
29	5% (*R*)-CP (**4**)	toluene	Et_3N	-40	65 h	57	17
30	5% (*R*)-CP (**4**)	DCM	Et_3N	-40	72 h	95	31
31	5% (*R*)-CP (**4**)	DCM	Et_3N	-80	72 h	60	40
32	5% (*R*)-CP (**4**)	acetone	Et_3N	-40	72 h	99	28
33	5% (*R*)-CP (**4**)	Et_2O	Et_3N	-40	65 h	32	25
34	5% (*R*)-CP (**4**)	THF	Et_3N	-40	65 h	7	35
35	5% (*R*)-CP (**4**)	neat	Et_3N	-40	24 h	47	10
36	5% (*R*)-CP (**4**)	MeOH[h]	Et_3N	-40	40 h	99	36
37	5% (*R*)-CP (**4**)	EtOH	Et_3N	-40	40 h	75	29
38	5% (*R*)-CP (**4**)	^{i}PrOH	Et_3N	-40	40 h	79	23
39	5% (*R*)-CP (**4**)	DCE	Et_3N	-40	40 h	28	38
40	5% (*R*)-CP (**4**)	$CHBr_3$/DCM (1:1)	Et_3N	-40	40 h	no reaction	N.D.
41	5% (*R*)-CP (**4**)	$CHCl_3$/acetone (5:1)	Et_3N	-80	17 h	78	49
42	10% (*R*)-CP (**4**)	$CHCl_3$/acetone (8:1)	Et_3N	-80	96 h	60	53
43	10% (*R*)-CP (**4**)	$CHCl_3$/acetone (8:1)	DBU	-80	24 h	94 (78%)[g]	55
44	10% (*R*)-CP (**4**)	$CHCl_3$/THF (8:1)	DBU	-80	24 h	90	55

[a]Conversion was determined by $^{31}P\{^{1}H\}$ NMR measurement of the crude mixture. [b]Enantiomeric excess was determined by chiral HPLC. [c]Significant amount of unidentified by-products were formed. [d]DMA: dimethylaniline. [e]TBD: 1,5,7-triazabicyclo[4.4.0]dec-5-ene. [f]TMG: 1,1,3,3-tetramethylguanidine. [g]Isolated yield in parentheses. [h]Remark: Methanol as solvent, TBD and TMG as external bases were reasonable choices based on these results; however, at -80 ^{o}C the obtained selectivity was low in the test reactions on substrate 3ca'.

2. Mechanistic studies

a) Role of palladium and base:

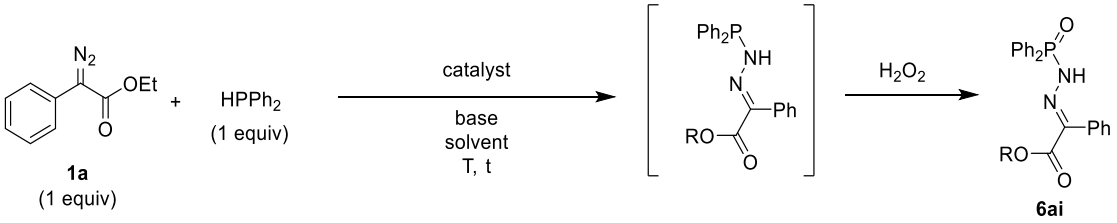

Table S2 Control experiments for mechanistic investigations.

Entry	Catalyst [mol%]	Solvent	Base (1 equiv)	T [°C]	t	Conversion[a] [%]
1	-	acetone	-	rt	15 h	8
2	-	acetone	Et_3N	rt	15 h	13
3	5% $Pd(OAc)_2$	acetone	Et_3N	rt	1.5 h	87 (80)[b]

[a]The conversion was calculated based on the $^{31}P\{^1H\}$ NMR measurement of the crude mixture. [b]Isolated yield in parentheses.

Table S2, entry 1: In the first test reaction, neither catalyst nor base was added to the reaction mixture. The product was formed in 8% conversion based on $^{31}P\{^1H\}$ NMR measurement during overnight.

Table S2, entry 2: In case if 1 equivalent triethylamine was added to the reactants, the conversion was slightly higher (13%).

Table S2, entry 3: If both palladium salt and triethylamine was applied, after 1,5 hours reaction time, **6ai** was produced in 87% NMR conversion and it was isolated in 80% yield. The presence of the base and the palladium salt significantly accelerated the reaction.

b) Coordination studies for catalyst-substrate interaction:

Our previous studies on asymmetric hydrophosphination of activated alkenes proved that the P-H addition can occur either via intra-[1, 2] or intermolecular[3] mechanism in the presence of palladacycle catalyst. In order to confirm any possible catalyst-substrate interaction between (*R*)-**4** and **1a**, coordination studies were conducted.

Coordination experiment 1:

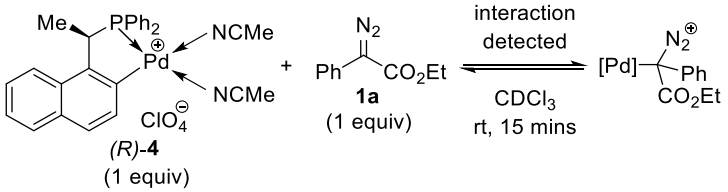

At first, equivalent amount of palladacycle and diazo substrate were mixed in $CDCl_3$ at room temperature, then multi nuclei NMR spectra were recorded of the mixture after 15 minutes. The observed spectra were compared with the pure (*R*)-**4** and **1a** NMR spectra (Figure S1).

Figure S1 Comparison of the ^{1}H NMR (400 MHz, $CDCl_3$) spectra of (*R*)-**4** (blue), **1a** (red) and coordination experiment 1 (green).

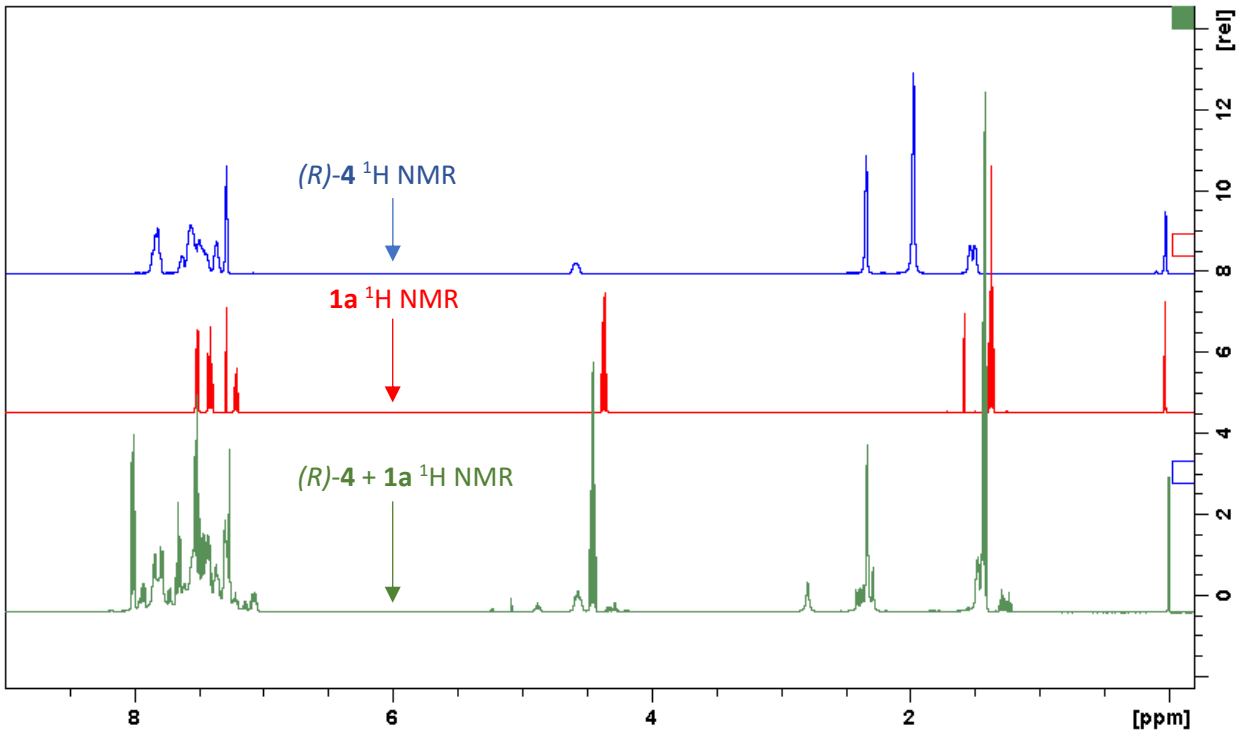

Full spectra

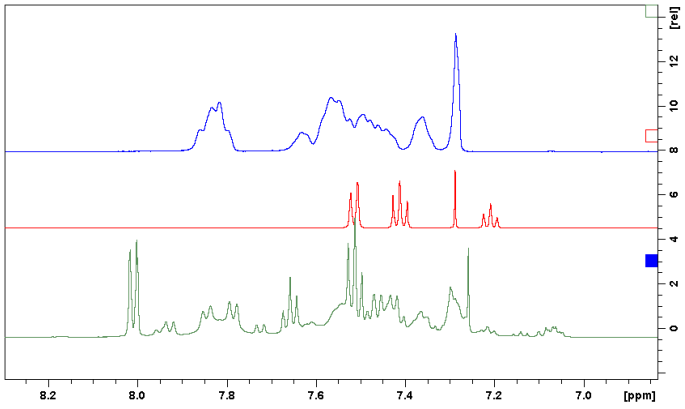

Aromatic region

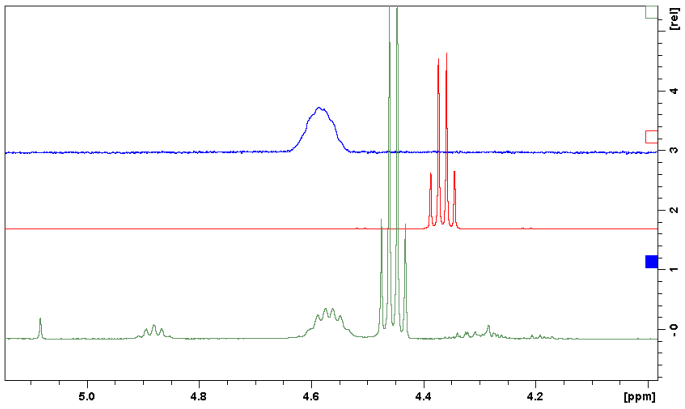

Aliphatic region

Figure S2 Comparison of the $^{13}C\{^{1}H\}$ NMR (101 MHz, $CDCl_3$) spectra of (*R*)-**4** (blue), **1a** (red) and coordination experiment 1 (green).

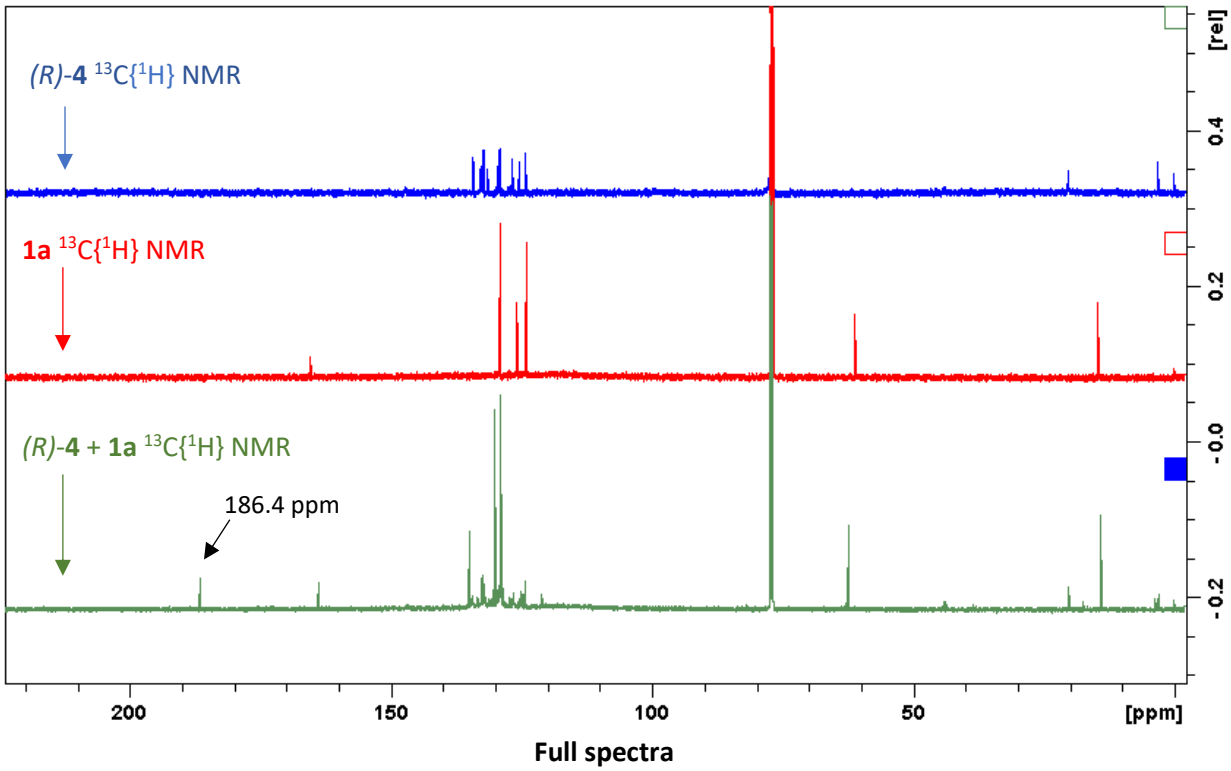

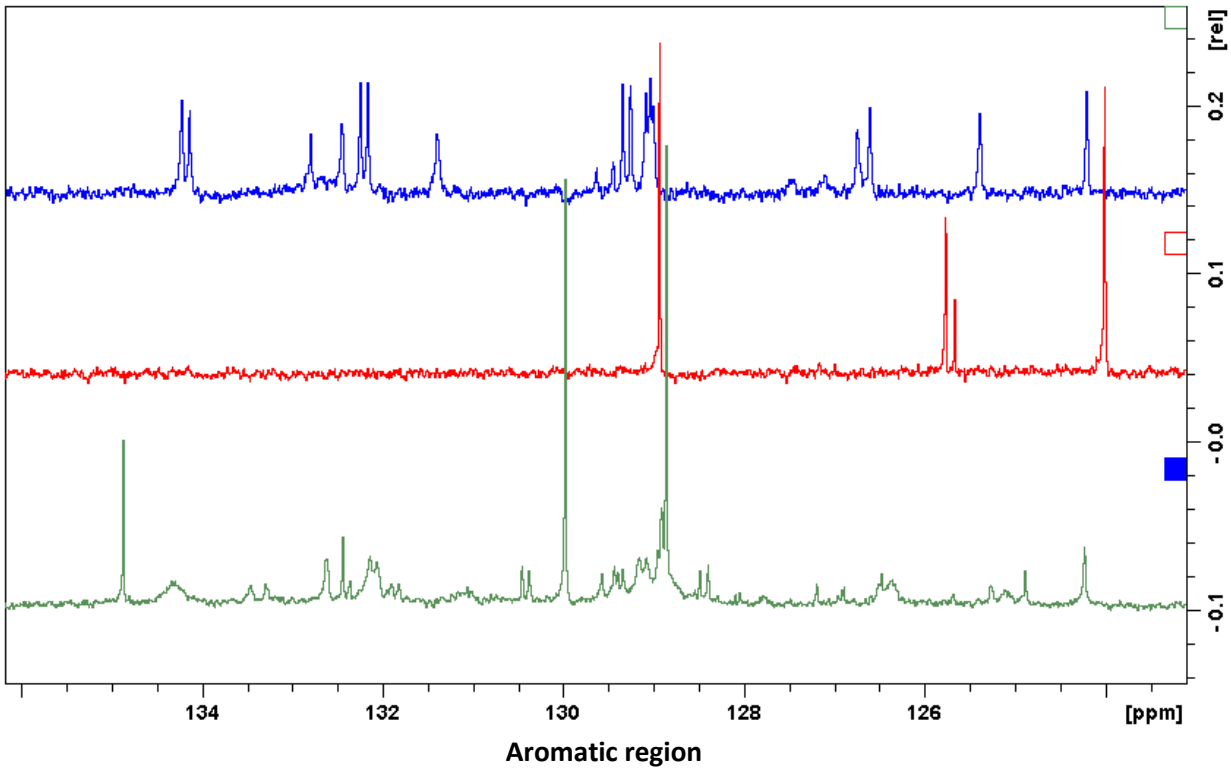

Figure S3 Comparison of the $^{31}P\{^{1}H\}$ NMR (162 MHz, $CDCl_3$) spectra of (*R*)-**4** (blue) and coordination experiment 1 (green).

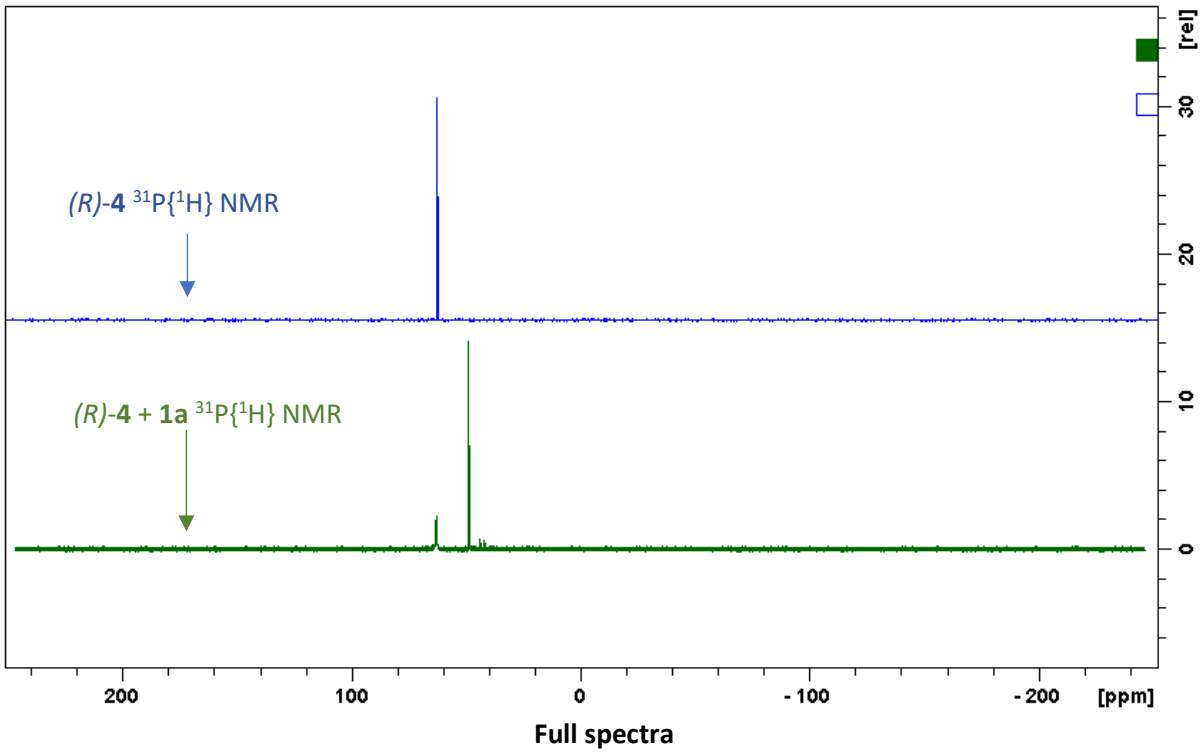

Full spectra

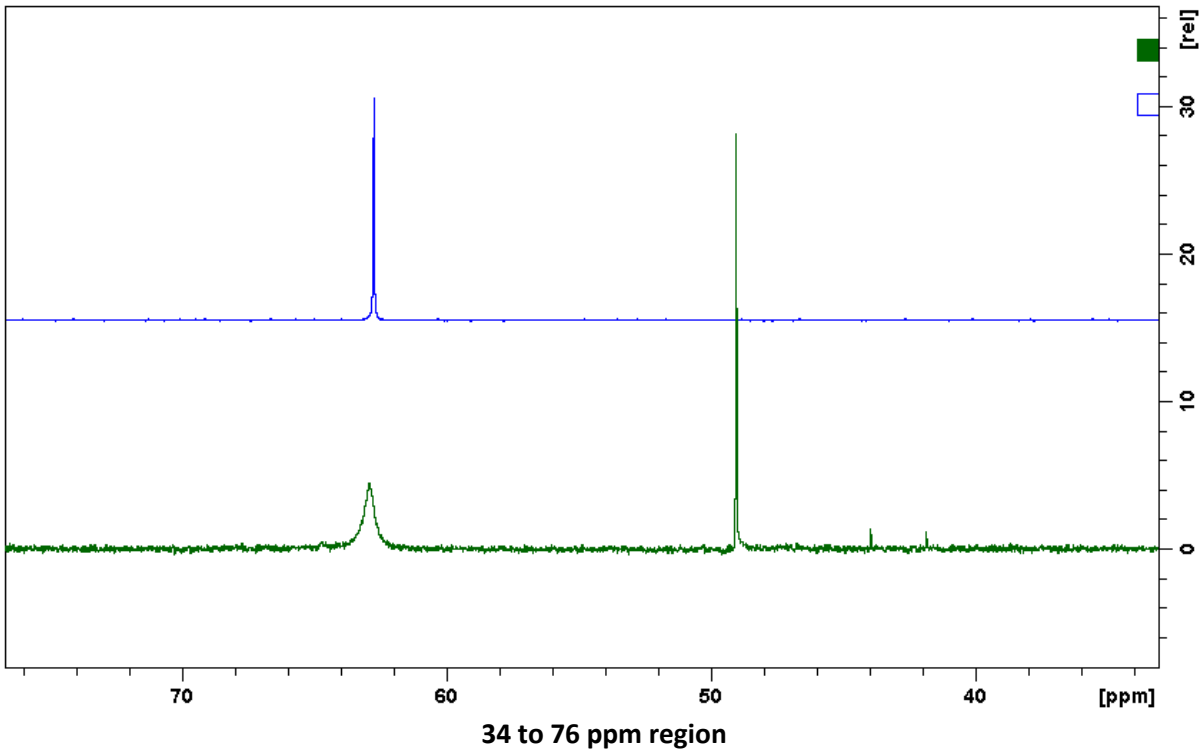

34 to 76 ppm region

In coordination experiment 1 established the interaction between (*R*)-**4** and **1a**. New chemical peaks appeared in both the ^{1}H, $^{13}C\{^{1}H\}$ and $^{31}P\{^{1}H\}$ NMR spectra after mixing the reactants in stoichiometric amount. Unfortunately, we were unable to fully characterize any exact structure based on these measurements; however, some general considerations have been made. Diazo compounds are known to develop various coordination modes to transition metals:[4-9]

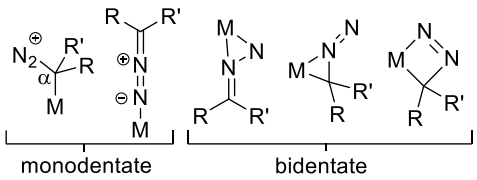

Among these structures, the monodentate coordination to the metal center via the α-carbon is well established, as the first step of metal carbene synthesis from diazo compounds.[10-12] Upon coordination, the α-carbon becomes highly electron-deficient in this species due to electron donation to the metal center. In the $^{13}C\{^{1}H\}$ ($CDCl_3$) NMR spectrum of coordination experiment 1, a new singlet peak can be detected in the low field region at δ 186.4 ppm after substrate addition. This peak also indicates the presence of an electron-deficient carbon. This observation supports the plausible mono-coordination of the α-carbon to the palladium.

Coordination experiment 2:

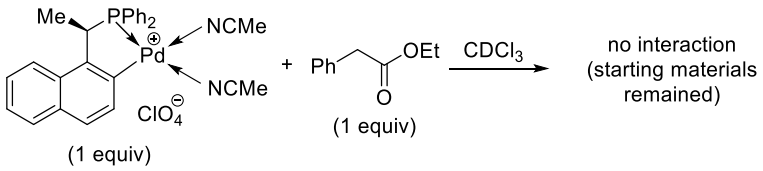

In order to prove or exclude any possible interaction between the diazoester's oxygen atom and the palladium, we performed control experiment 2 by mixing stoichiometric amount of (*R*)-**4** and ethyl phenylacetate. In this case, we did not observe any interaction between the reactants.

Figure S4 Comparison of the ^{1}H NMR (400 MHz, $CDCl_3$) spectra of (*R*)-**4** (blue), ethyl phenylacetate (red) and coordination experiment 2 (green).

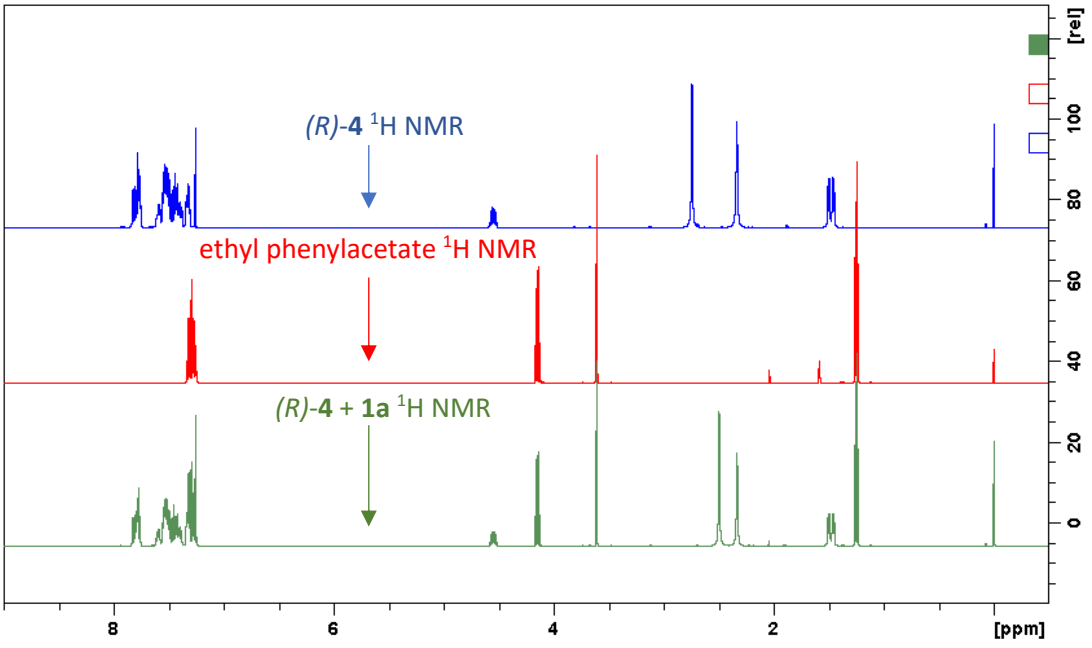

Figure S5 Comparison of the $^{13}C\{^{1}H\}$ NMR (101 MHz, $CDCl_3$) spectra of (*R*)-**4** (blue), ethyl phenylacetate (red) and coordination experiment 2 (green).

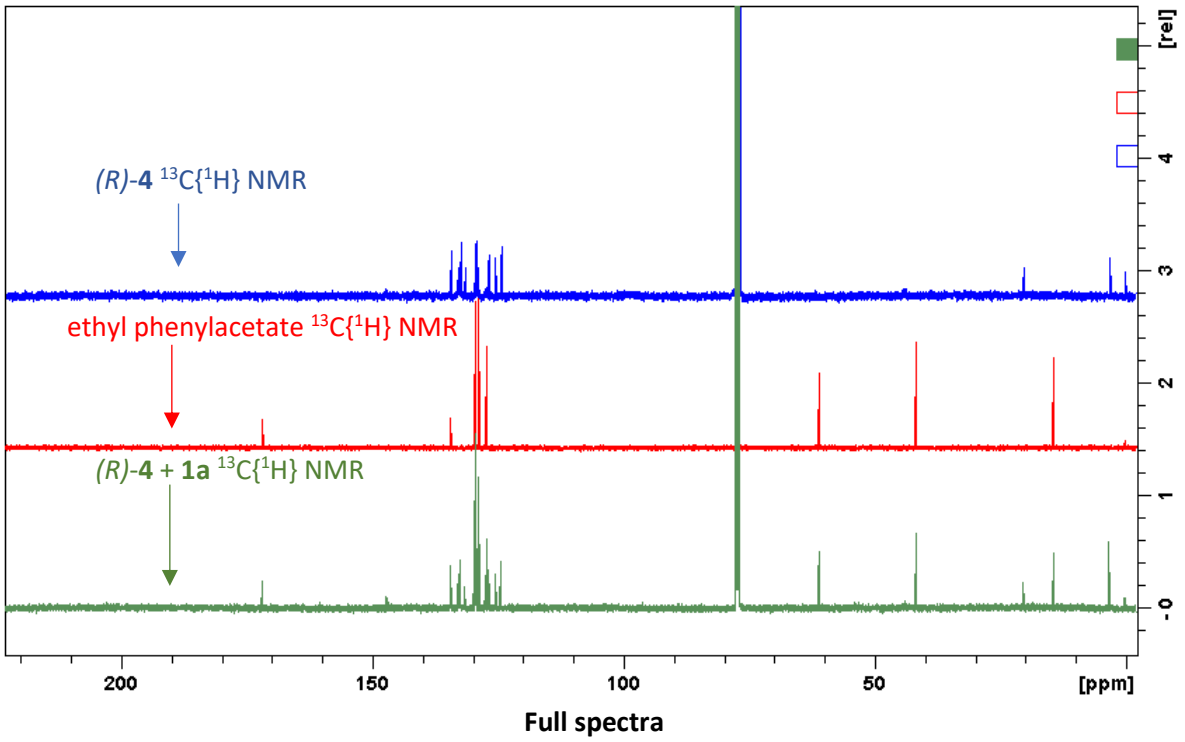

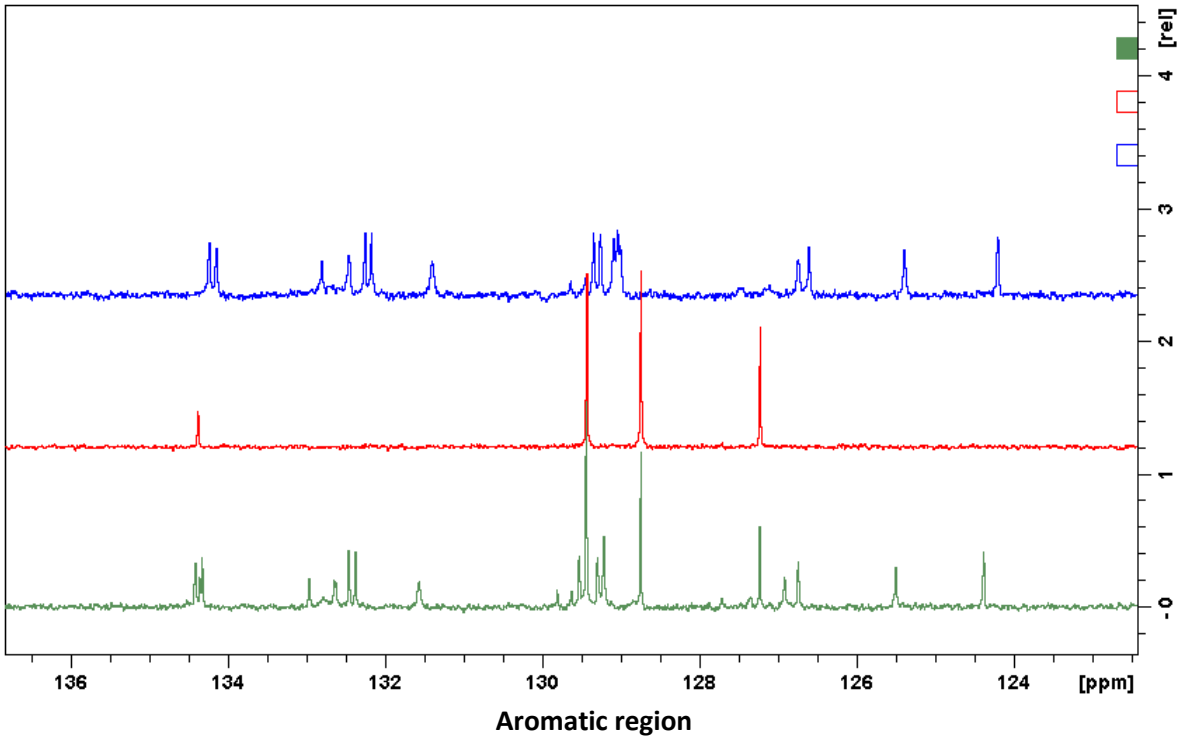

Coordination experiment 3:

To gain more information on the substrate's coordination mode in the presence of phosphines, further control experiments were performed:

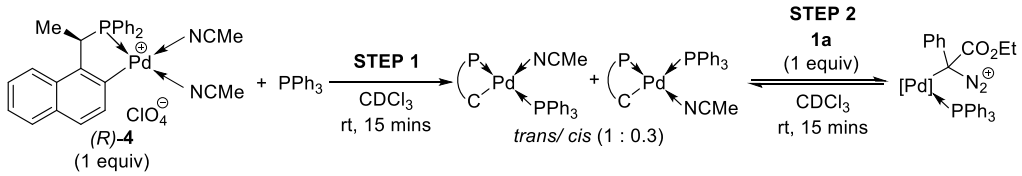

STEP 1:

For this coordination study, triphenylphosphine was used to replace the secondary phosphine, to avoid any product formation and to allow us to examine the coordinating properties. In the first step, stoichiometric amount of palladacycle was mixed with triphenylphosphine at room temperature, then multi nuclei NMR spectra were recorded after 15 minutes.

Figure S6 ^{1}H NMR (500 MHz, $CDCl_3$) spectrum of **STEP 1**.

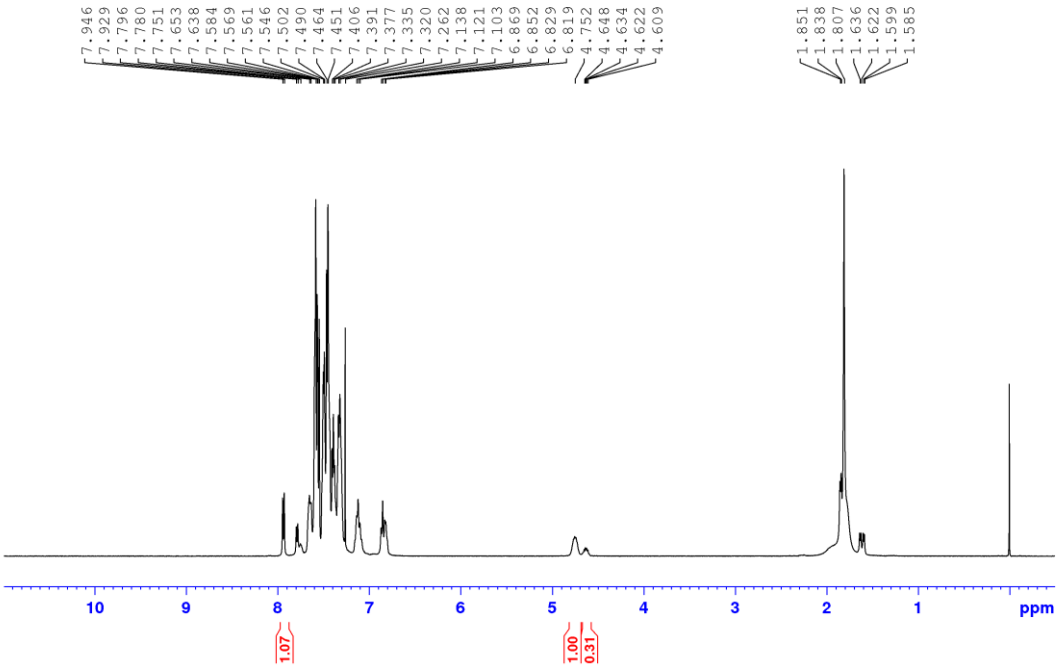

Figure S7 $^{13}C\{^{1}H\}$ NMR (126 MHz, $CDCl_3$) spectrum of **STEP 1**.

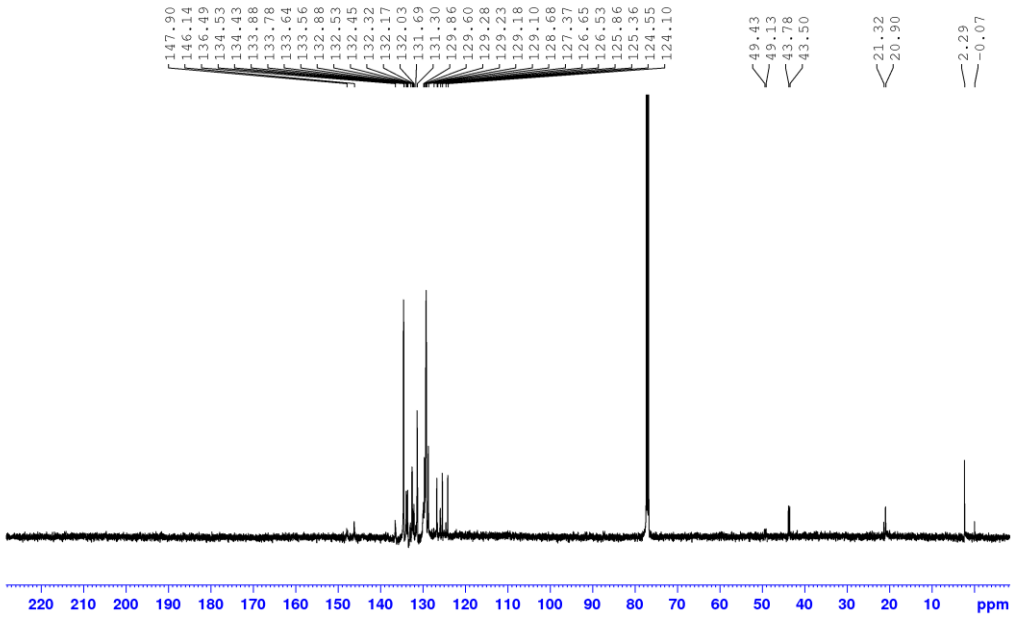

Figure S8 $^{31}P\{^{1}H\}$ NMR (162 MHz, $CDCl_3$) spectrum of **STEP 1**.

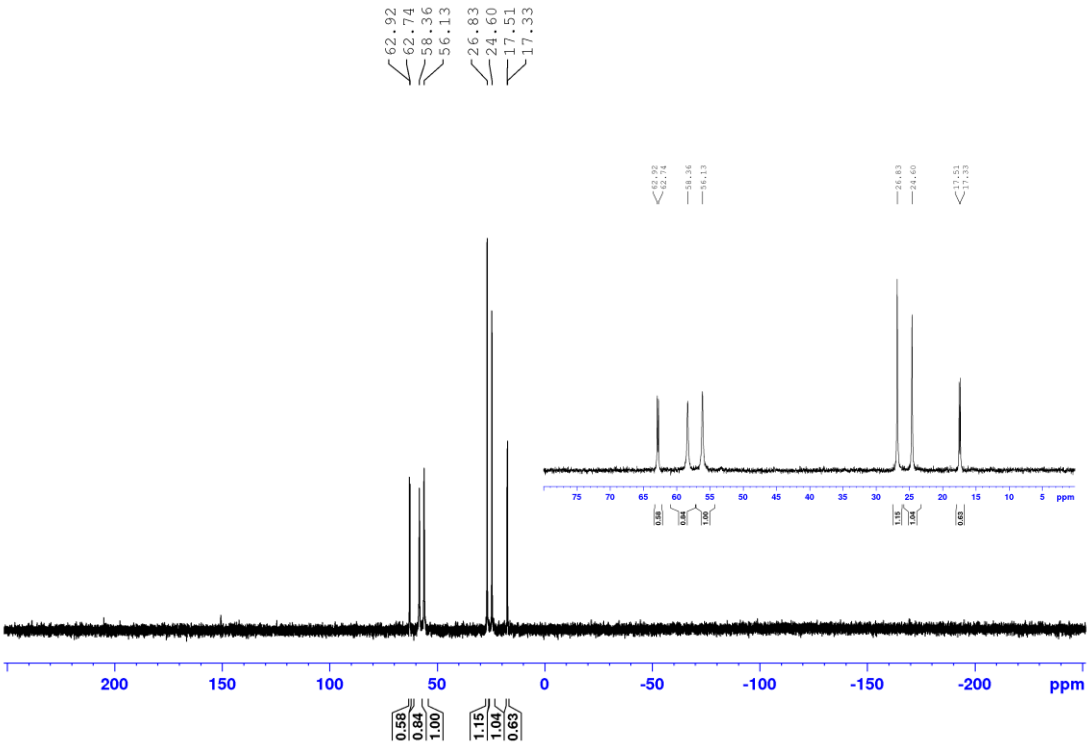

At this stage, the recorded $^{31}P\{^{1}H\}$ ($CDCl_3$) NMR spectrum shows two pairs of doublets, which are consistent to the formation of two isomers, compound **A** and **B** in 1 to 0.3 ratio. Significantly higher coupling constant (d, $J_{PP(trans)}$=361.5 Hz) belongs to the *trans* P-Pd-P moiety in compound **A** (at δ 57.25 and 25.72 ppm), compared to the *cis* P-Pd-P fragment (d, $J_{PP(cis)}$=29 Hz) in case of compound **B** (at δ 62.83 and 17.42 ppm). The observed ratio of the generated complexes indicates that the coordination of the triphenylphosphine to the *cis* position is less favorable compared to *trans* to the palladacycle's phosphorus atom. This phenomenon is consistent to our previous studies on the stereoelectronic properties of the CP palladacycle complex, which established that the aromatic carbon donor of the metallacycle induces a significantly stronger *trans*-influence than the phosphorus atom.[13] Due to the significant electron withdrawing effect of the aromatic ring, the d-orbitals of the palladium are less available for backdonation in *trans* position to the carbon donor. The weaker backdonation indicates more labile ligand coordination to this site. This feature is important in our proposed mechanism.

STEP 2

In the second step of our control experiment, equivalent amount of α-diazoacetate was introduced to the same reaction mixture, followed by the spectroscopic measurements after 15 minutes stirring:

Figure S9 ^{1}H NMR (400 MHz, $CDCl_3$) spectrum of **STEP 2.**

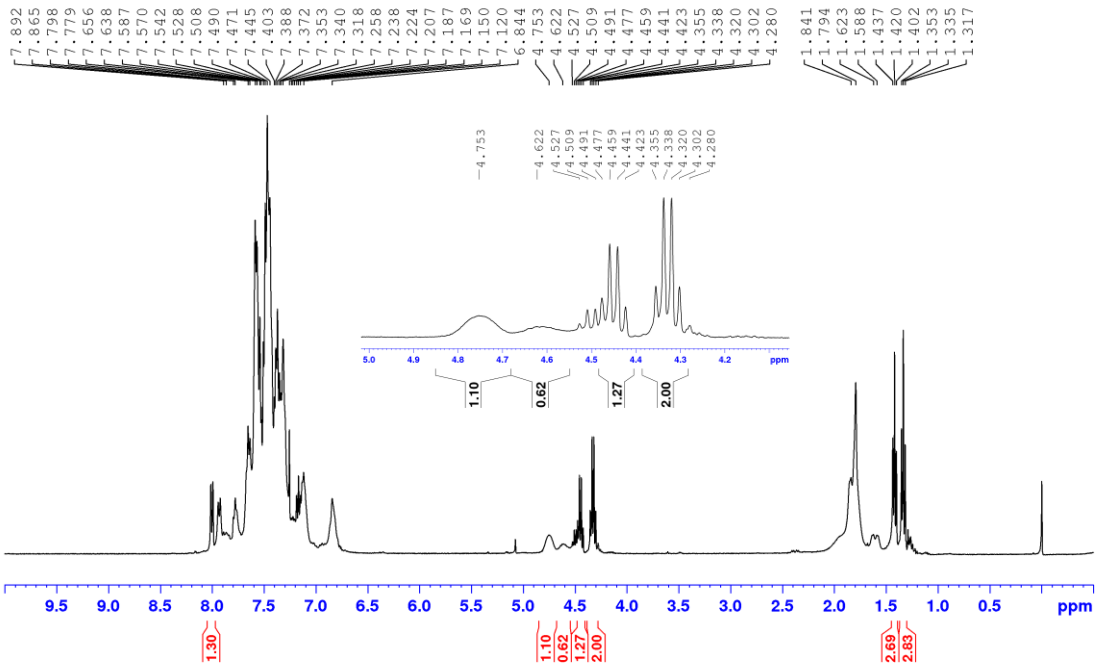

Figure S10 $^{13}C\{^{1}H\}$ NMR (101 MHz, $CDCl_3$) spectrum of **STEP 2**.

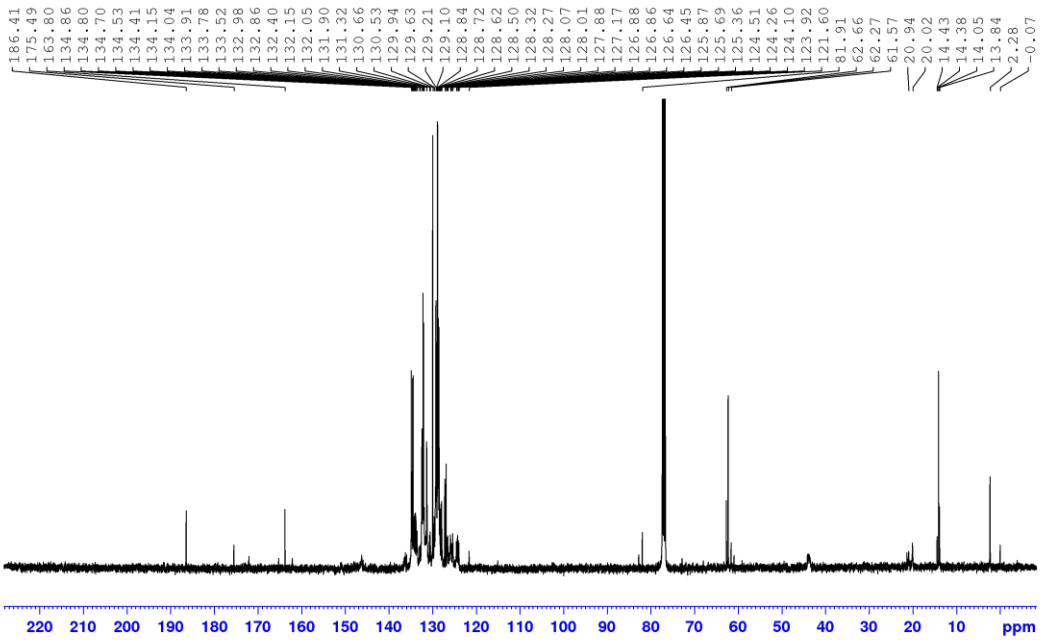

Figure S11 $^{31}P\{^{1}H\}$ NMR (162 MHz, $CDCl_3$) spectrum of **STEP 2**.

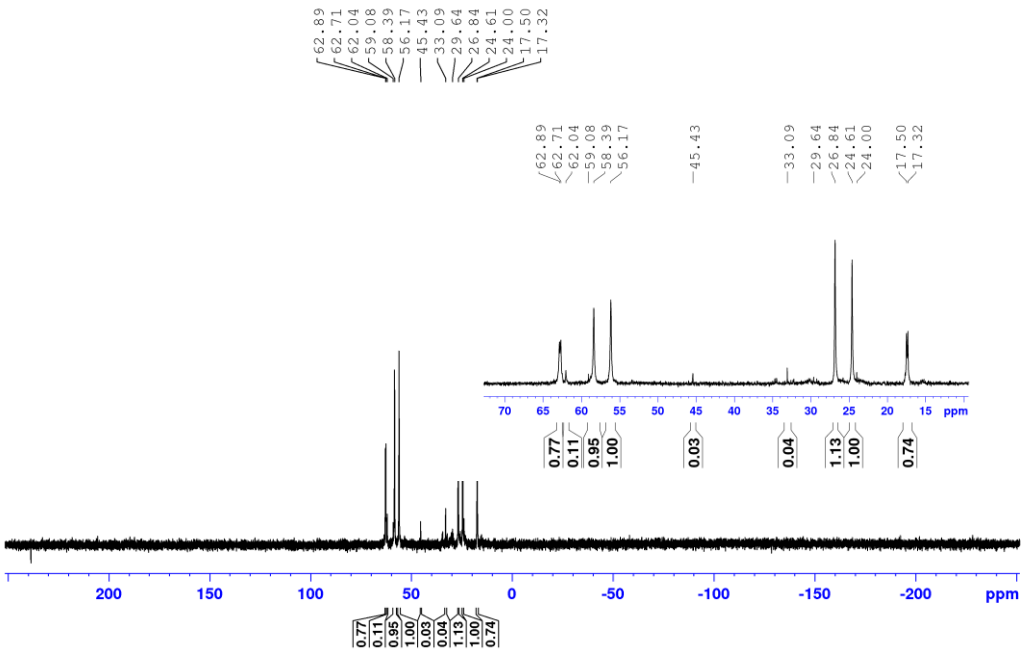

NMR spectroscopic measurements revealed that interactions between the diazo substrate and the complexes arose, just as we have seen it in the first coordination study. In the $^{13}C\{^1H\}$ ($CDCl_3$) NMR spectrum, the singlet carbon peak in the low field (at δ 186.4 ppm) was detected again, as in the previous experiment. In this case, we predict only *trans* coordination to the aromatic carbon donor, due to the labile ligand interaction at this position. The diazo substrate's coordination properties are not strong enough to replace the coordinated phosphines in the *cis* position to the carbon donor. The recorded $^{31}P\{^1H\}$ ($CDCl_3$) NMR spectrum at this stage shows similar chemical peak pattern as we observed in the first step of this experiment (STEP 1); however, a few new minor peaks arose upon the diazoester addition. This suggests the formation of new species in the reaction mixture; however, the small intensity indicates continuous coordination-decoordination between the diazo acetate and the palladium complexes. Bidentate substrate coordination in this case can be excluded, due to the single coordination site available at one time around the metal center.

The special electronic features of the palladacycle is one of the reasons why we did not observe any nitrogen molecule elimination from the diazoester. As we have mentioned above, the diazo compounds tend to coordinate to transition metals via the α-carbon to generate metal carbene species via nitrogen elimination. In the Fisher type metal carbenes, the sp^2-hybridized carbenic carbon donates σ electrons to the vacant d-orbital of the metal and at the same time, π-backdonation takes place from the metal's d-orbital to the available p-orbital of the carbon. Since the CP-ligand scaffold of the applied palladacycle catalyst ((*R*)-**4**) develops significant backdonation from the palladium to both of the phosphorus and the aromatic carbon donor, the d-orbitals of the metal are much less available for backdonation to the coordinating diazosubstrate. This is one of the reasons why the formation of metal carbene species was not observed in our case; however, further investigations are necessary to establish this statement.

Coordination experiment 4:

The first step of the proposed mechanism is the replacement of the coordinated acetonitrile molecules of complex **4** to secondary phosphines. In our proposed mechanism, intermediate **A** contains two molecules of phosphines coordinated to the metal center. To experimentally prove the existence of intermediate **A**, the following coordination experiment was performed:

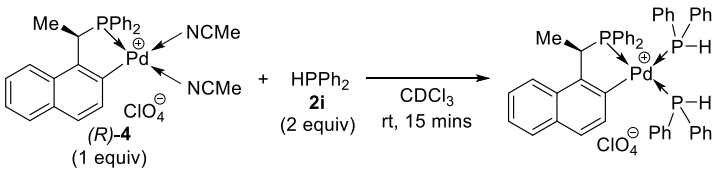

In this experiment, 1 equivalent of **4** was mixed with 2 equivalents of **2i** at room temperature in chloroform. After 15 minutes, multi-nuclei NMR spectra were recorded (Figures S12 to S14). By analyzing the $^{31}P\{^1H\}$ NMR spectrum of the experiment (Figure S14), it can be clearly seen that all the diphenylphosphine molecules took part in the coordination, which is supported by the absence of the non-coordinated diphenylphosphine chemical peak at -40 ppm. The chemical peak at 59.5 ppm belongs to the phosphorus of the bidentate ligand scaffold (integration value: 1) and the chemical peaks at -7.4 ppm (integration value: 2) support the coordination of the phosphine compounds to the palladium. The observed broad peaks and the absence of P-P coupling represent labile ligand coordination.

Figure S12 ^{1}H NMR (400 MHz, $CDCl_3$) spectrum of coordination experiment 4.

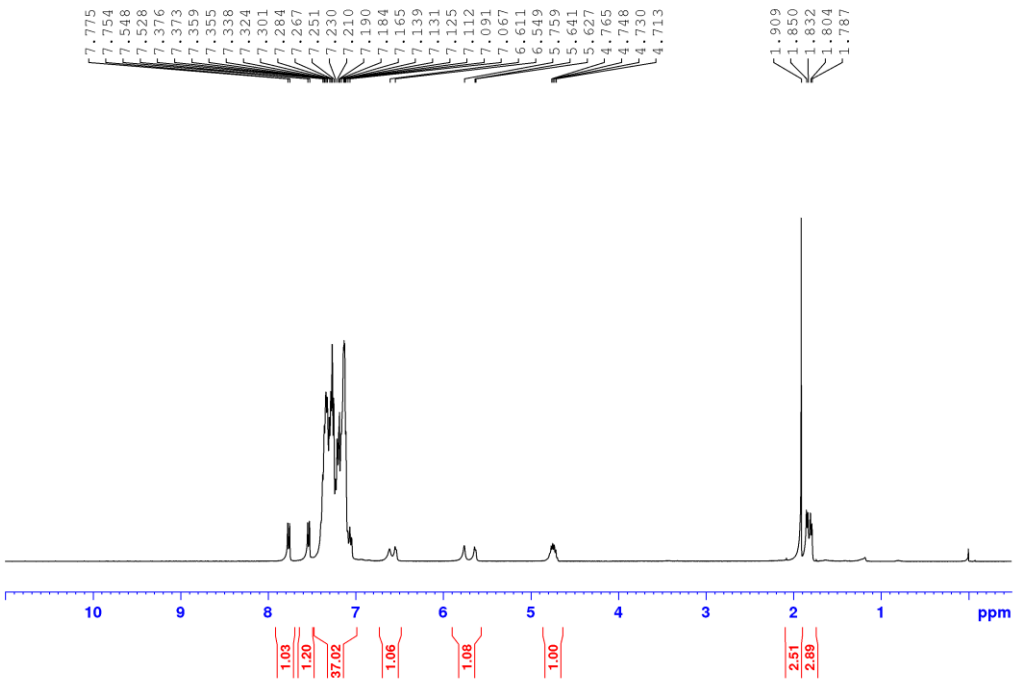

Figure S13 $^{13}C\{^{1}H\}$ NMR (101 MHz, $CDCl_3$) spectrum of coordination experiment 4.

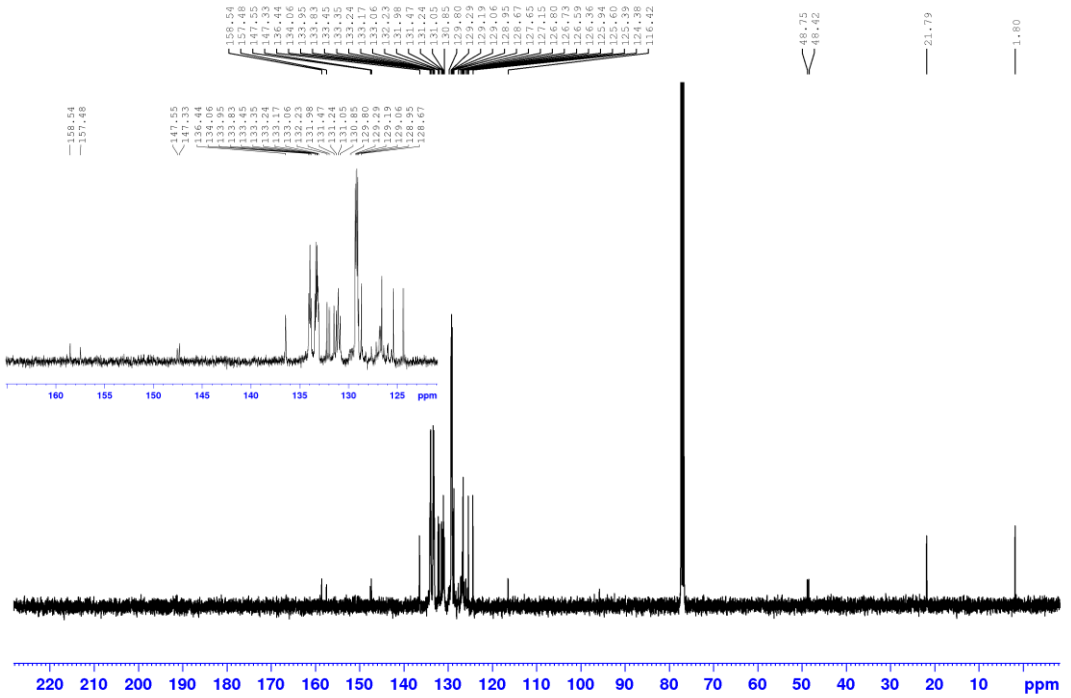

Figure S14 $^{31}P\{^{1}H\}$ NMR (162 MHz, $CDCl_3$) spectrum of coordination experiment 4.

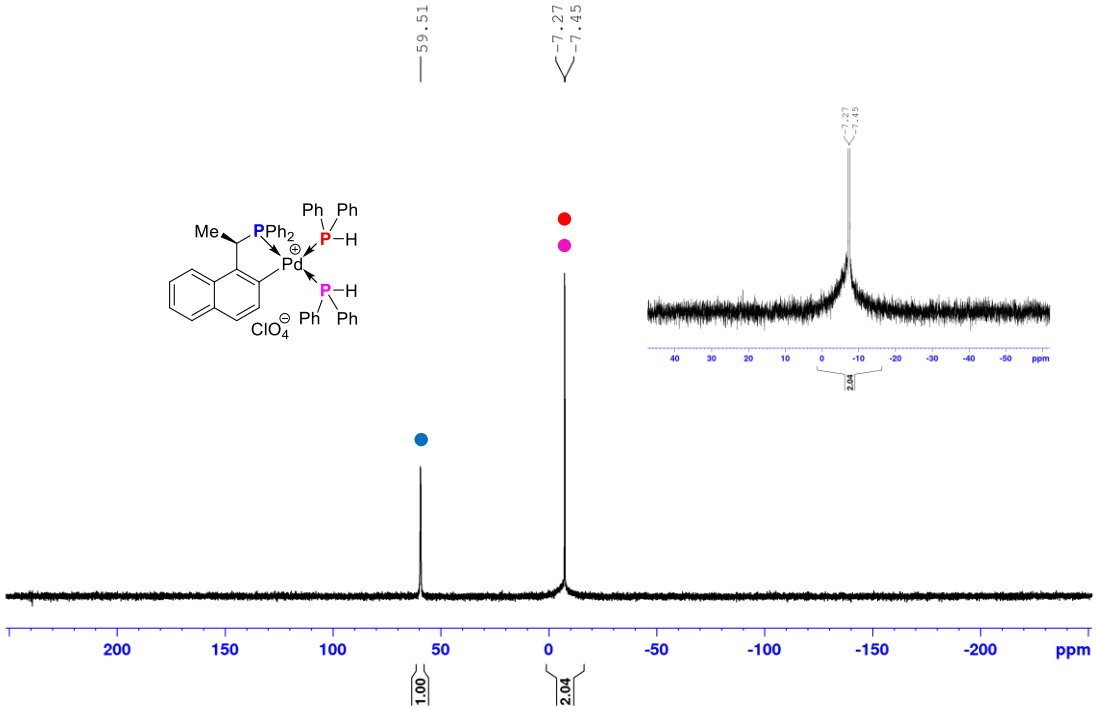

Considering all of the results of our control investigations, we have proposed a possible intramolecular mechanism for the diazoacetate phosphination:

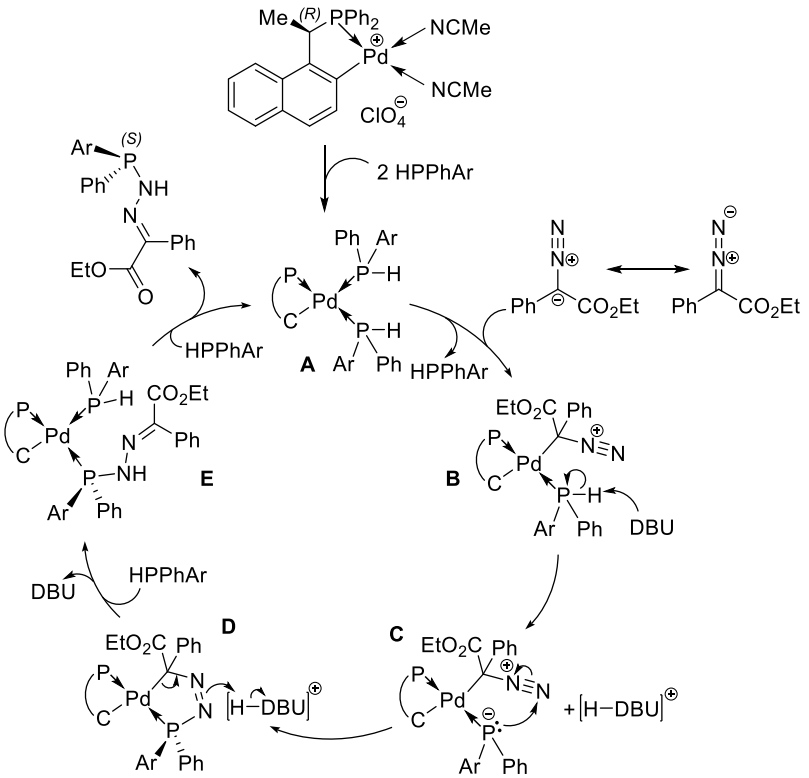

In the first step of the proposed mechanism, the secondary phosphines occupy the two available coordination sites around the palladium center (**A**). The next step is the coordination of the diazoester, followed by the deprotonation of the racemic secondary phosphine by external base to generate a prochiral phosphido species (**B**). Nucleophilic attack on the terminal nitrogen of the coordinated diazoester by the phosphide species (**C**) results in the formation of a five-member chelate to the palladium (**D**). Noteworthy to mention, that according to our previous findings, asymmetric hydrophosphinations of activated alkenes proceed via six-member ring at this stage of the catalytic cycle.[1, 2] Due to the rigid nature of the five-member ring, this can be an explanation why the phosphination of the diazoacetates are significantly slower compared to the alkene substrates. In the last step of the catalytic cycle, a new set of diarylphosphines coordinate to palladium causing the elimination of the final product and regeneration of the active catalyst (**E** to **A**).

3. NMR spectra

Figure S15 ^{1}H NMR (400 MHz, $CDCl_3$) spectrum of **2a**.

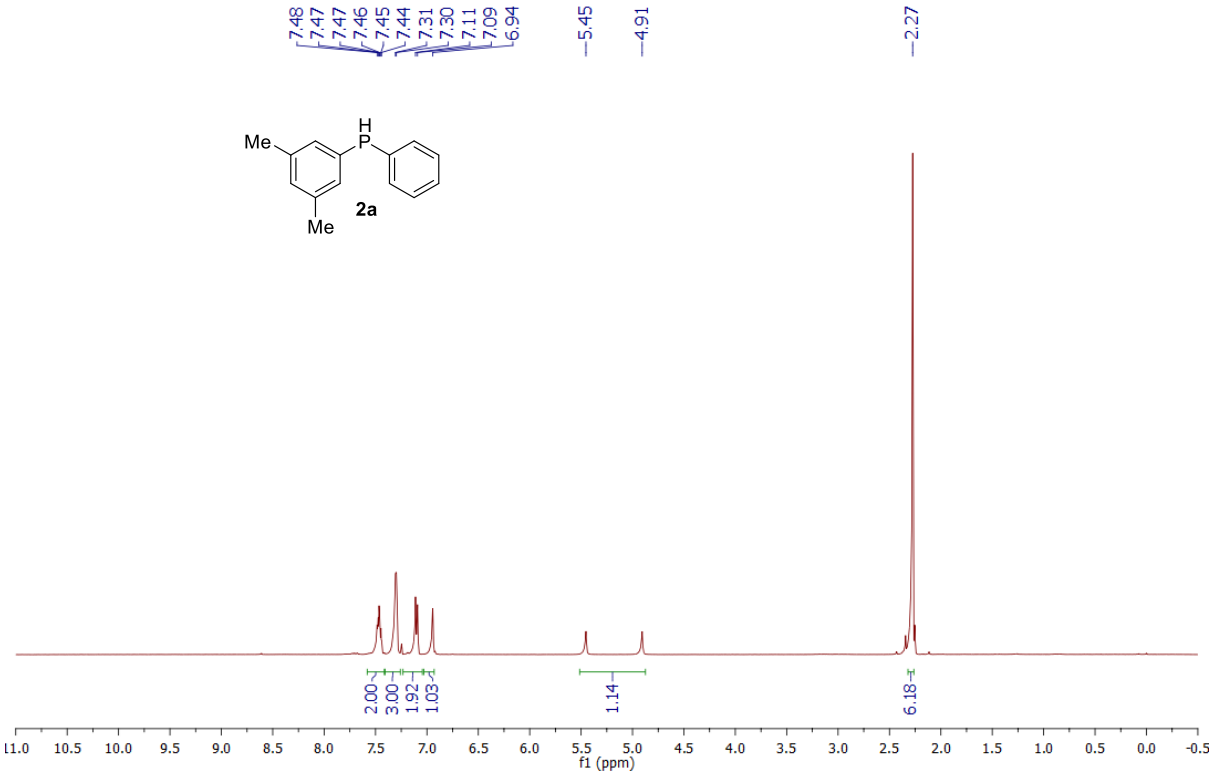

Figure S16 $^{13}C\{^{1}H\}$ NMR (101 MHz, $CDCl_3$) spectrum of **2a**.

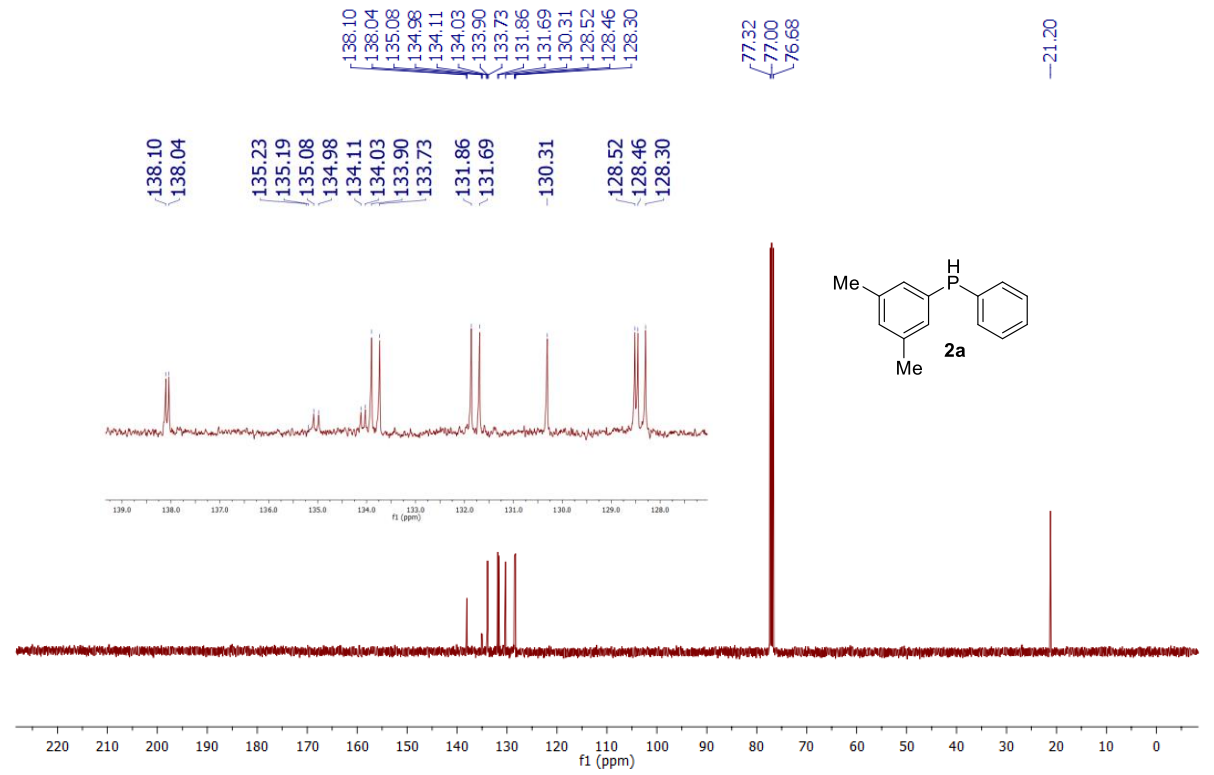

Figure S17 $^{31}P\{^{1}H\}$ NMR (162 MHz, $CDCl_3$) spectrum of **2a**.

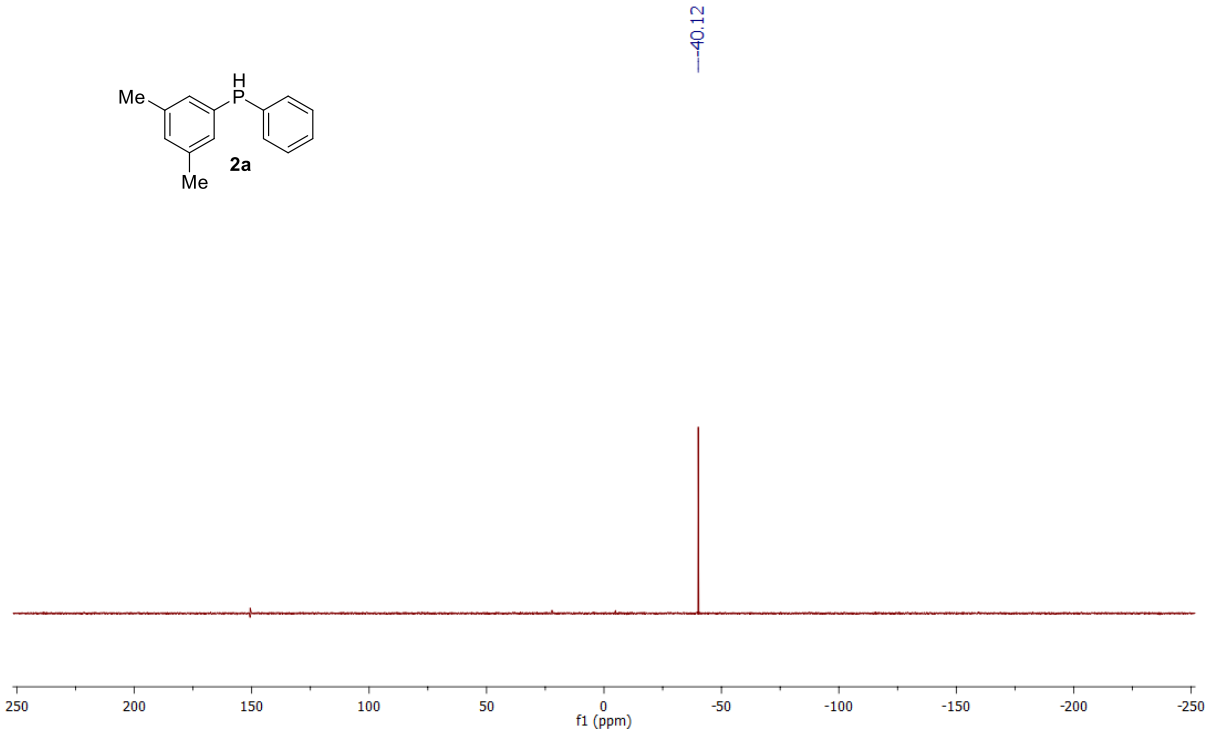

Figure S18 ^{1}H NMR (400 MHz, $CDCl_3$) spectrum of **2b**.

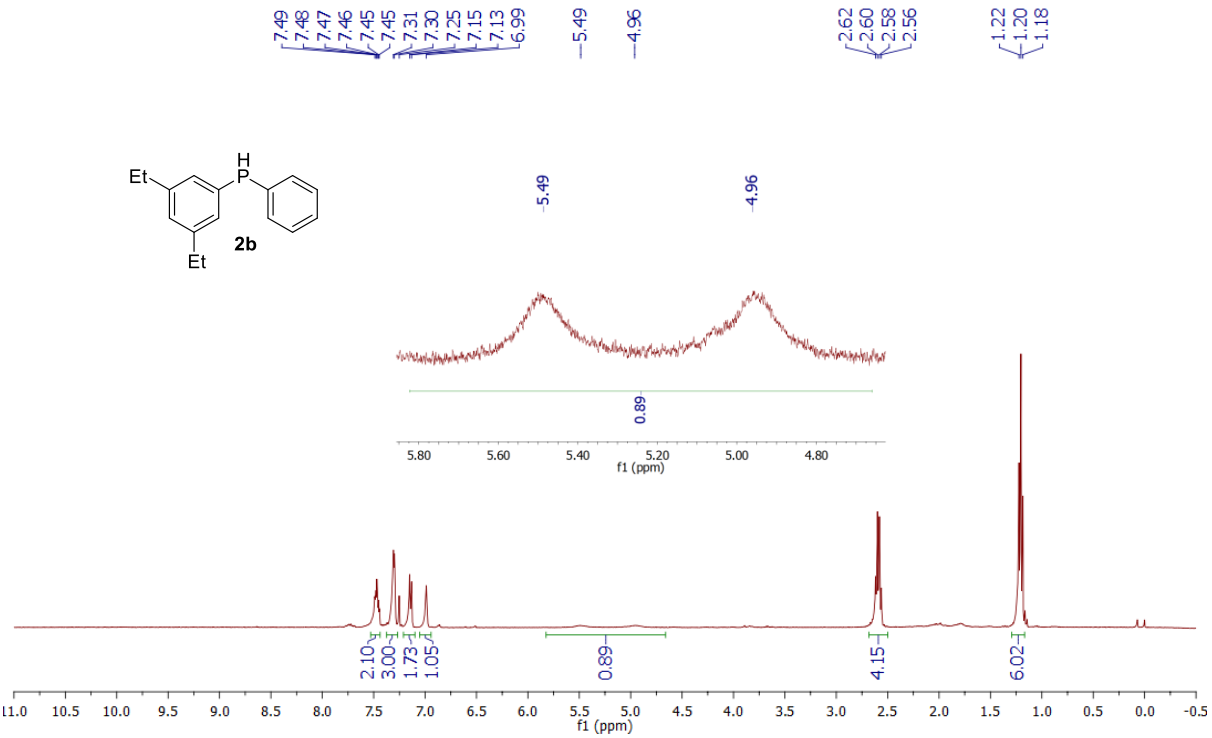

Figure S19 $^{13}C\{^{1}H\}$ NMR (101 MHz, $CDCl_3$) spectrum of **2b**.

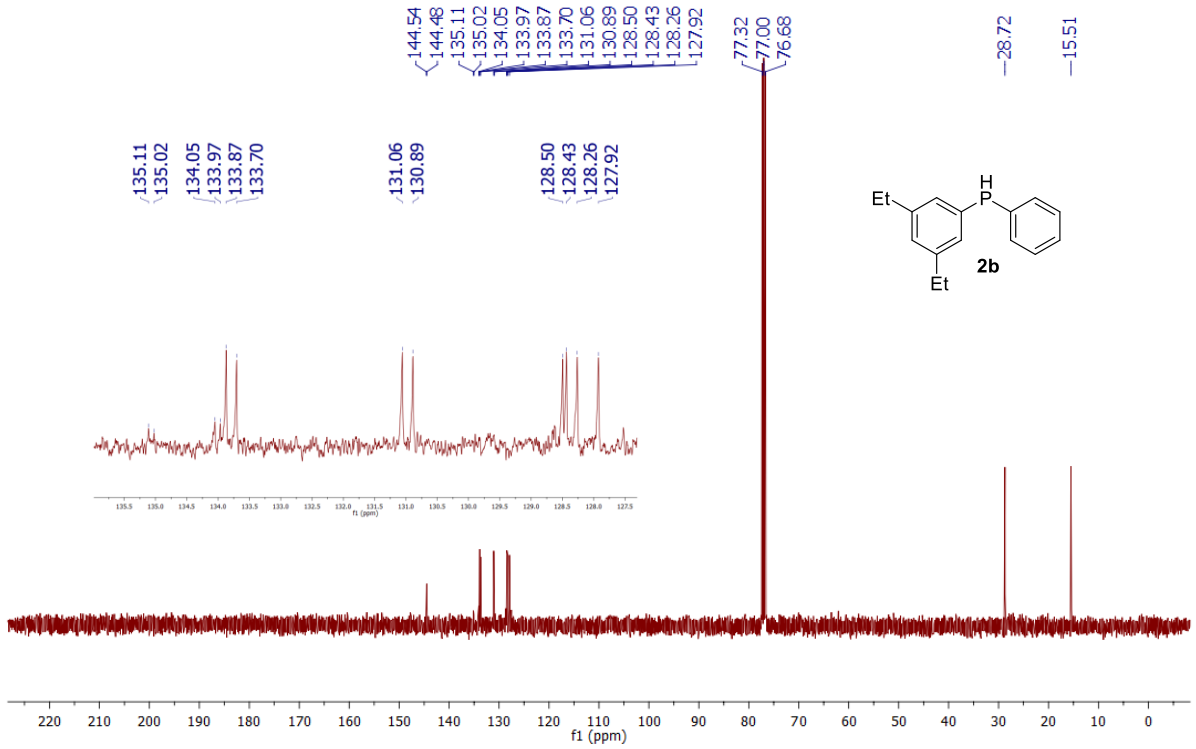

Figure S20 $^{31}P\{^{1}H\}$ NMR (162 MHz, $CDCl_3$) spectrum of **2b**.

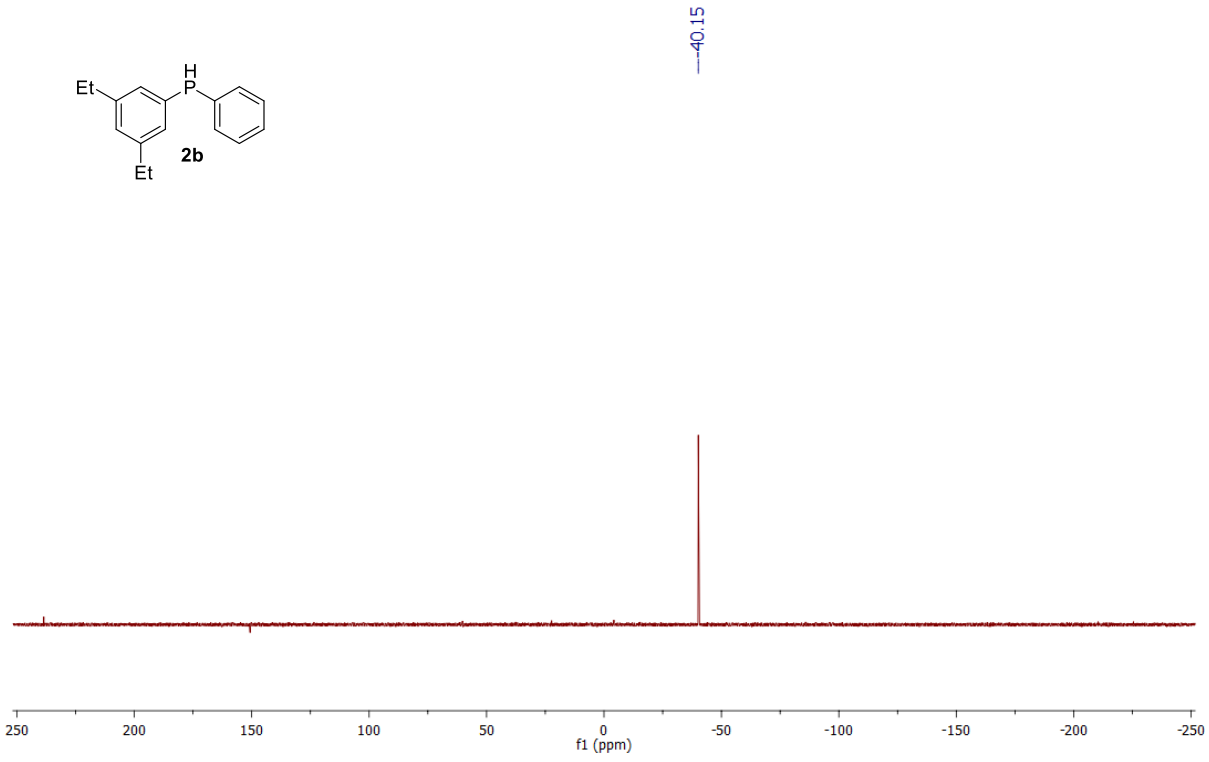

Figure S21 ^{1}H NMR (400 MHz, $CDCl_3$) spectrum of **2c**.

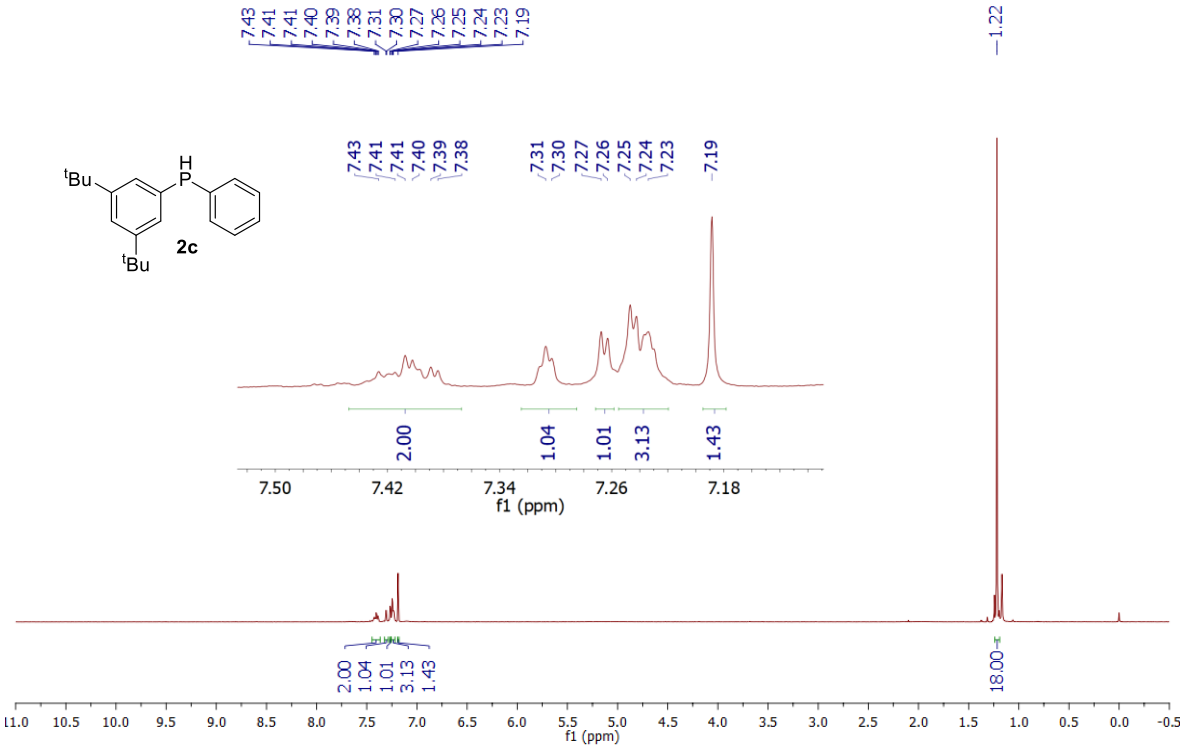

Figure S22 $^{13}C\{^{1}H\}$ NMR (75 MHz, $CDCl_3$) spectrum of **2c**.

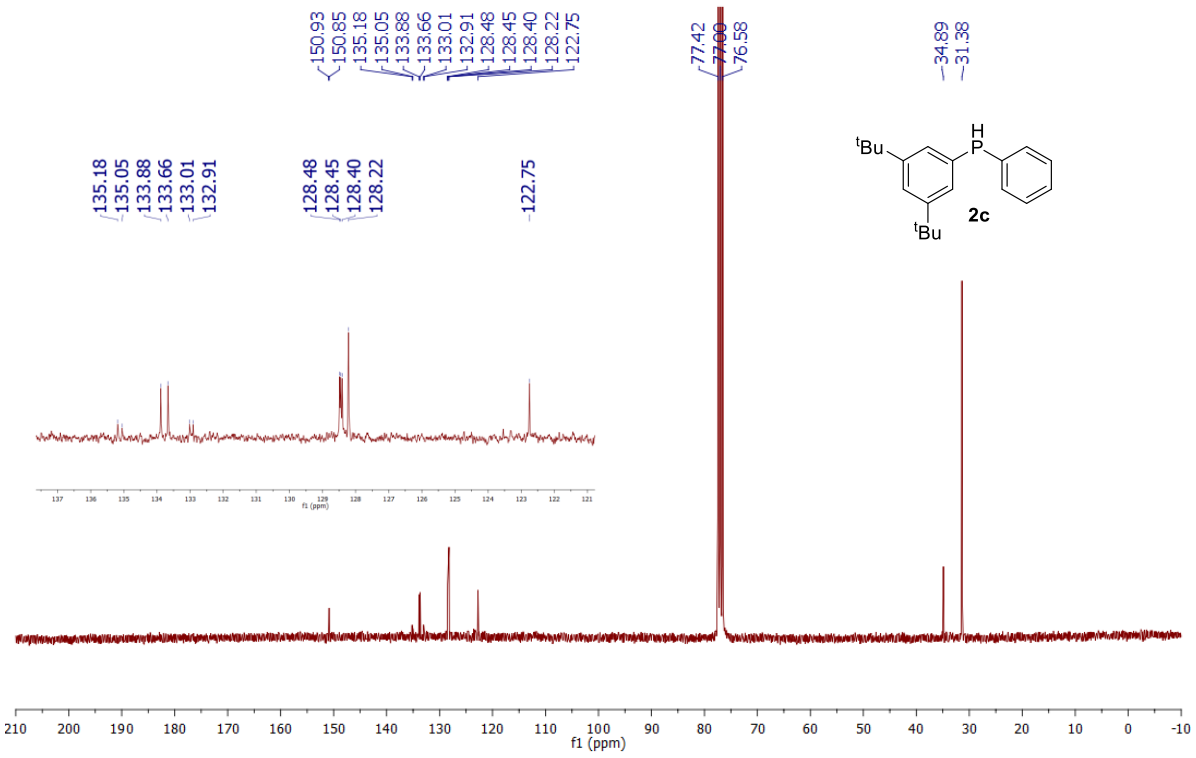

Figure S23 $^{31}P\{^{1}H\}$ NMR (162 MHz, $CDCl_3$) spectrum of **2c**.

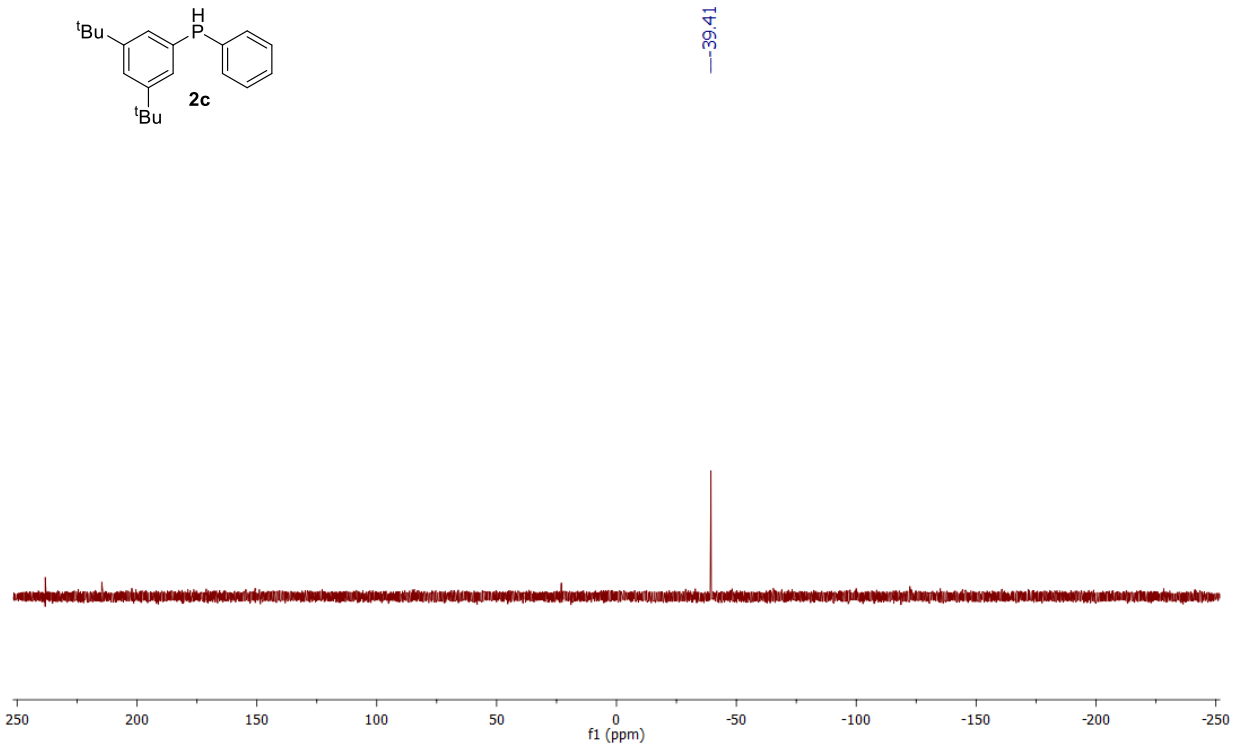

Figure S24 ^{1}H NMR (400 MHz, $CDCl_3$) spectrum of **2d**.

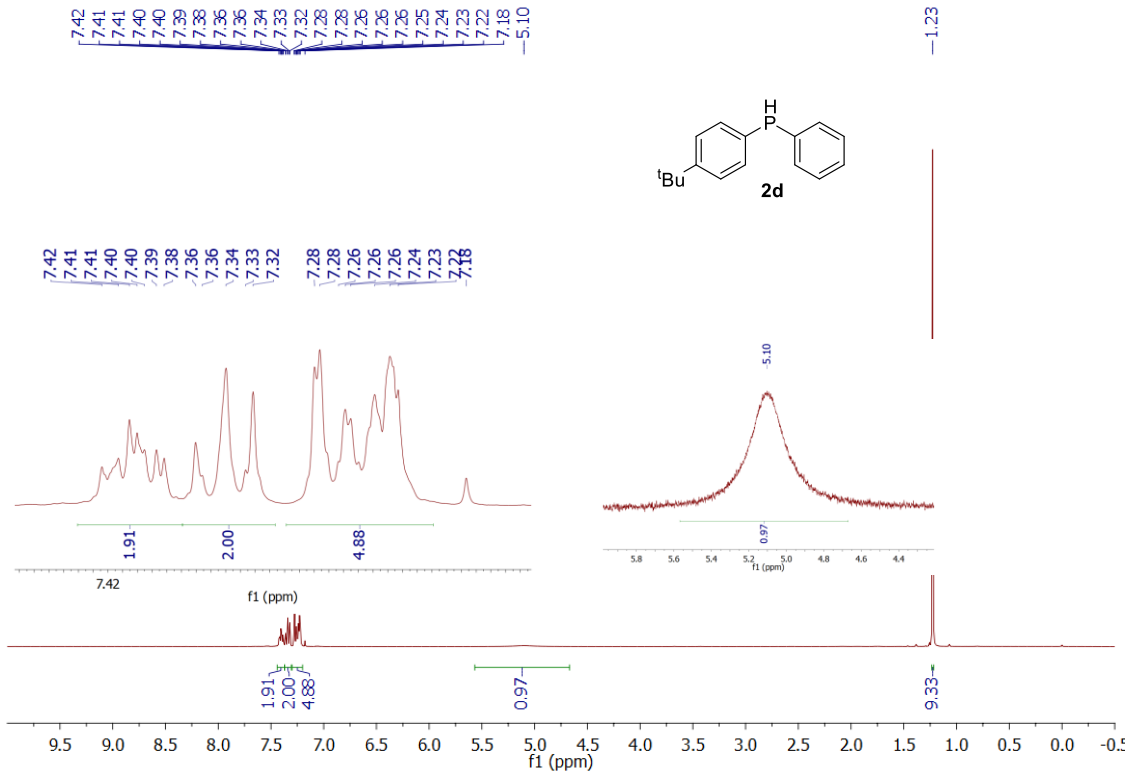

Figure S25 $^{13}C\{^{1}H\}$ NMR (101 MHz, $CDCl_3$) spectrum of **2d**.

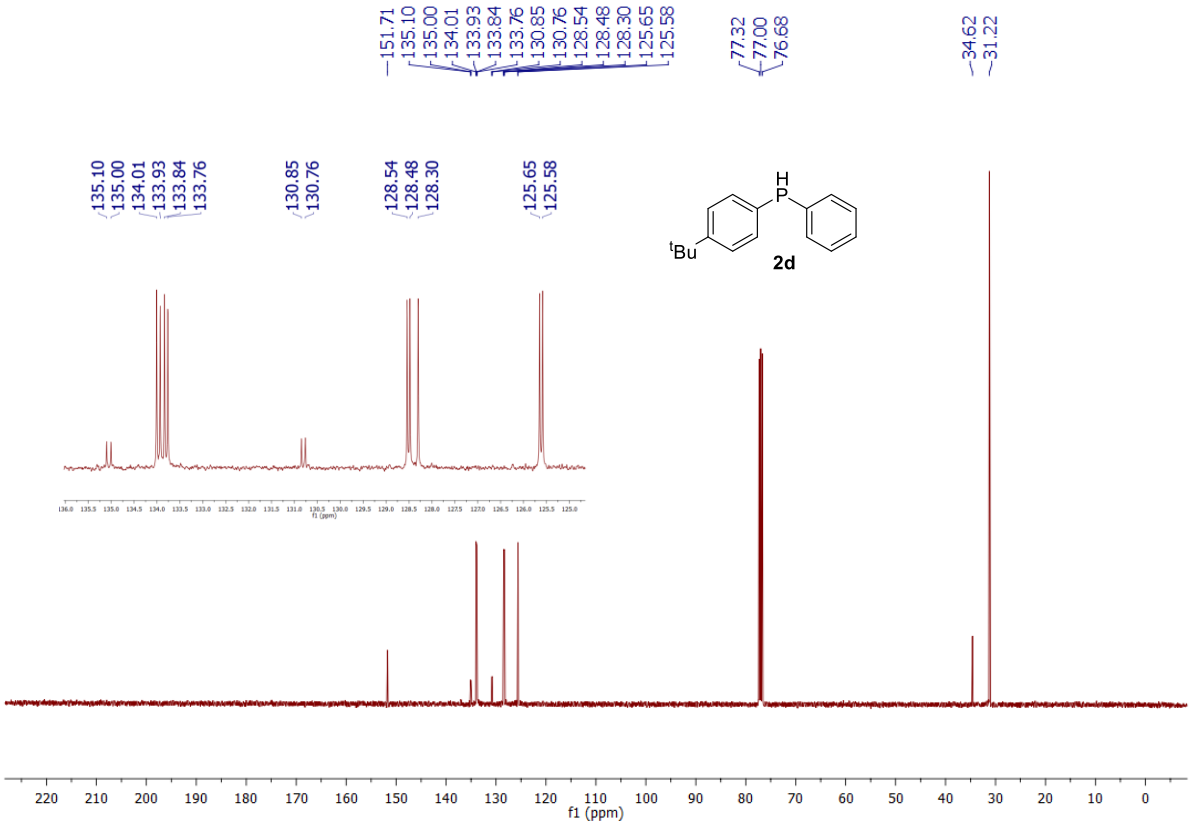

Figure S26 $^{31}P\{^{1}H\}$ NMR (162 MHz, $CDCl_3$) spectrum of **2d**.

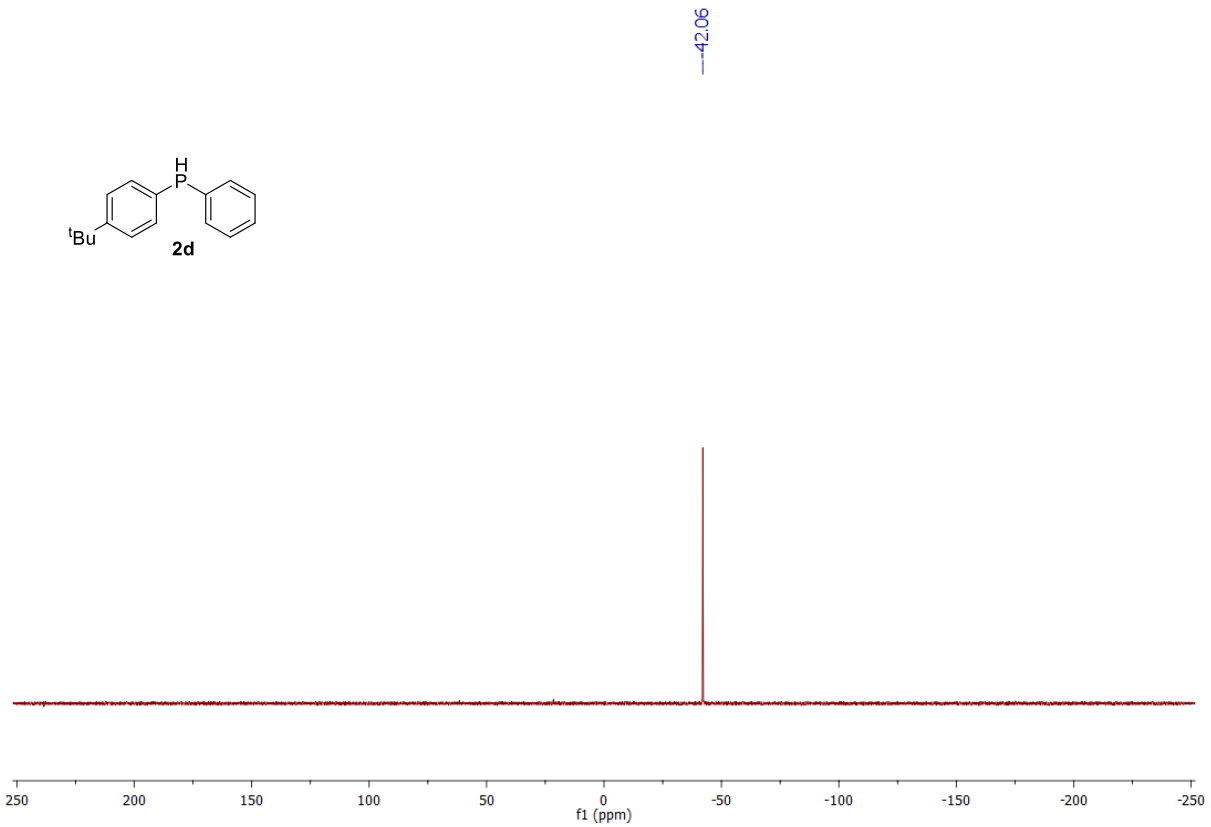

Figure S27 ^{1}H NMR (400 MHz, $CDCl_3$) spectrum of **1b**.

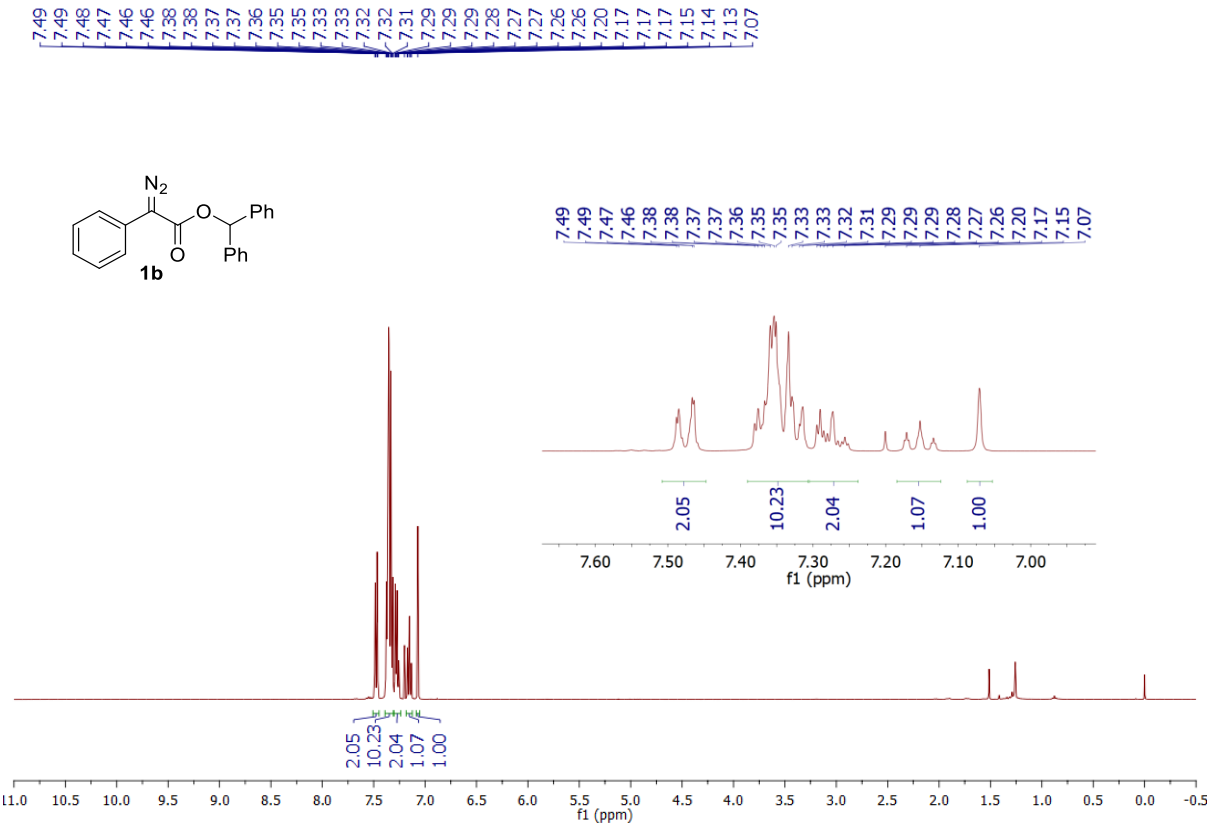

Figure S28 $^{13}C\{^{1}H\}$ NMR (101 MHz, $CDCl_3$) spectrum of **1b**.

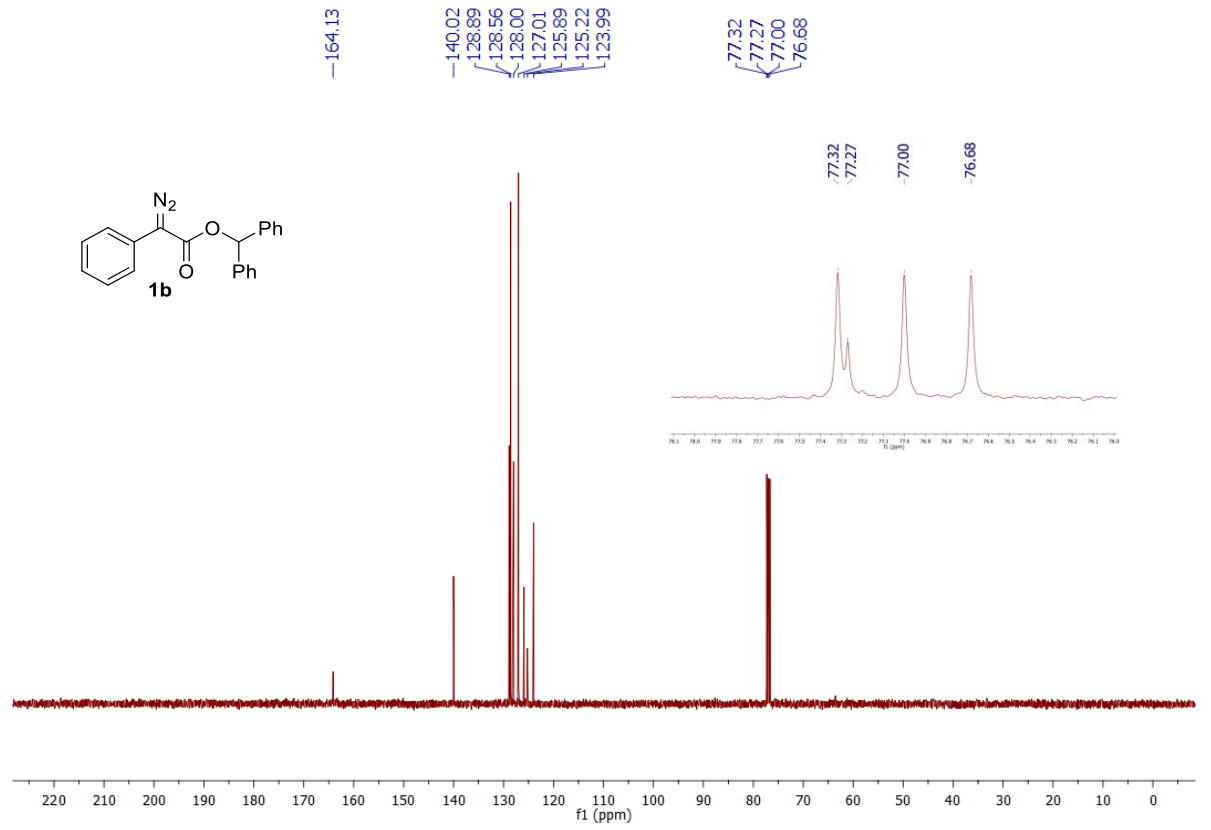

Figure S29 ^{1}H NMR (400 MHz, $CDCl_3$) spectrum of **1d**.

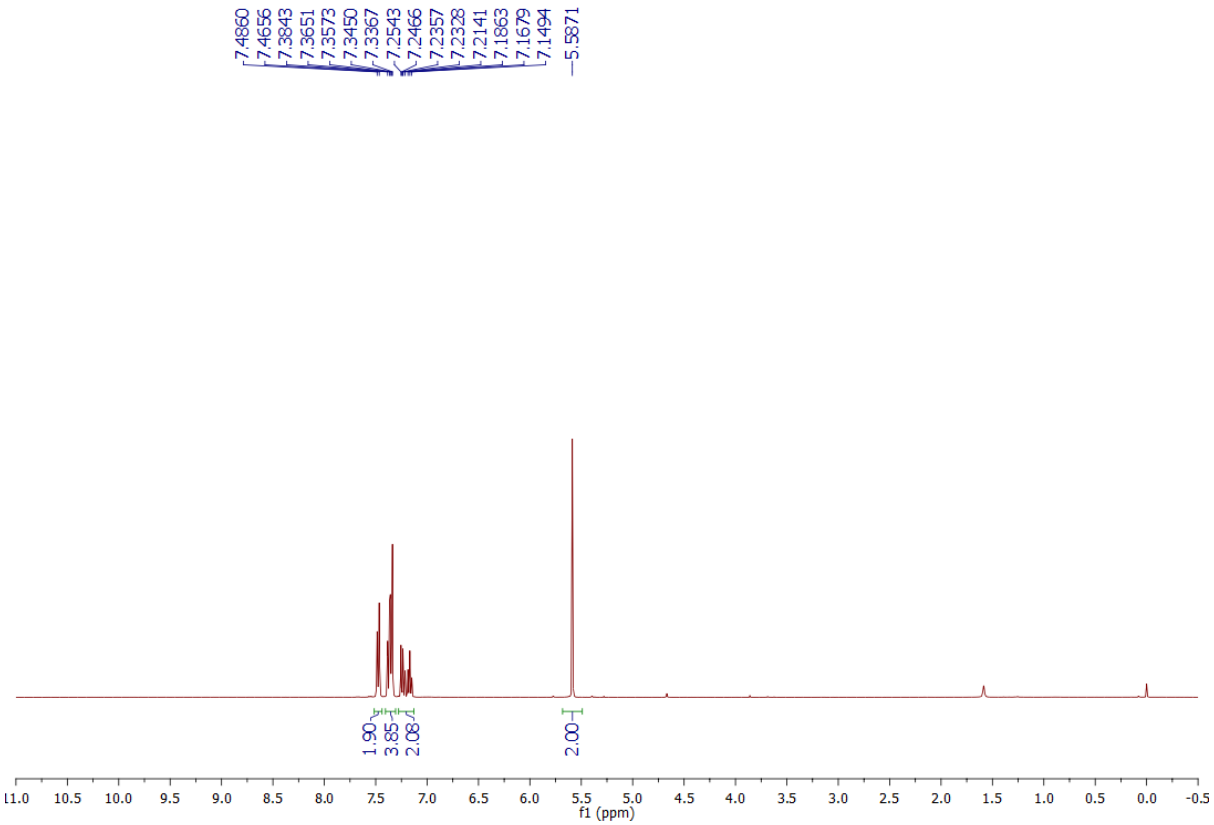

Figure S30 $^{13}C\{^{1}H\}$ NMR (101 MHz, $CDCl_3$) spectrum of **1d**.

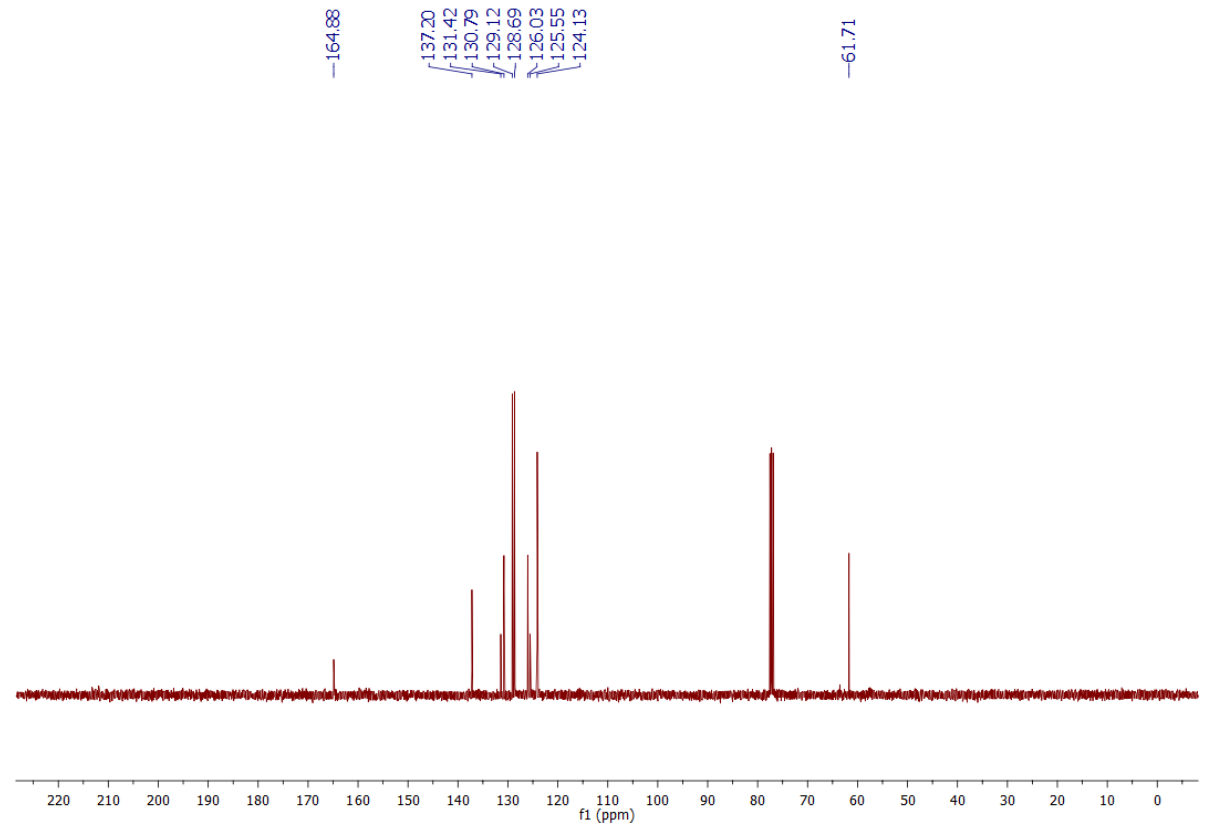

Figure S31 ^{1}H NMR (400 MHz, $CDCl_3$) spectrum of **3aa.**

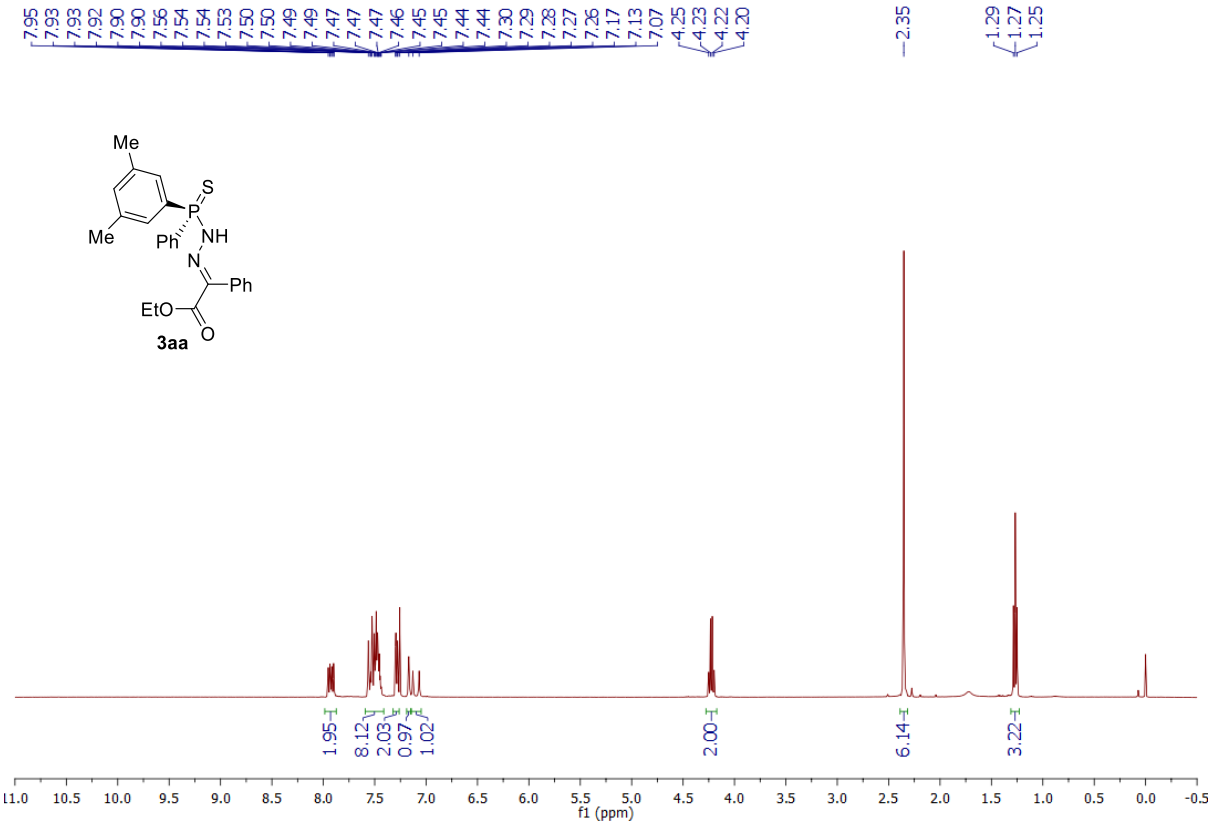

Figure S32 $^{13}C\{^{1}H\}$ NMR (101 MHz, $CDCl_3$) spectrum **3aa.**

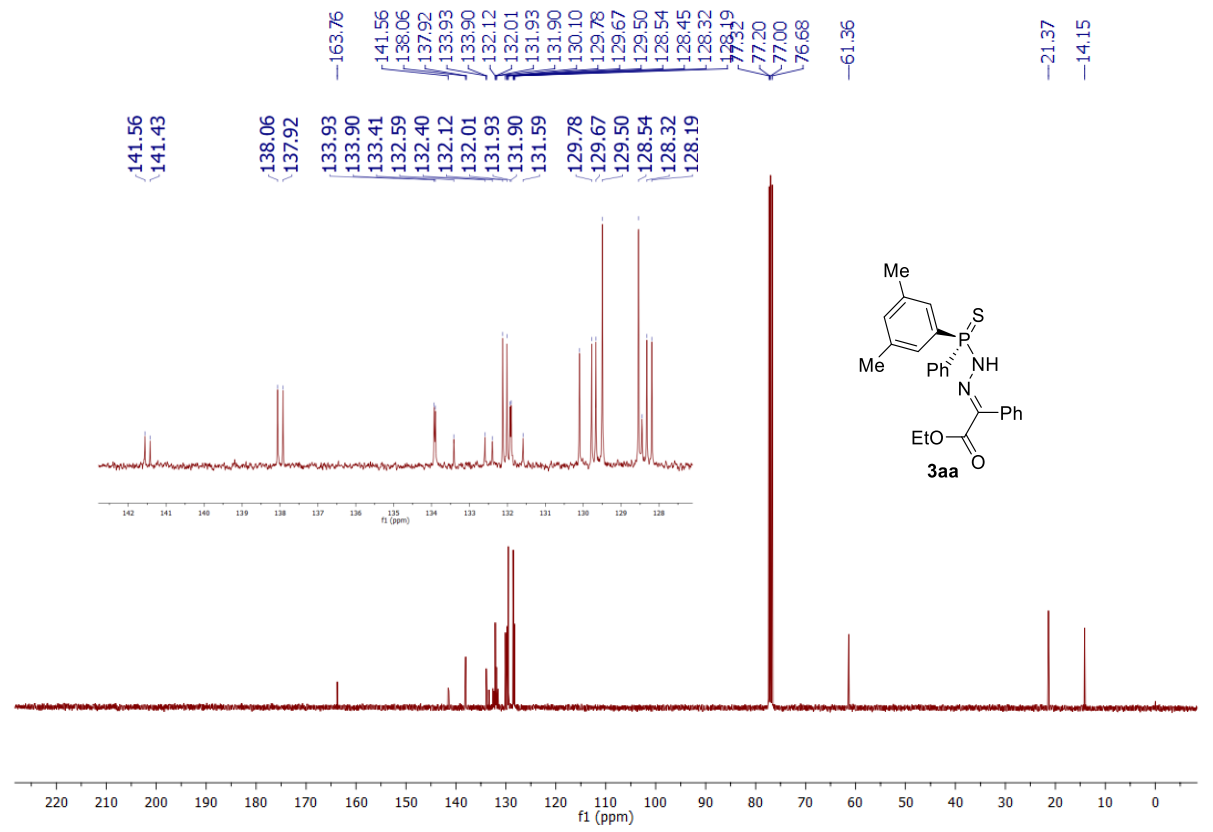

Figure S33 $^{31}P\{^{1}H\}$ NMR (162 MHz, $CDCl_3$) spectrum of **3aa.**

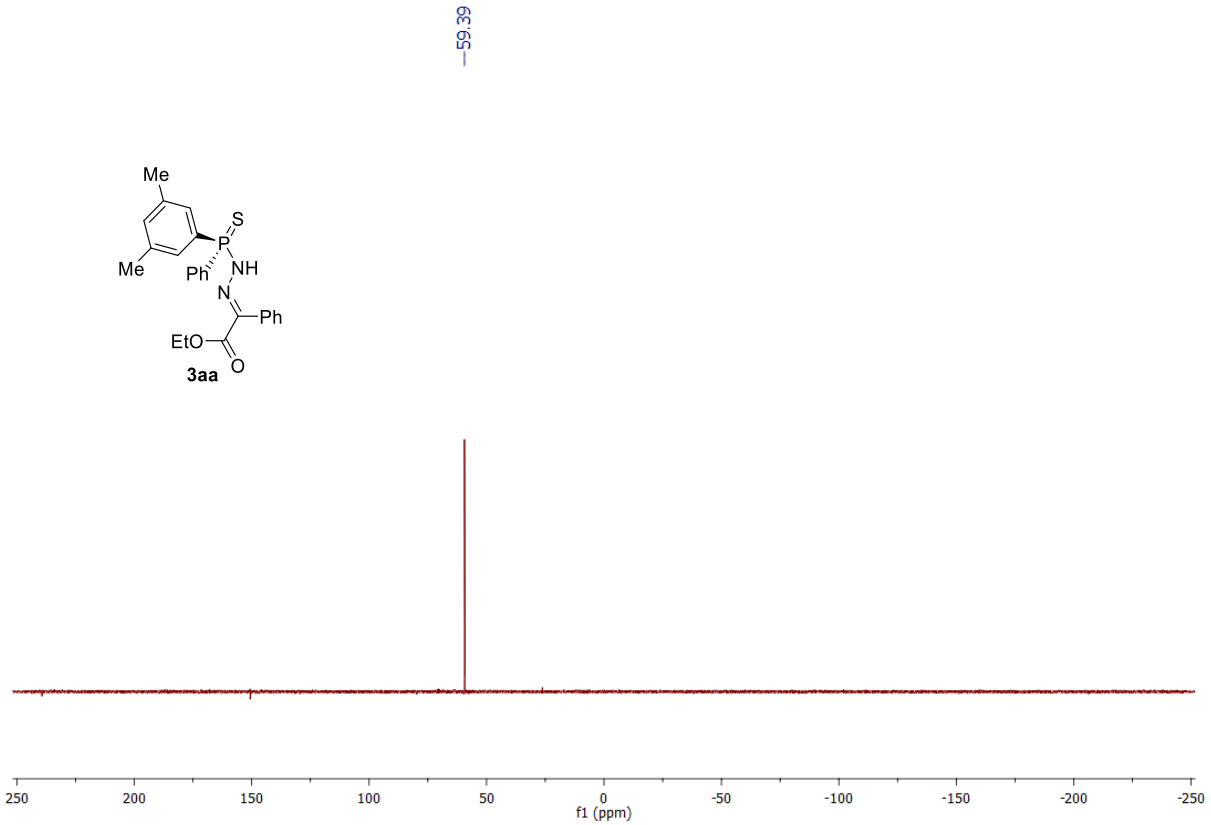

Figure S34 ^{1}H NMR (400 MHz, $CDCl_3$) spectrum of **6aa**.

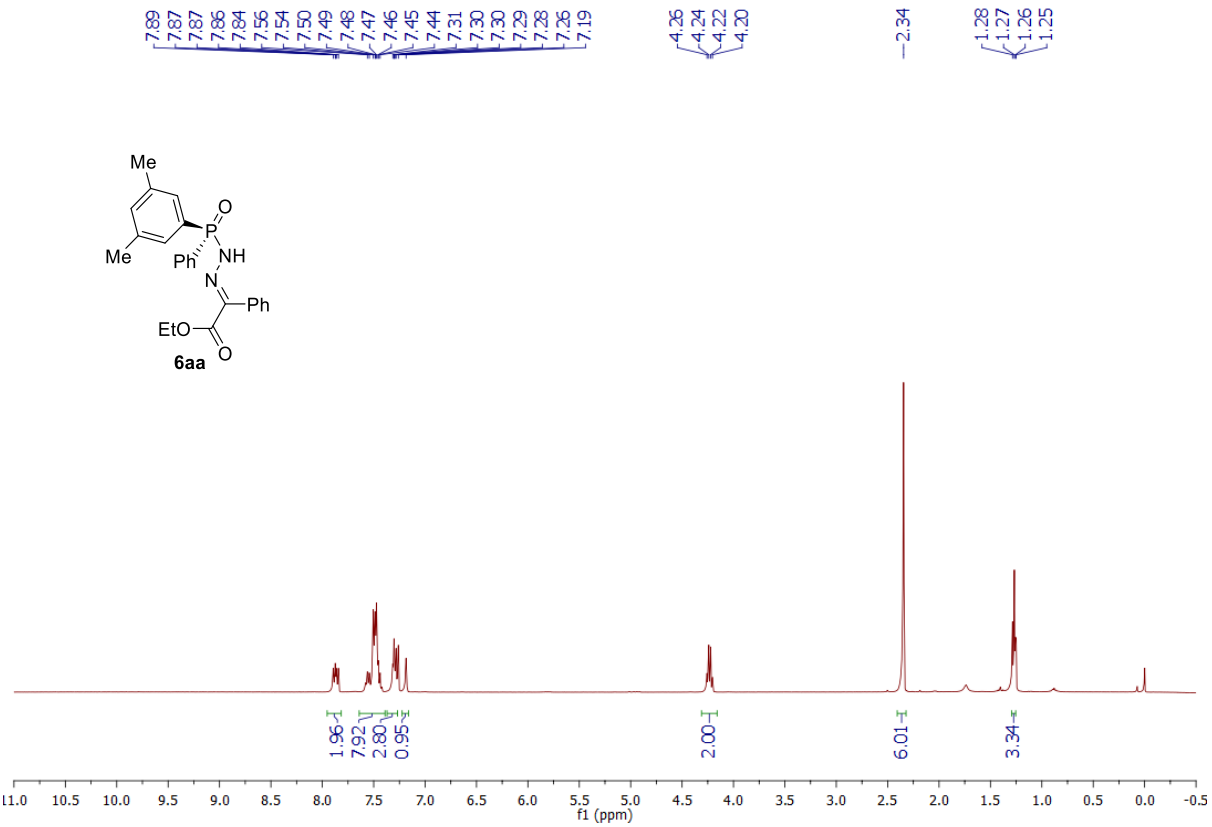

Figure S35 $^{13}C\{^{1}H\}$ NMR (101 MHz, $CDCl_3$) spectrum **6aa**.

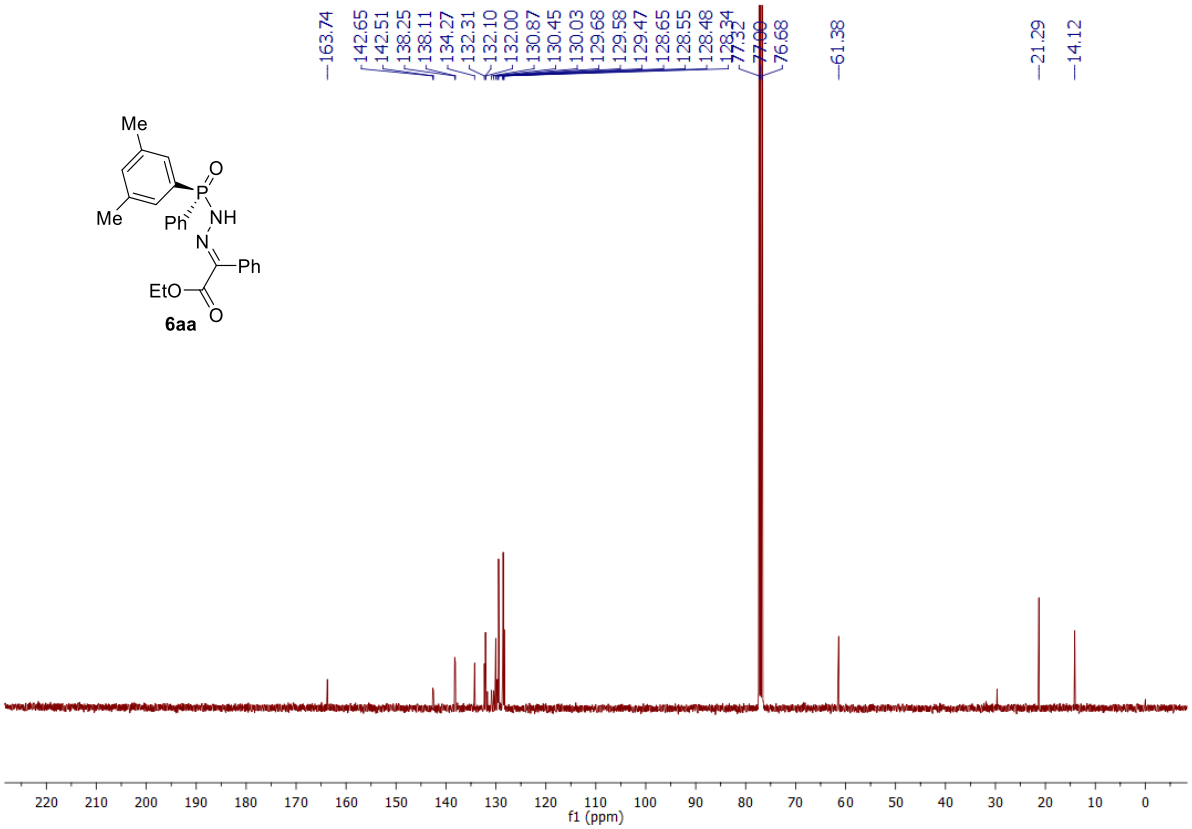

Figure S36 $^{31}P\{^{1}H\}$ NMR (162 MHz, $CDCl_3$) spectrum of **6aa**.

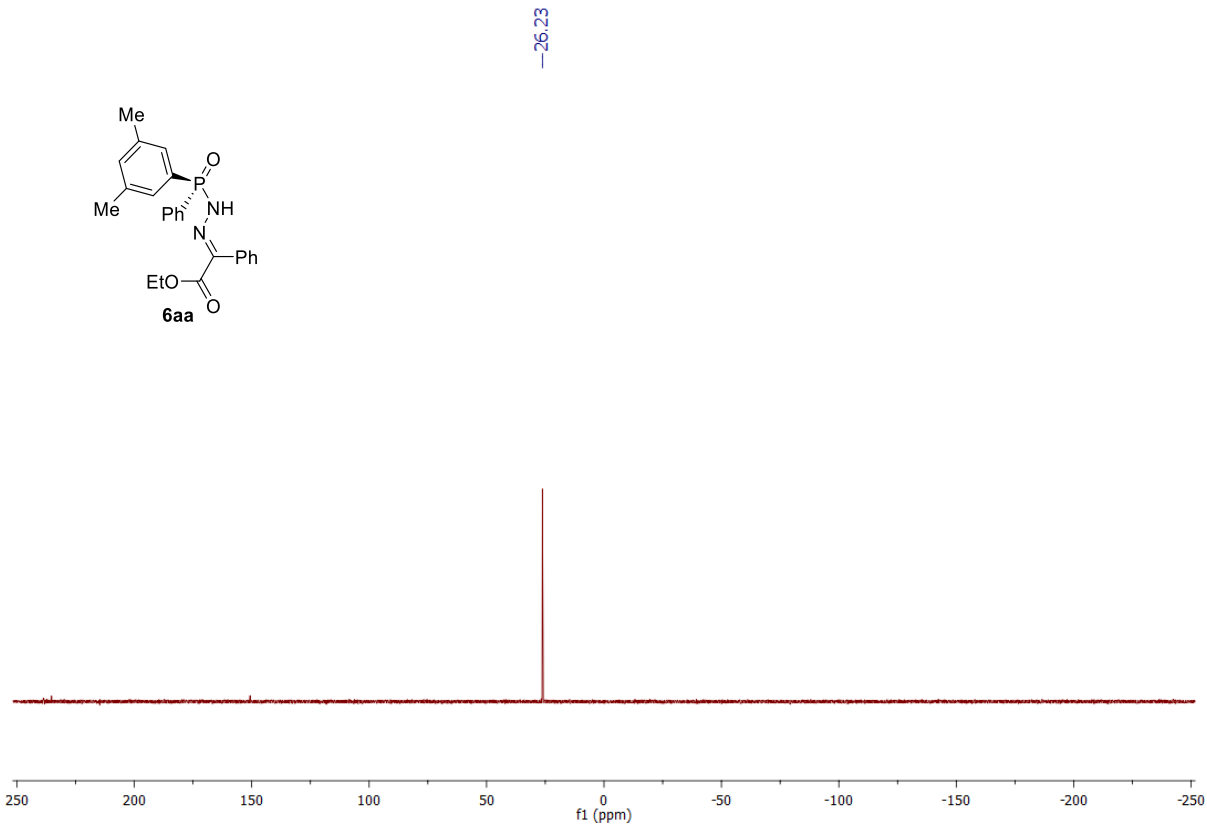

Figure S37 ^{1}H NMR (500 MHz, $CDCl_3$) spectrum of **6ba.**

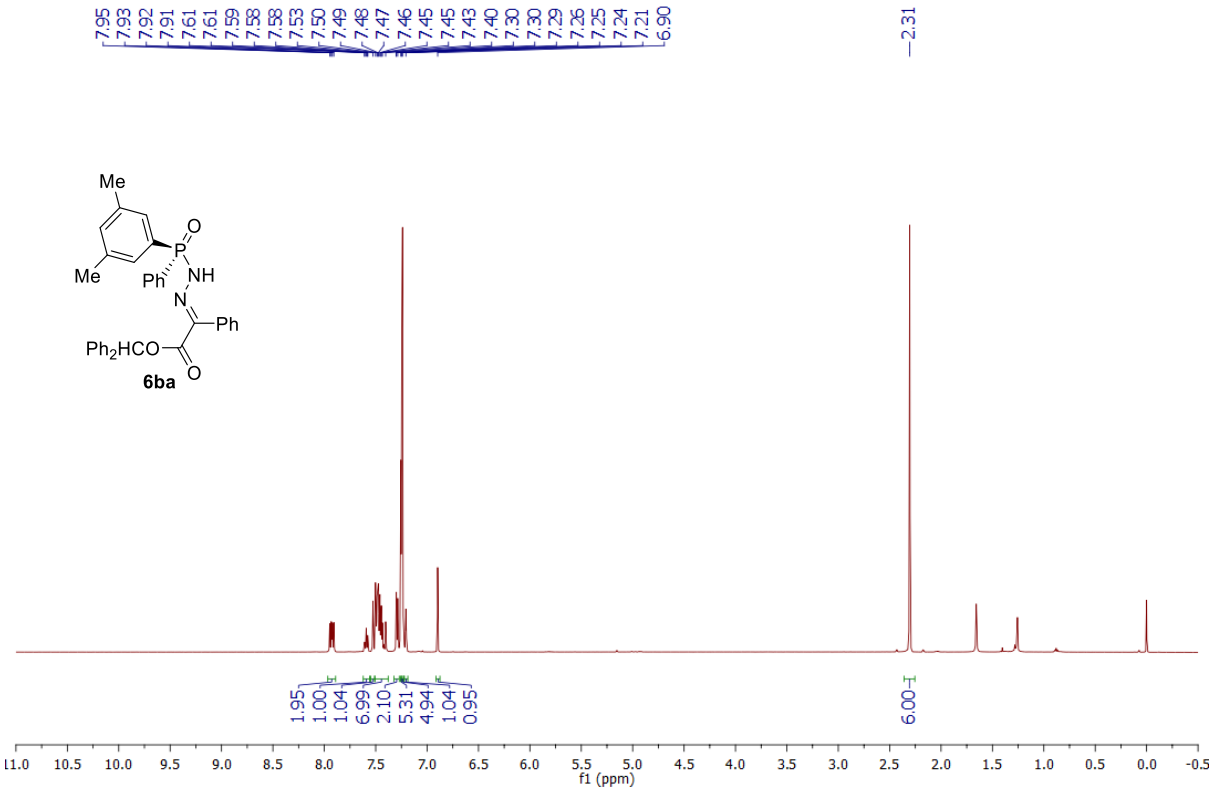

Figure S38 $^{13}C\{^{1}H\}$ NMR (101 MHz, $CDCl_3$) spectrum **6ba.**

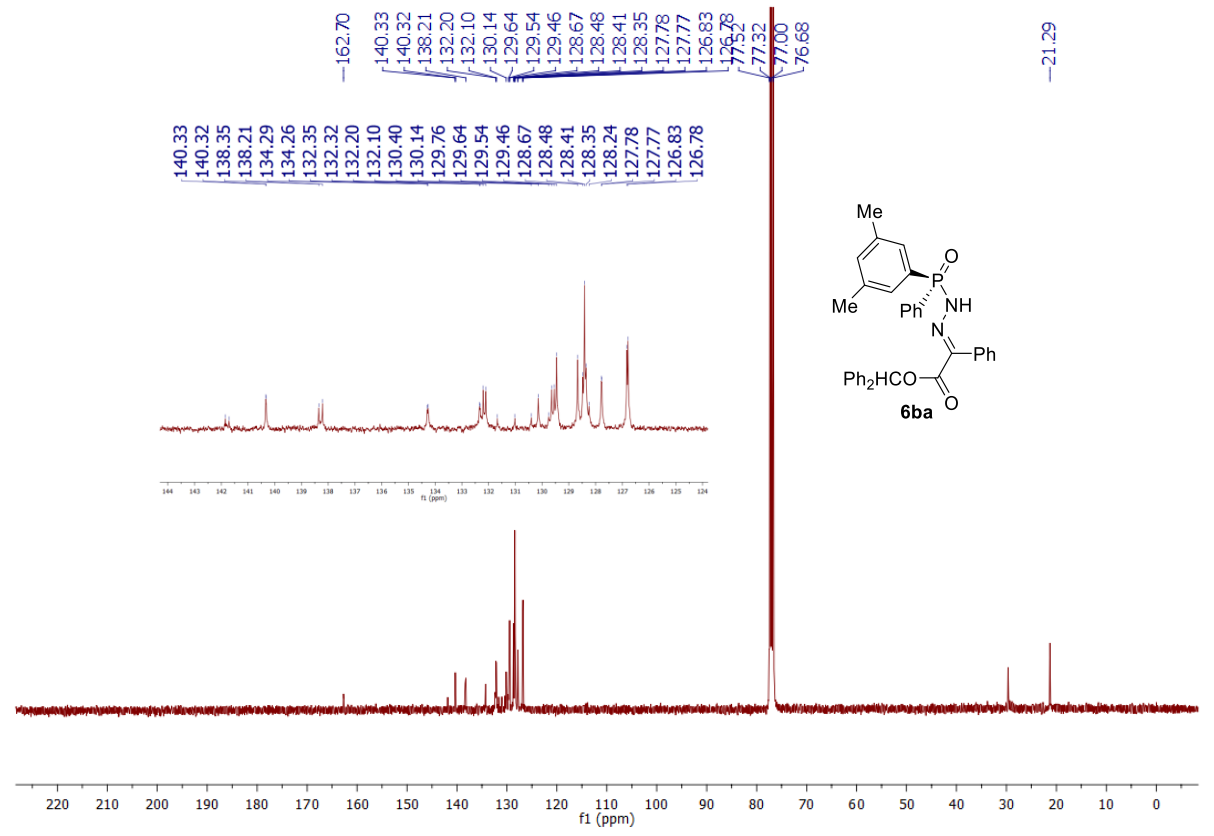

Figure S39 $^{31}P\{^{1}H\}$ NMR (162 MHz, $CDCl_3$) spectrum of **6ba.**

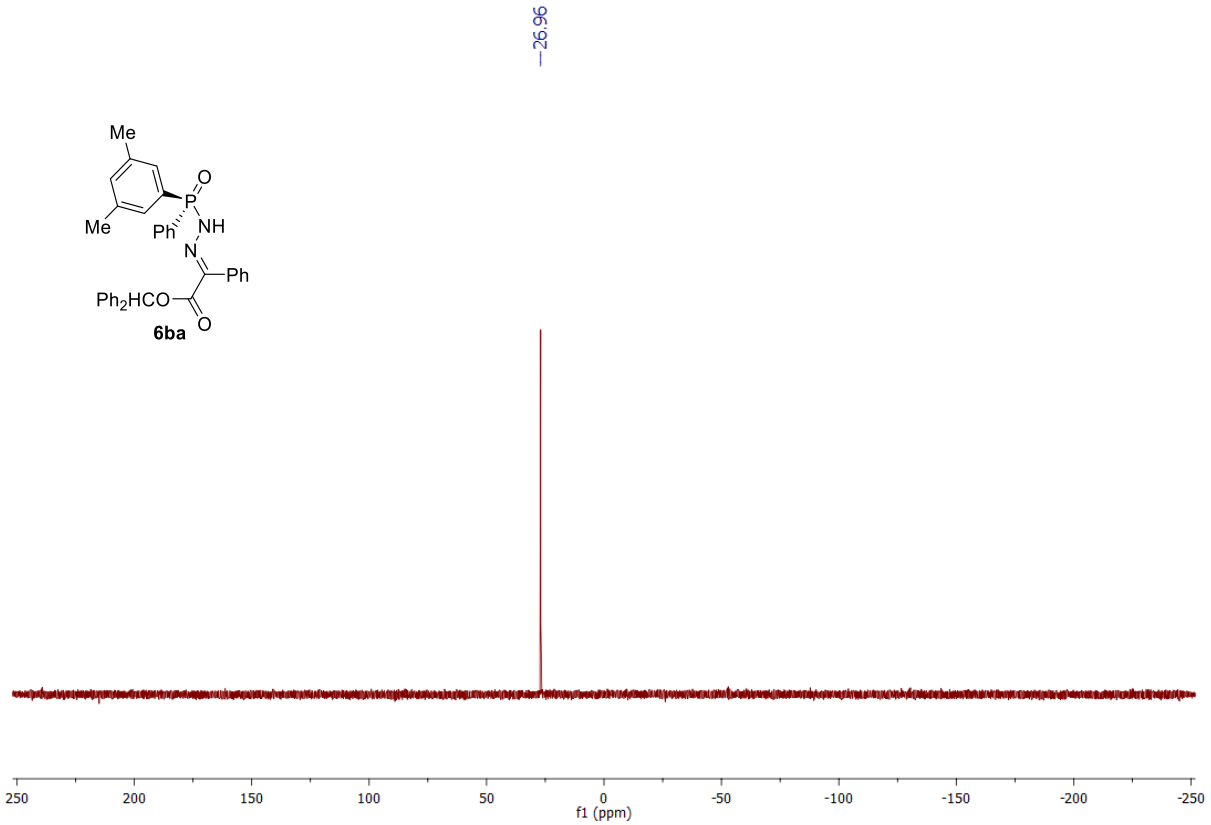

Figure S40 ^{1}H NMR (400 MHz, $CDCl_3$) spectrum of **6ca.**

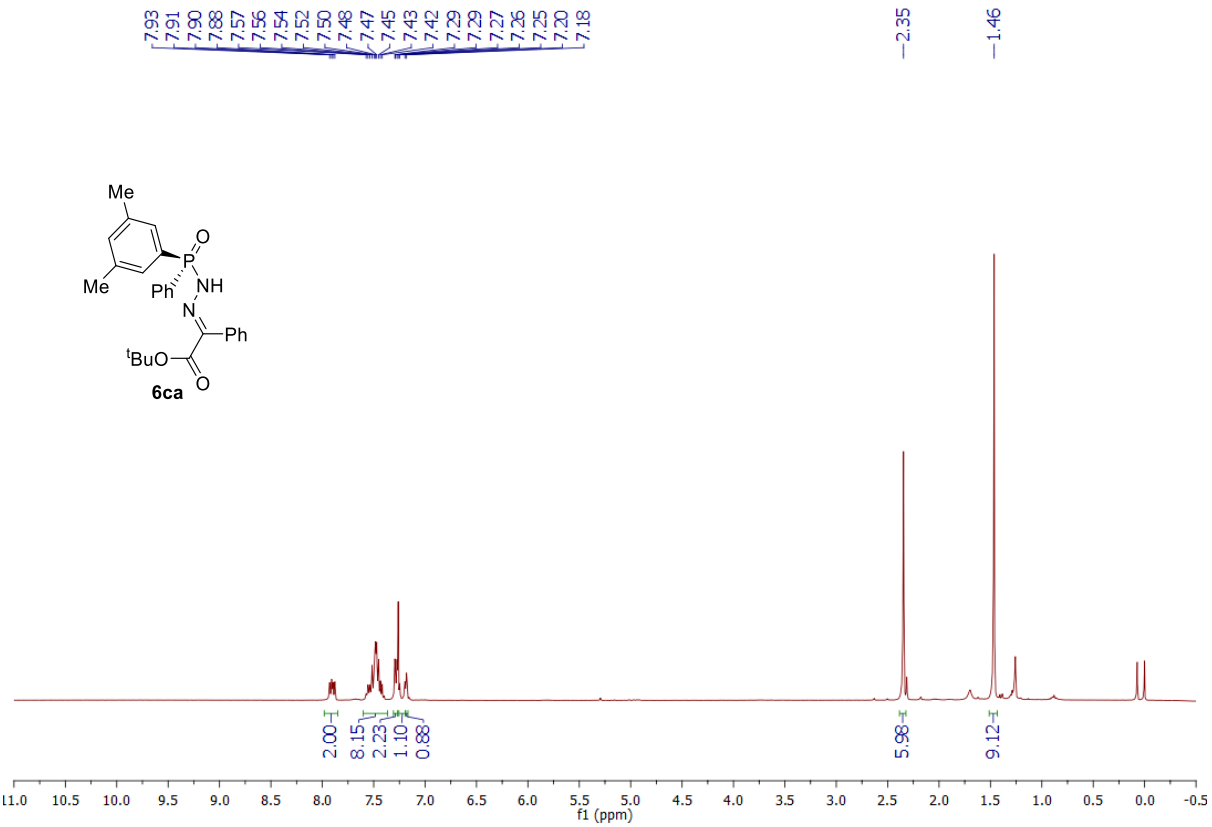

Figure S41 $^{13}C\{^{1}H\}$ NMR (101 MHz, $CDCl_3$) spectrum **6ca**.

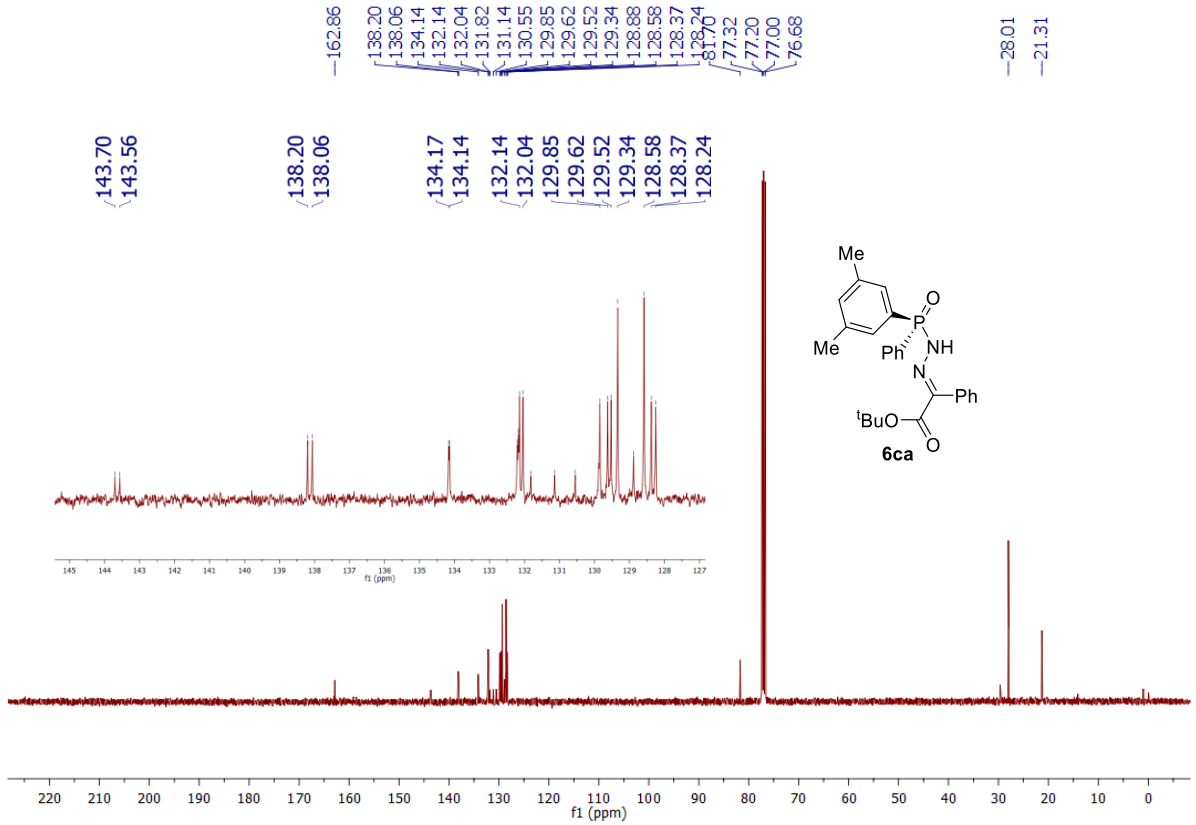

Figure S42 $^{31}P\{^{1}H\}$ NMR (162 MHz, $CDCl_3$) spectrum of **6ca.**

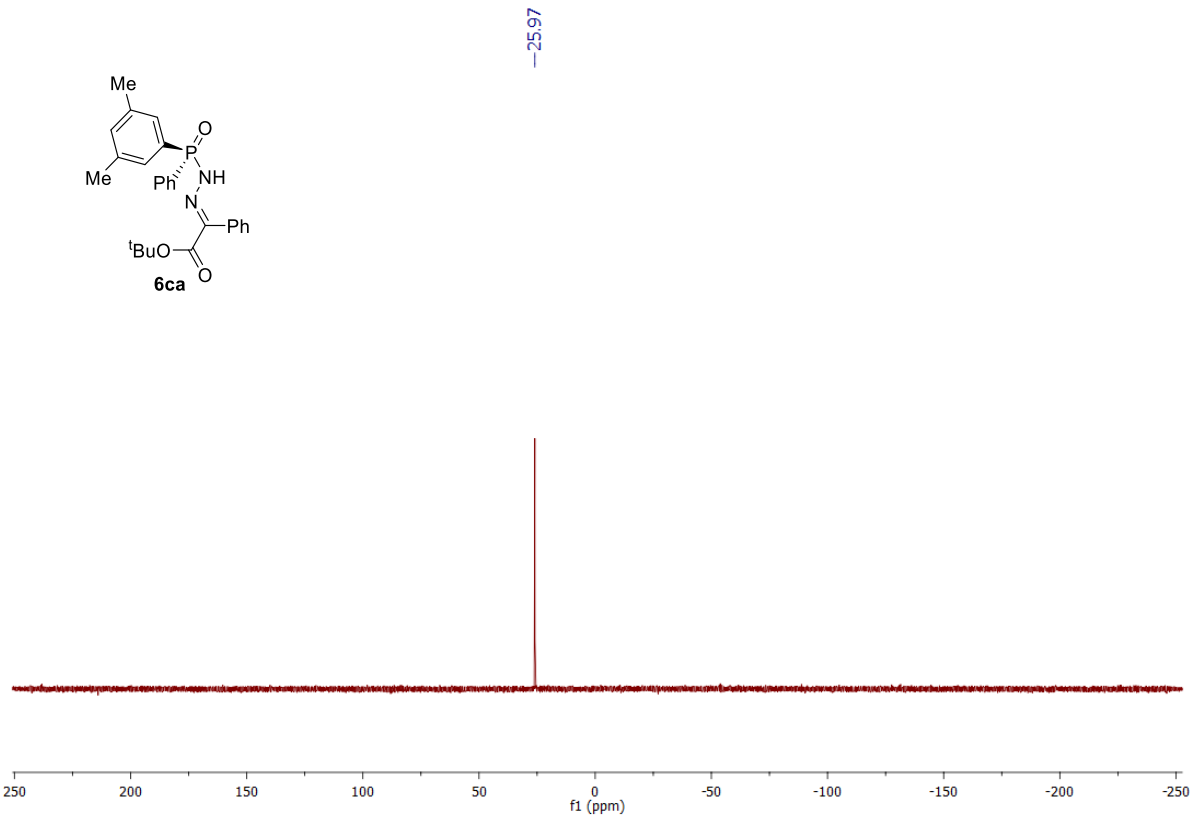

Figure S43 ^{1}H NMR (500 MHz, $CDCl_3$) spectrum of **6cb.**

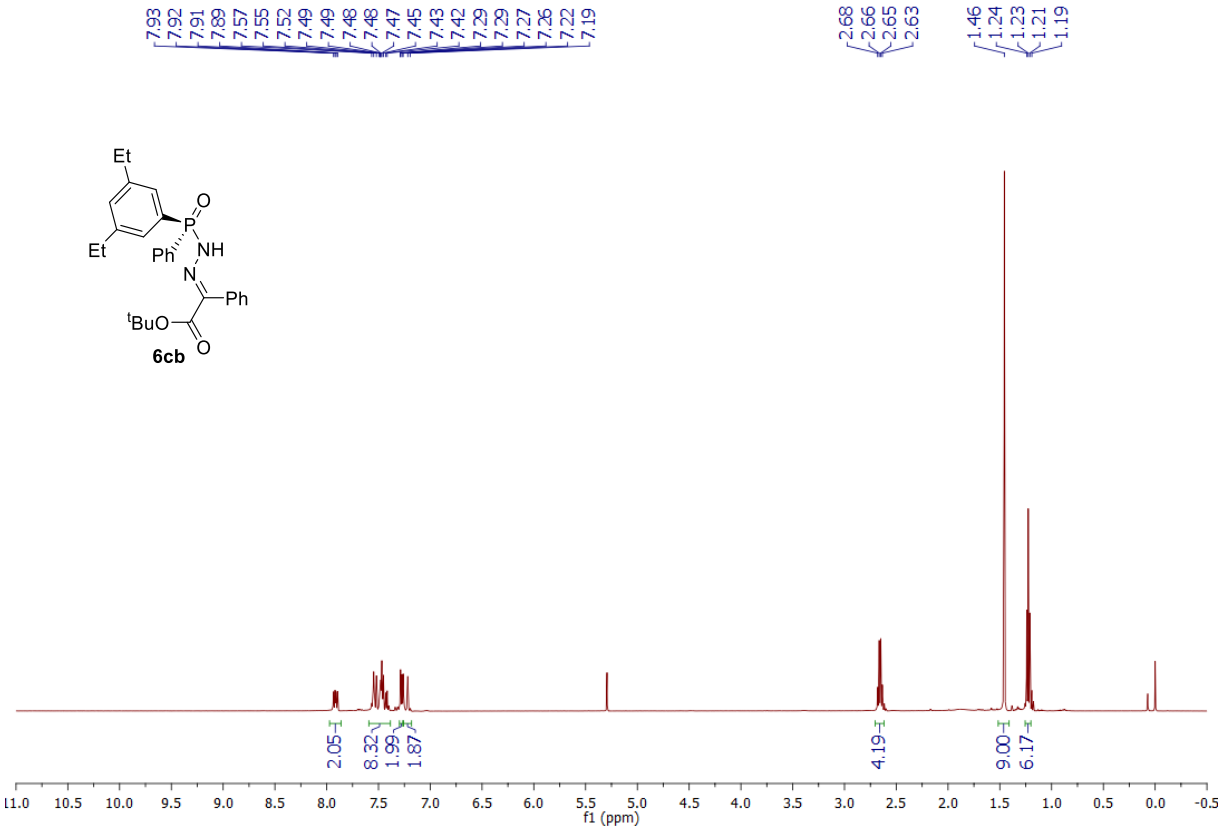

Figure S44 $^{13}C\{^{1}H\}$ NMR (126 MHz, $CDCl_3$) spectrum **6cb**.

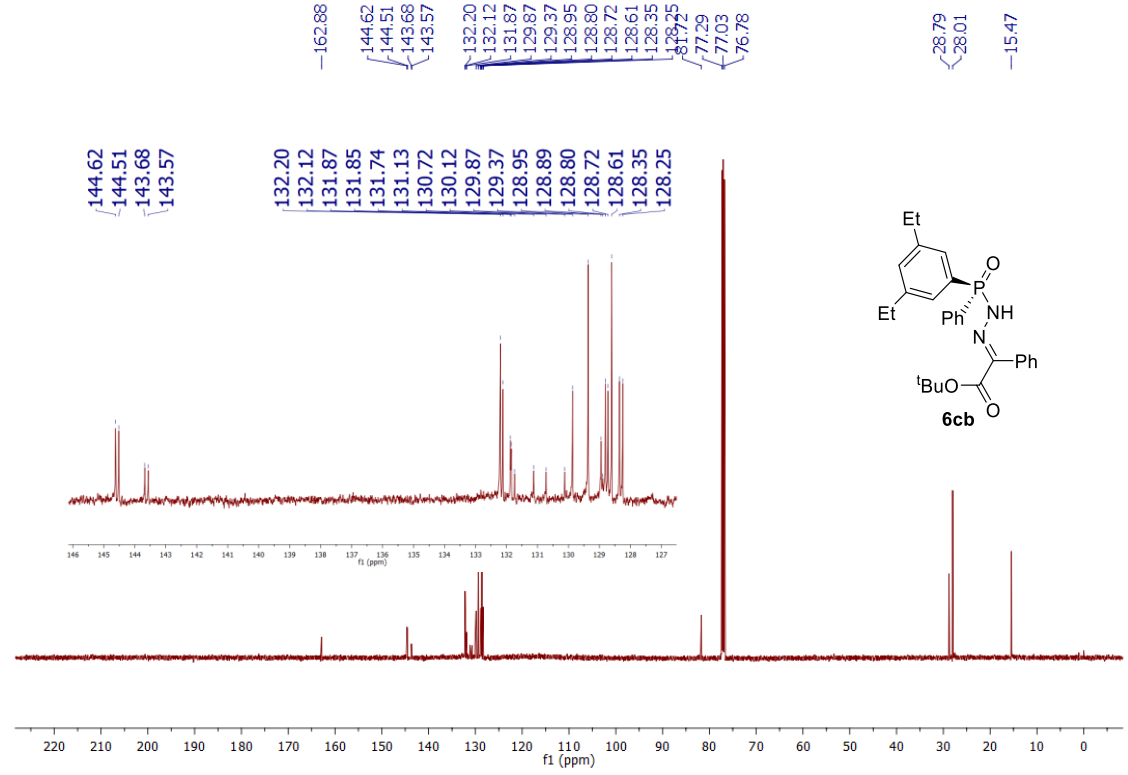

Figure S45 $^{31}P\{^{1}H\}$ NMR (162 MHz, $CDCl_3$) spectrum of **6cb.**

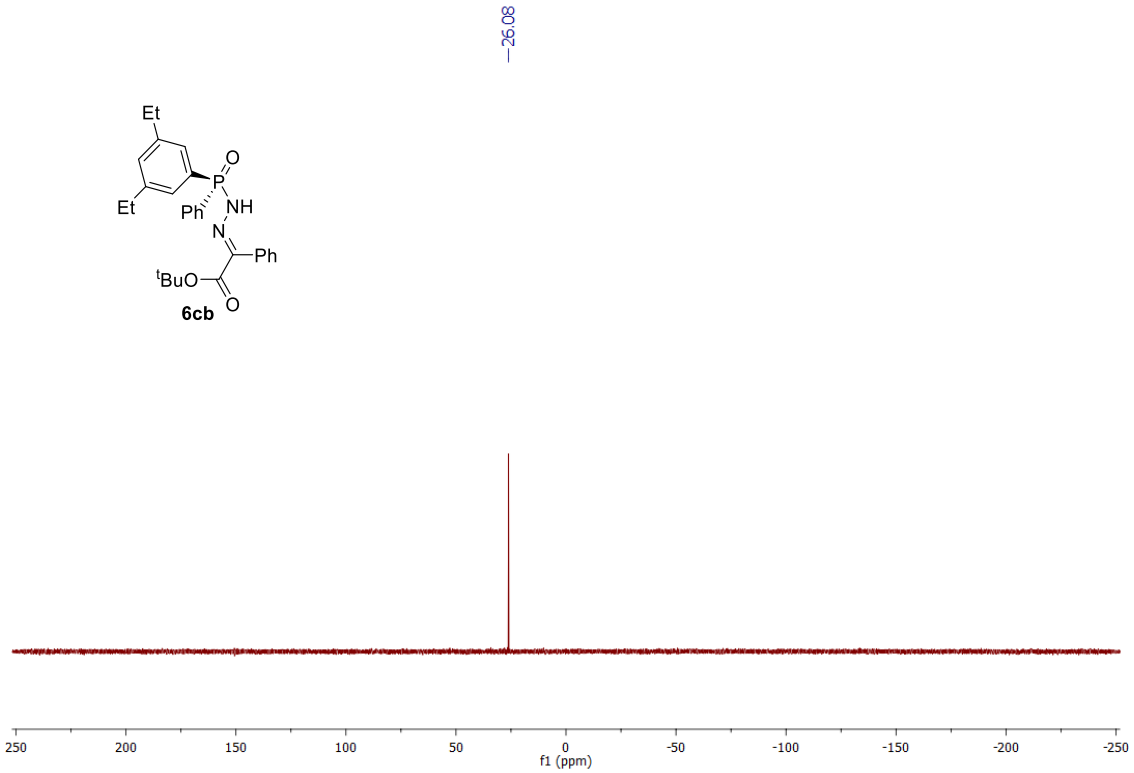

Figure S46 ^{1}H NMR (500 MHz, $CDCl_3$) spectrum of **6db.**

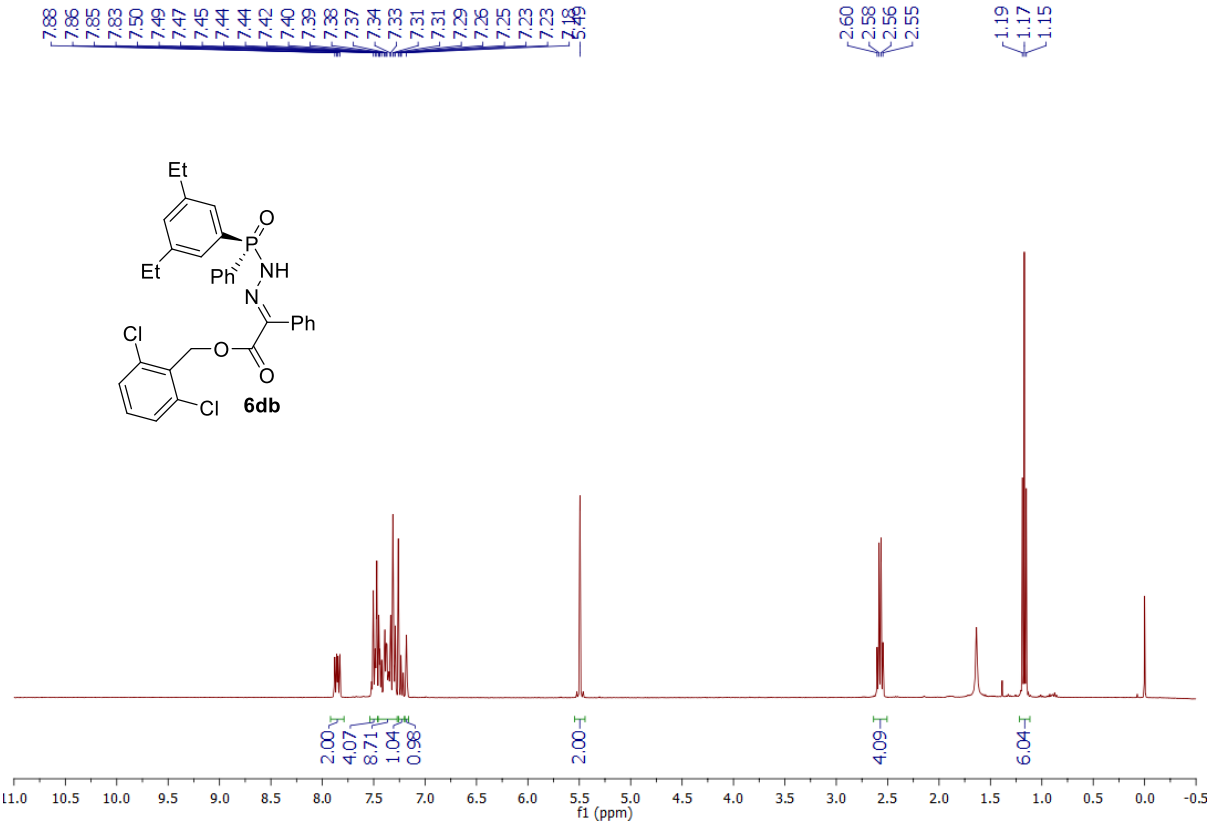

Figure S47 $^{13}C\{^{1}H\}$ NMR (126 MHz, $CDCl_3$) spectrum **6db**.

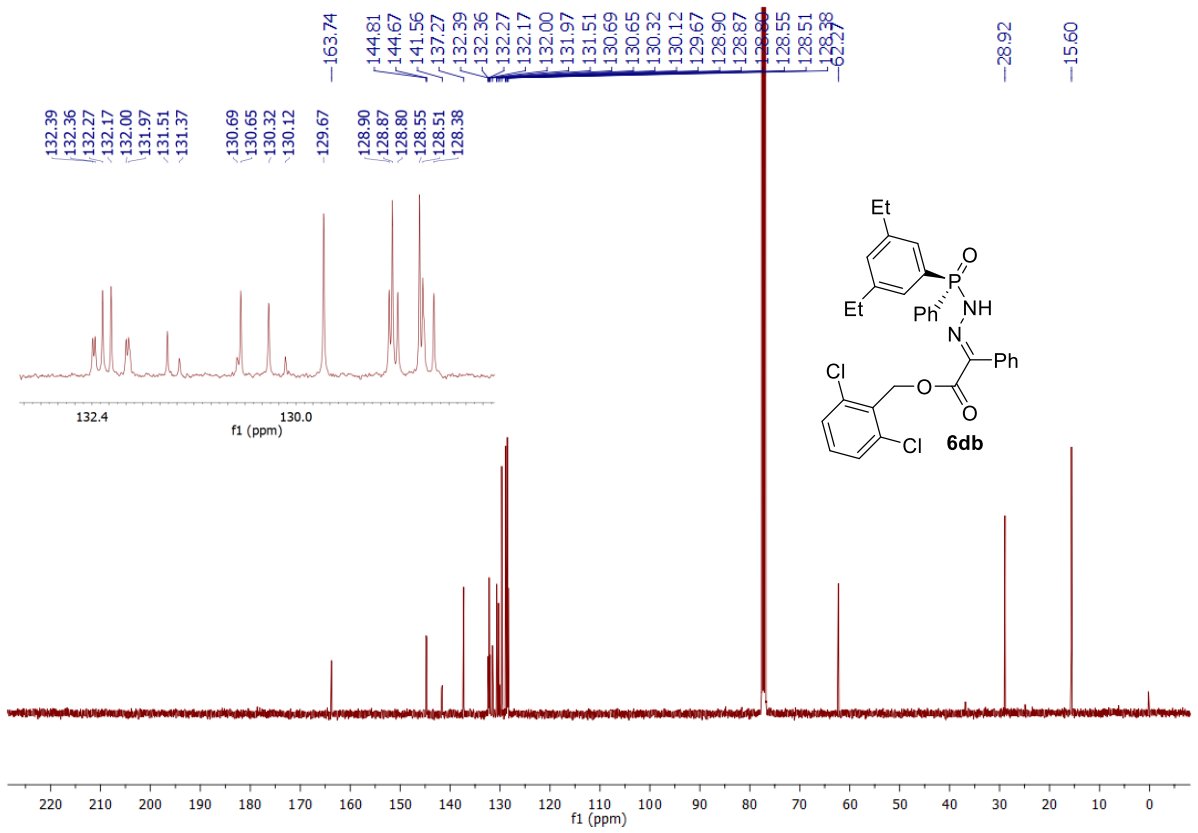

Figure S48 $^{31}P\{^{1}H\}$ NMR (162 MHz, $CDCl_3$) spectrum of **6db.**

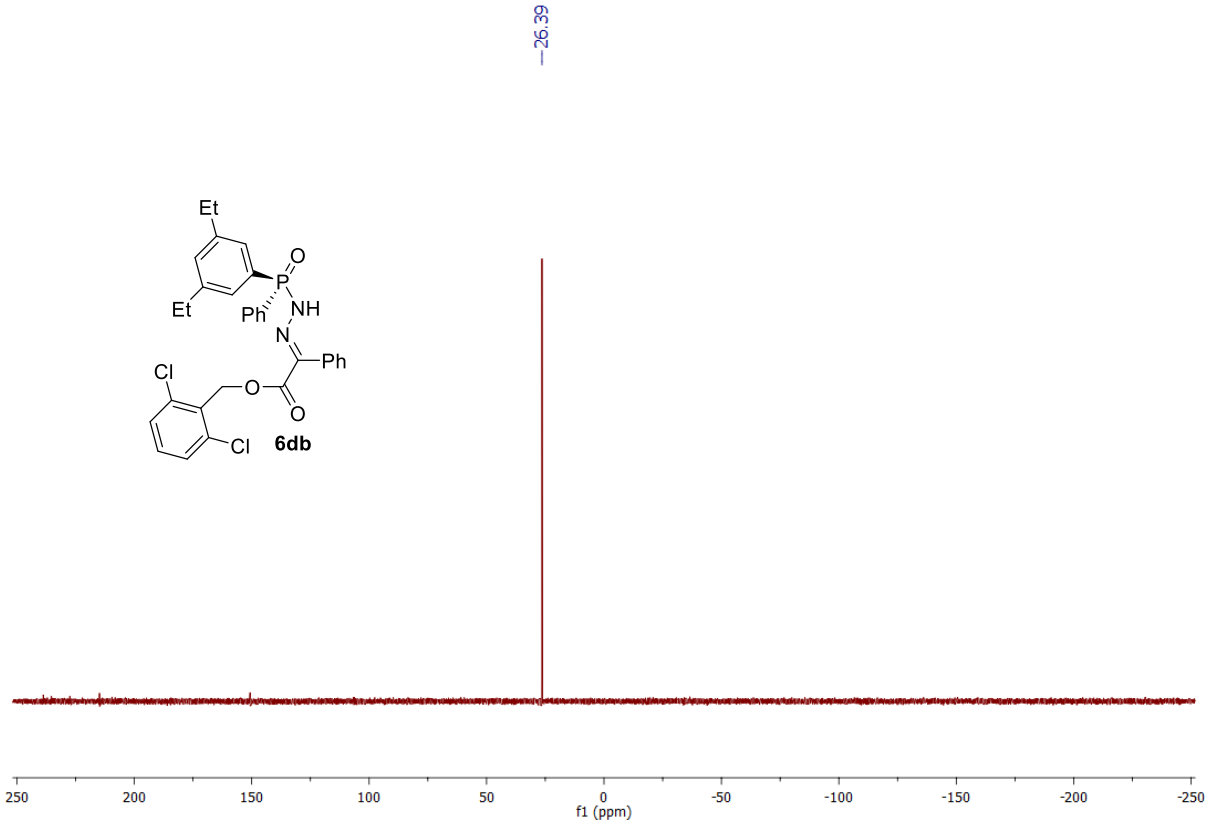

Figure S49 ^{1}H NMR (300 MHz, $CDCl_3$) spectrum of **6bc.**

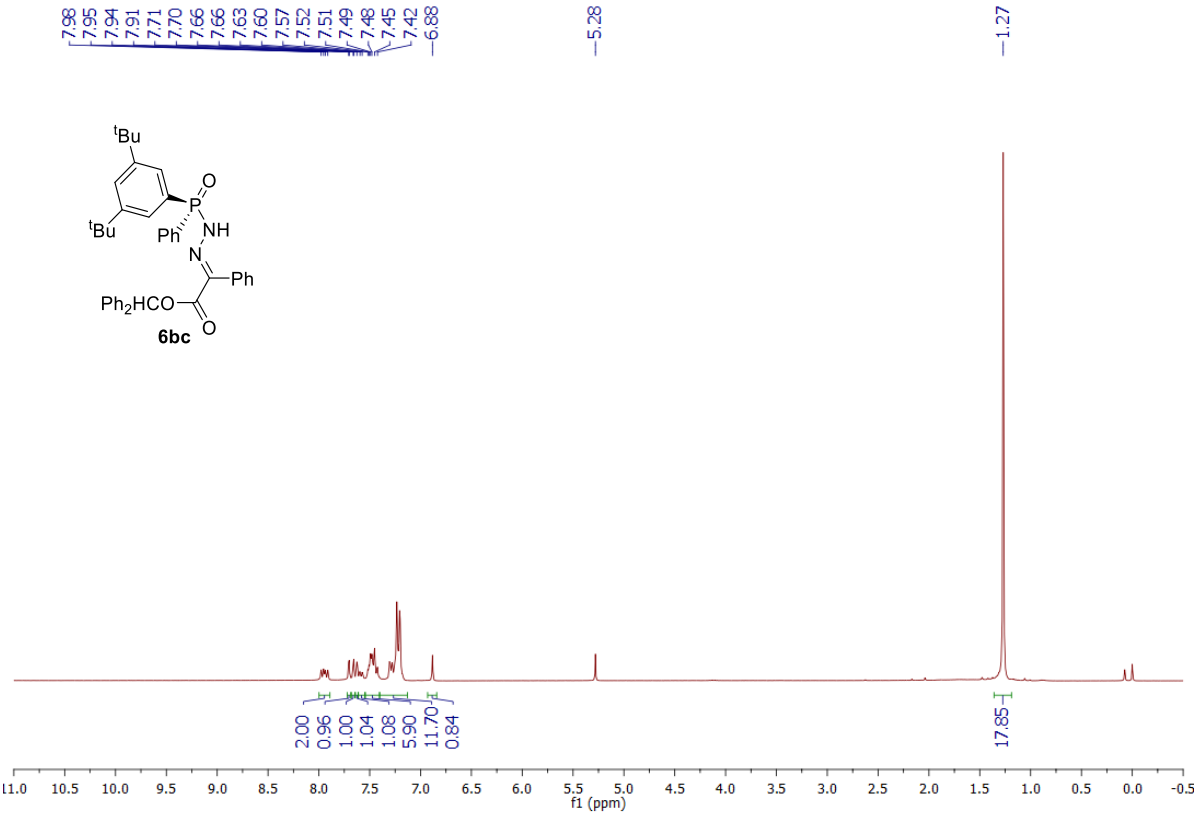

Figure S50 $^{13}C\{^{1}H\}$ NMR (101 MHz, $CDCl_3$) spectrum **6bc**.

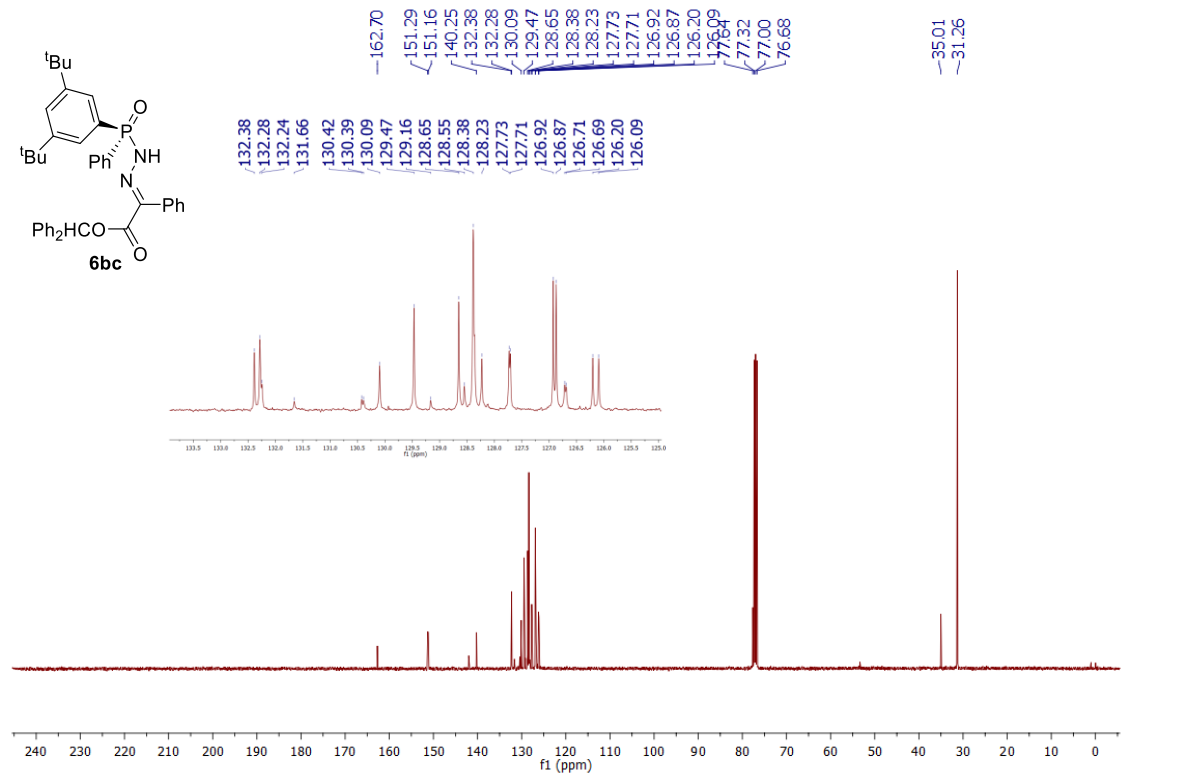

Figure S51 $^{31}P\{^{1}H\}$ NMR (162 MHz, $CDCl_3$) spectrum of **6bc.**

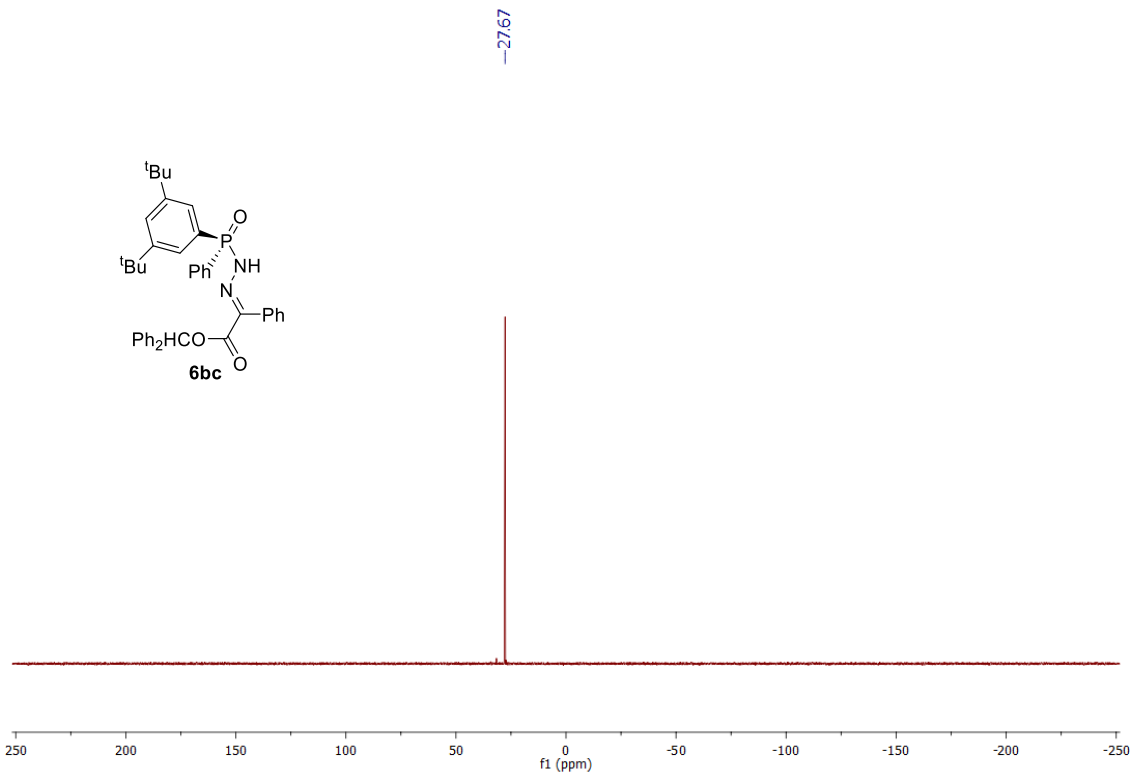

Figure S52 ^{1}H NMR (400 MHz, $CDCl_3$) spectrum of **6cc.**

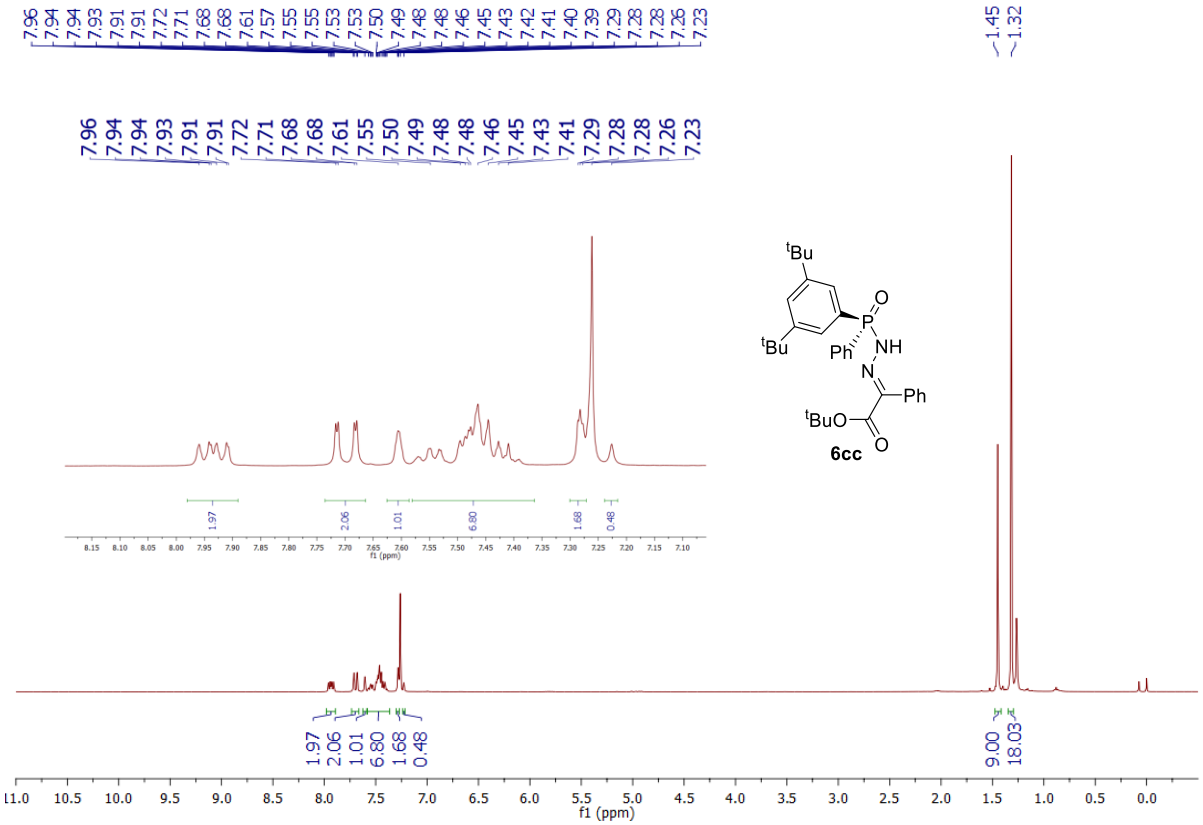

Figure S53 $^{13}C\{^{1}H\}$ NMR (101 MHz, $CDCl_3$) spectrum **6cc**.

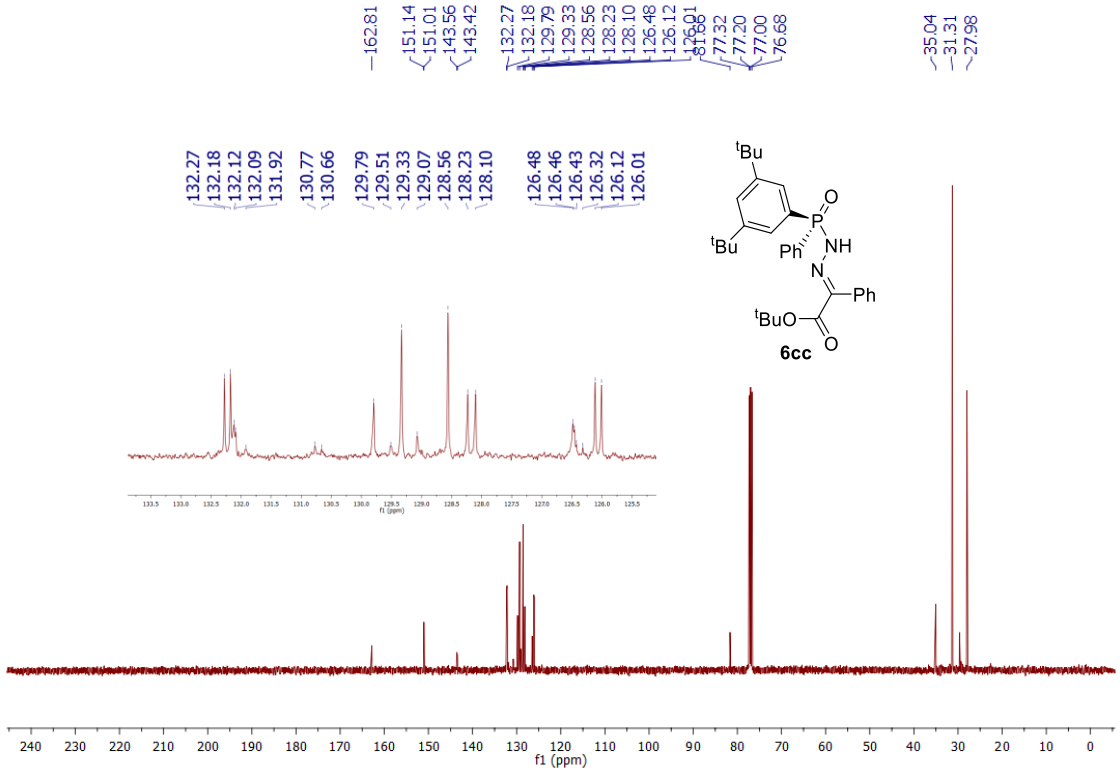

Figure S54 $^{31}P\{^{1}H\}$ NMR (162 MHz, $CDCl_3$) spectrum of **6cc.**

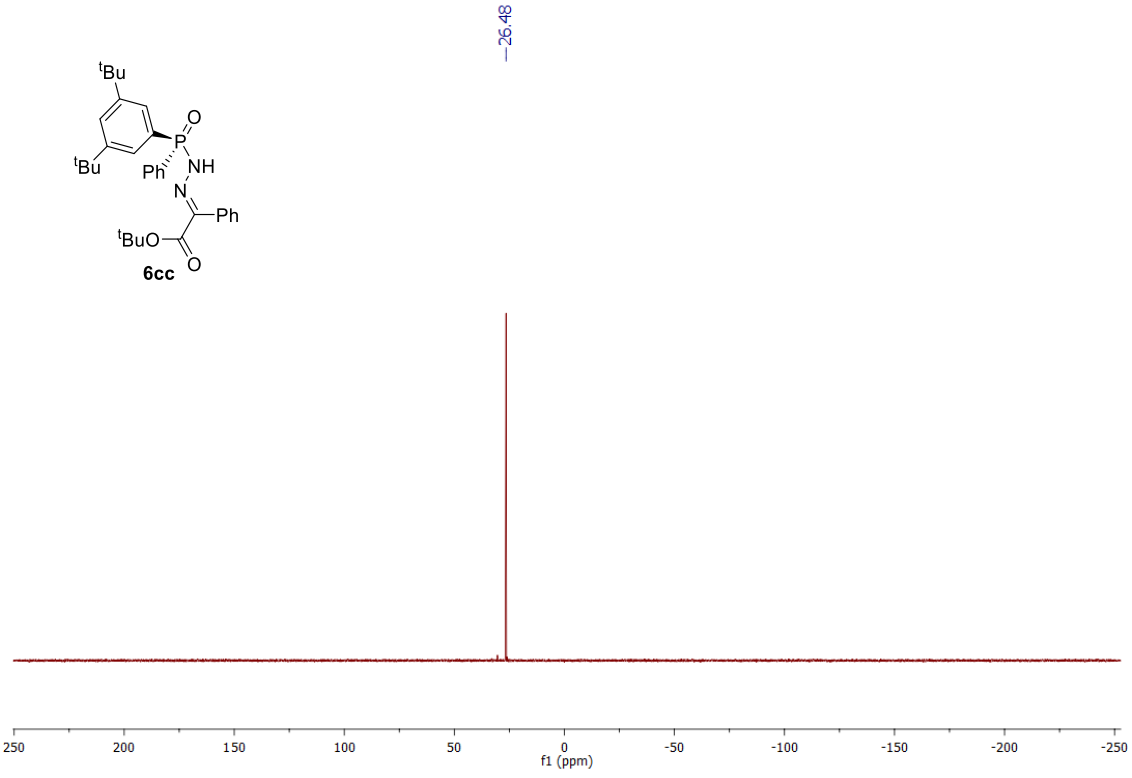

Figure S55 ^{1}H NMR (400 MHz, $CDCl_3$) spectrum of **6cd.**

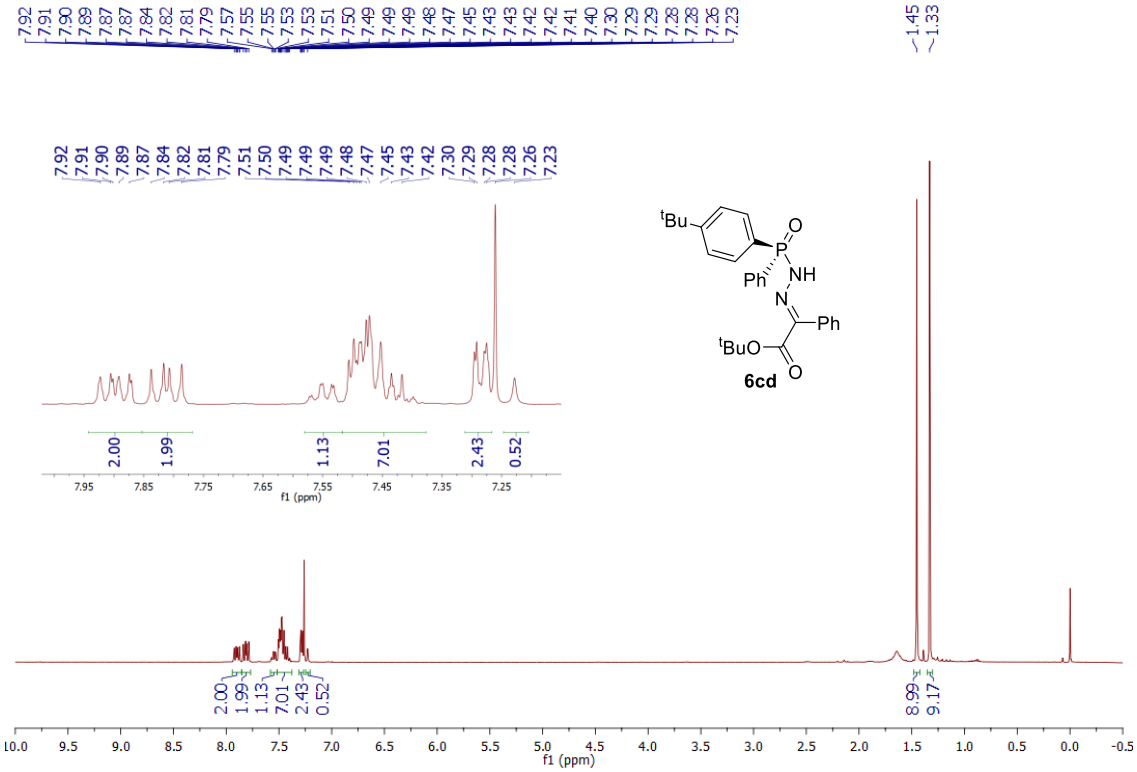

Figure S56 $^{13}C\{^{1}H\}$ NMR (101 MHz, $CDCl_3$) spectrum **6cd**.

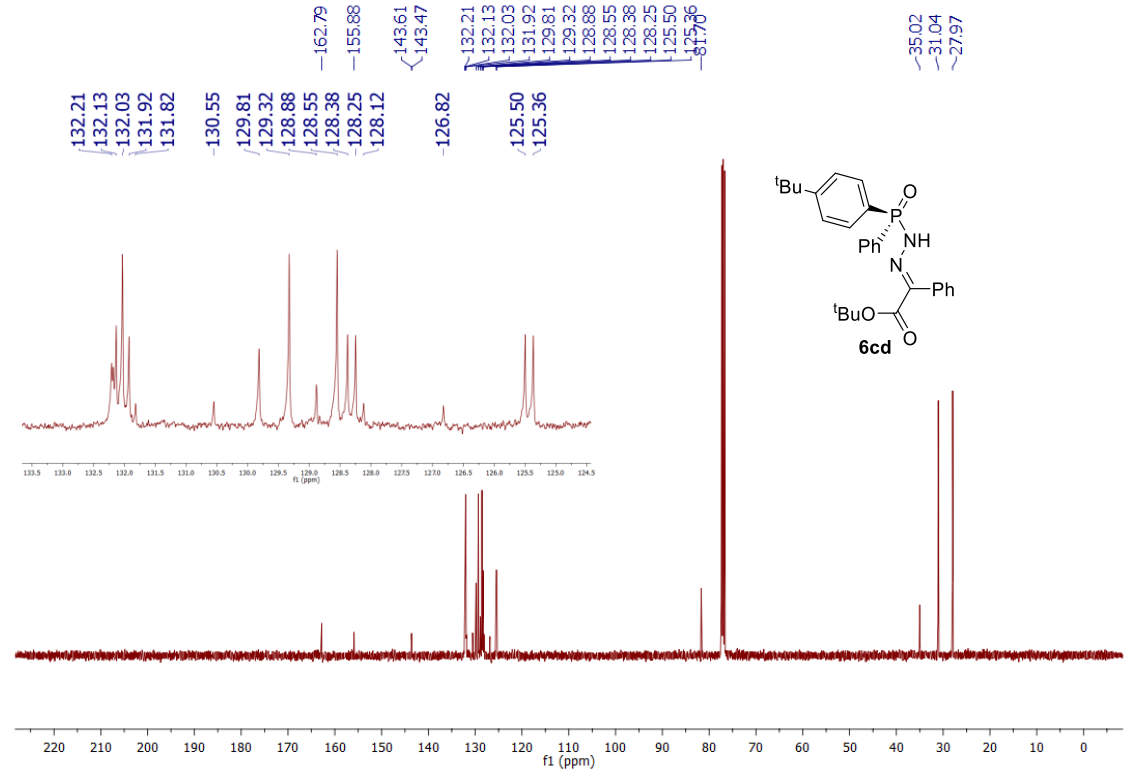

Figure S57 $^{31}P\{^{1}H\}$ NMR (162 MHz, $CDCl_3$) spectrum of **6cd.**

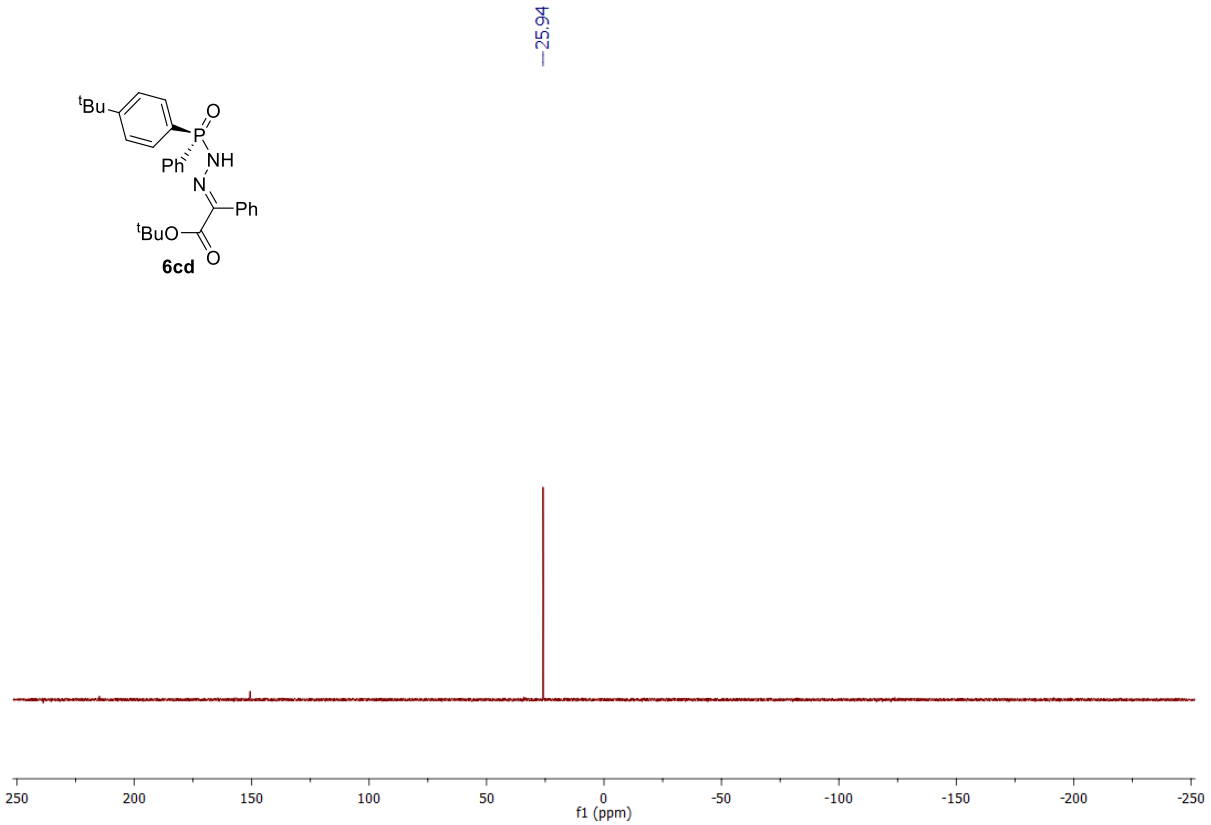

Figure S58 ^{1}H NMR (500 MHz, $CDCl_3$) spectrum of **6ce.**

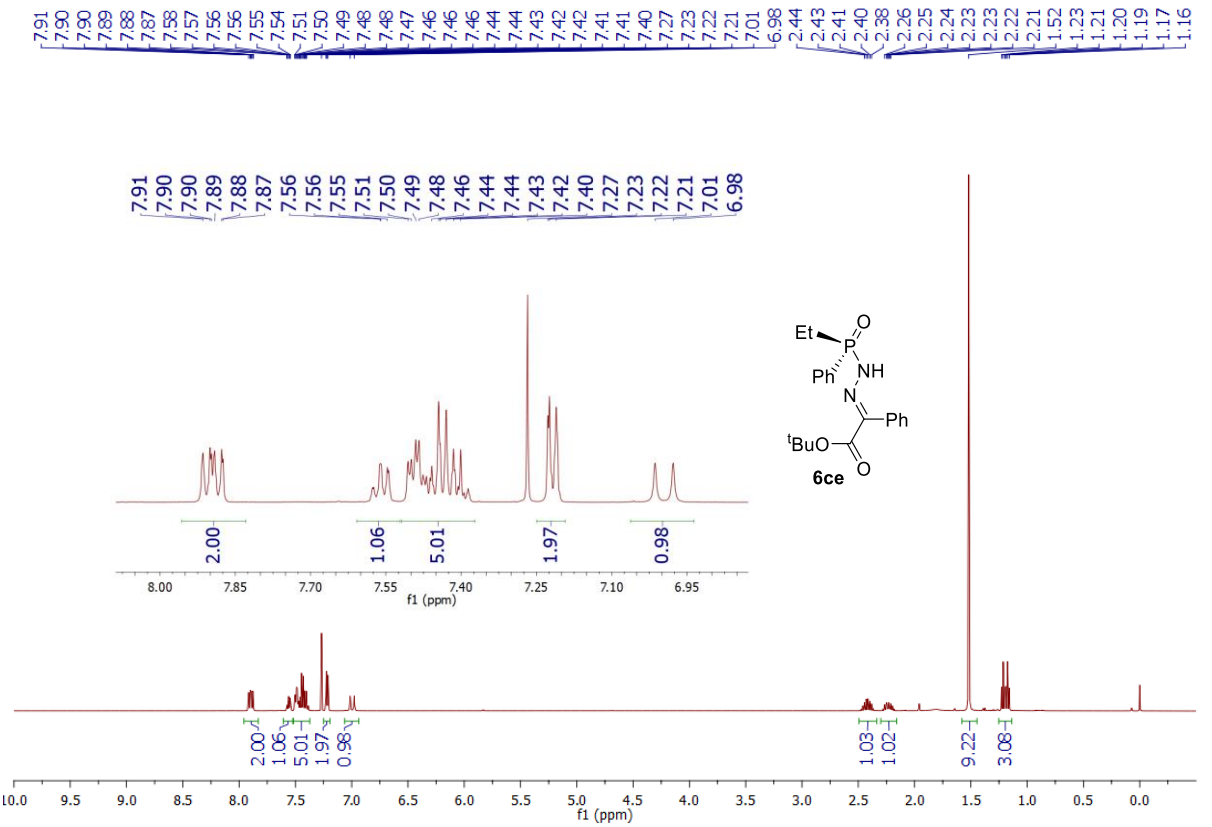

Figure S59 $^{13}C\{^{1}H\}$ NMR (126 MHz, $CDCl_3$) spectrum **6ce**.

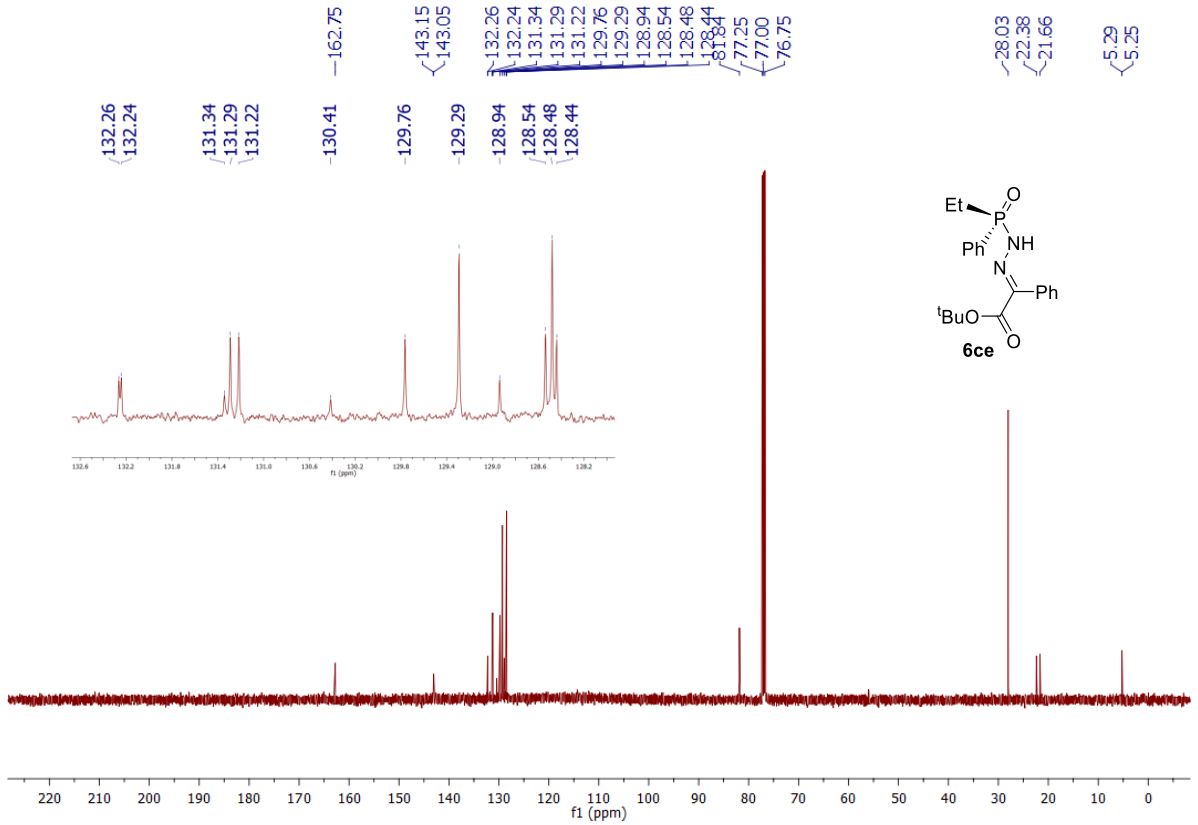

Figure S60 $^{31}P\{^{1}H\}$ NMR (162 MHz, $CDCl_3$) spectrum of **6ce.**

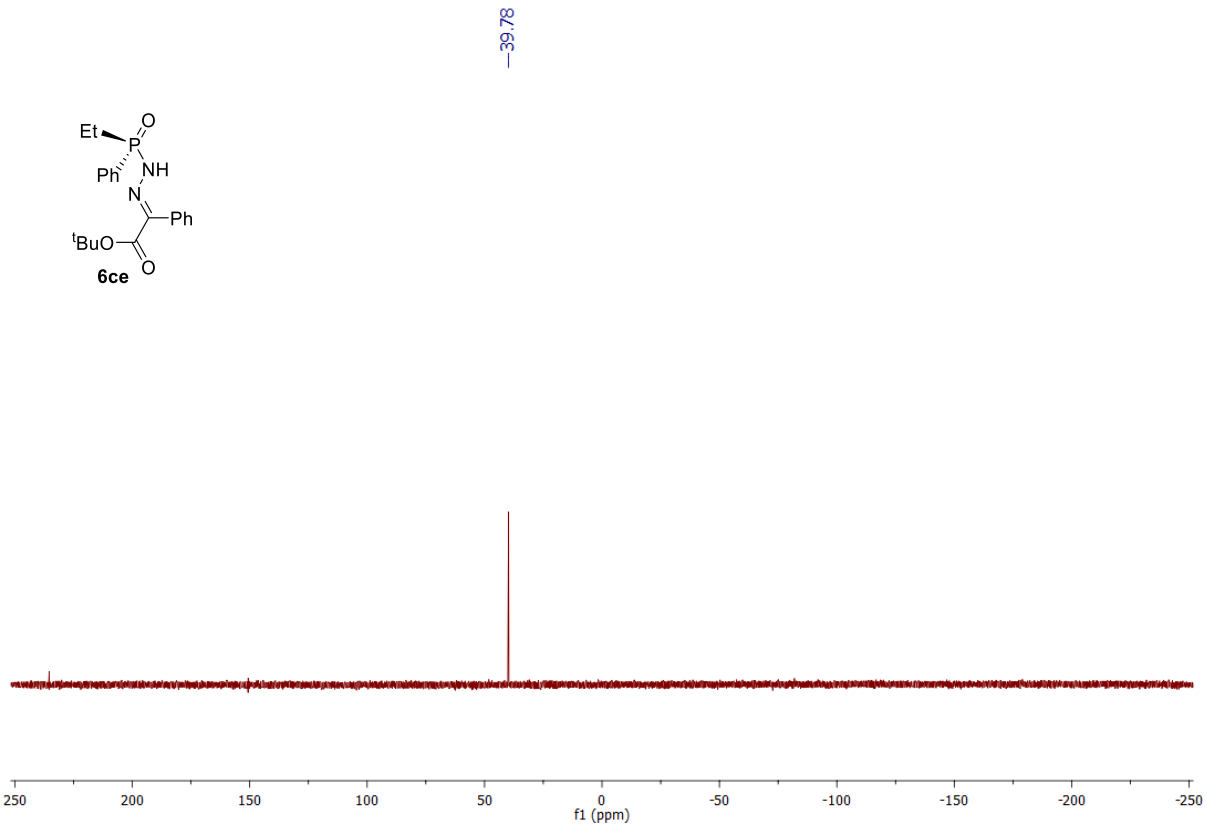

Figure S61 ^{1}H NMR (500 MHz, $CDCl_3$, mixture, *de*=68%) spectrum of (*R,S,R,R*)-**6eb** (major isomer).

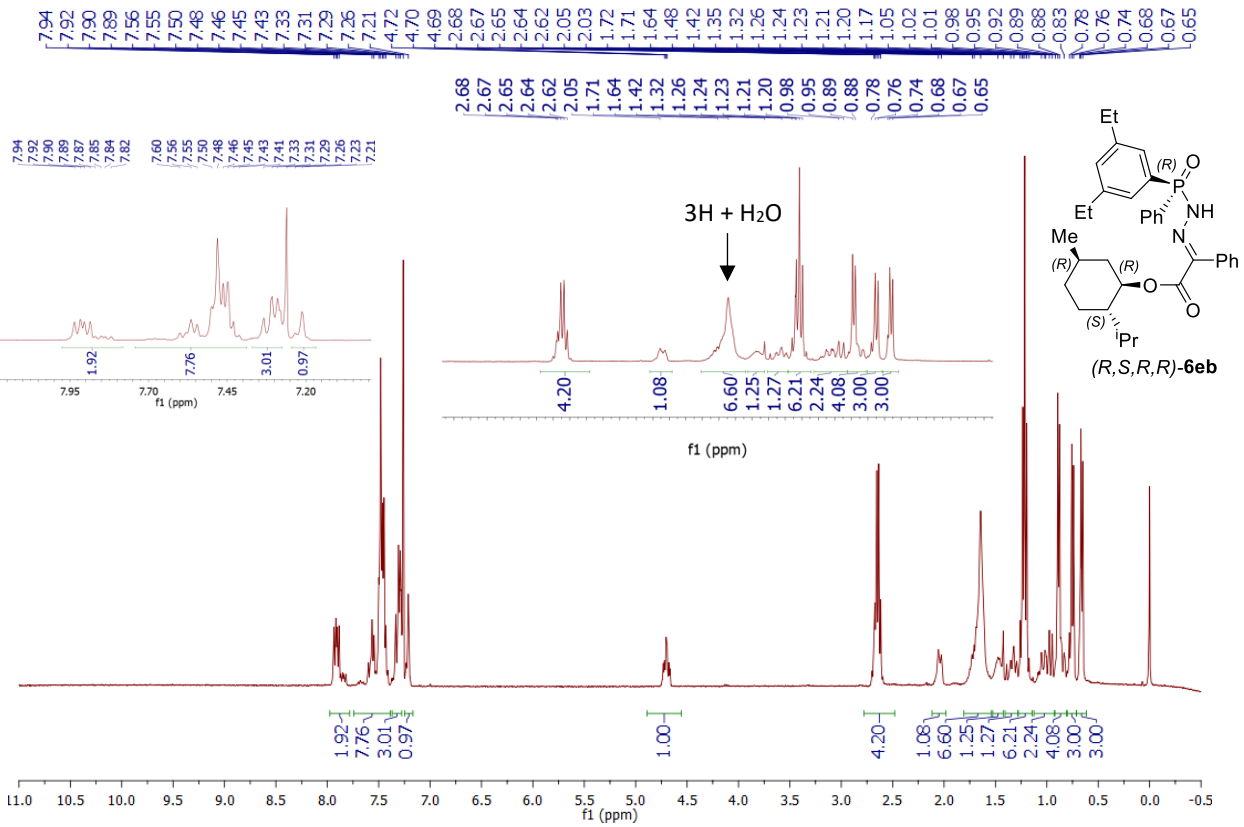

Figure S62 $^{13}C\{^{1}H\}$ NMR (126 MHz, $CDCl_3$, mixture, *de*=68%) spectrum (*R,S,R,R*)-**6eb** (major isomer).

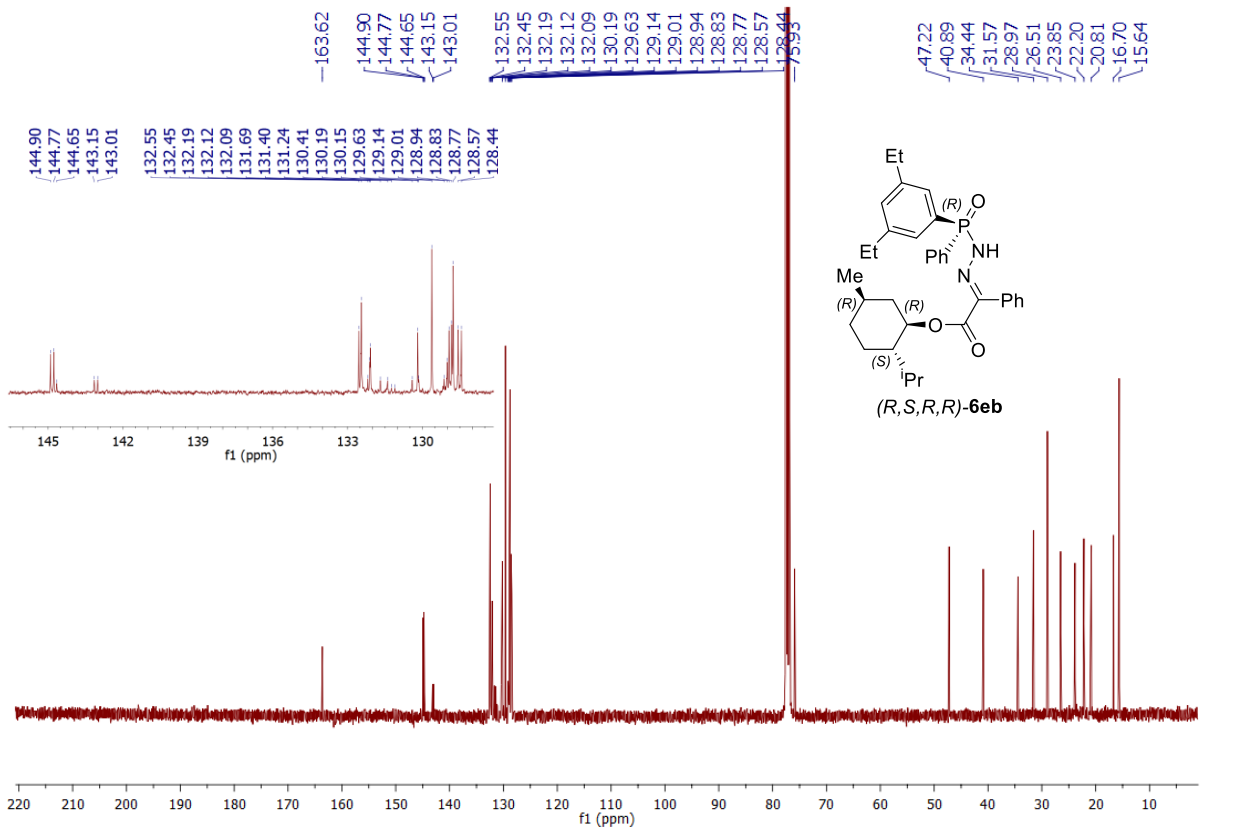

Figure S63 $^{31}P\{^{1}H\}$ NMR (162 MHz, $CDCl_3$, mixture, *de*=68%) spectrum of (*R,S,R,R*)-**6eb** (major isomer).

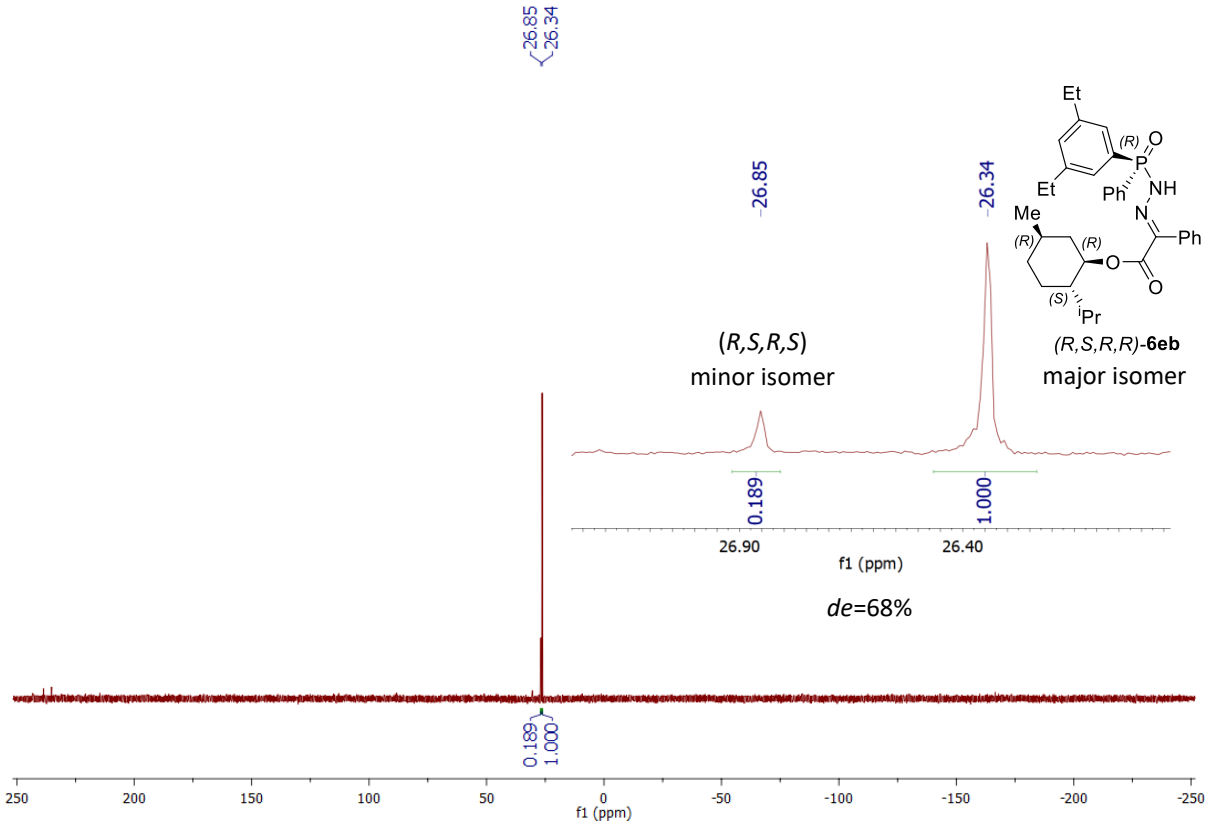

Figure S64 ^{1}H NMR (500 MHz, $CDCl_3$, mixture, *de*=70%) spectrum of (*R,S,R,S*)-**6eb** (major isomer).

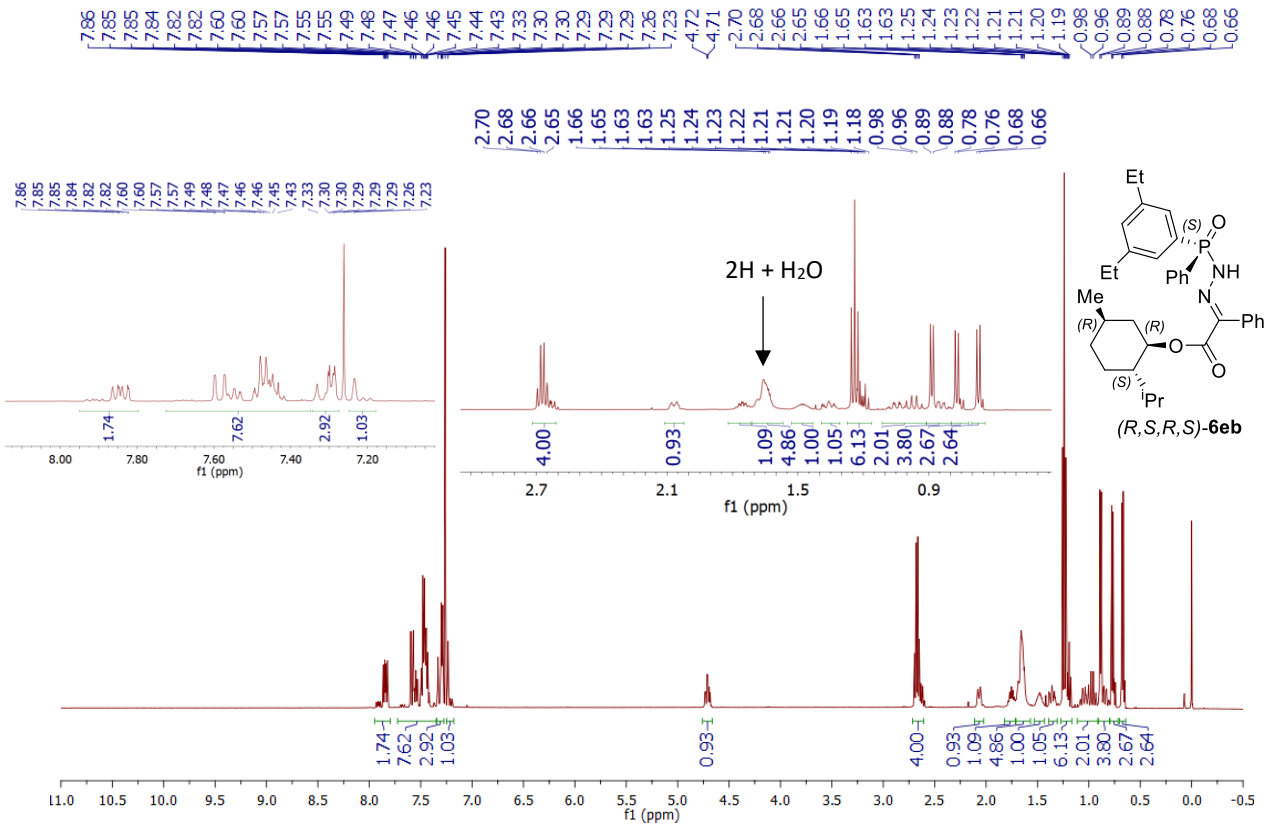

Figure S65 $^{13}C\{^{1}H\}$ NMR (126 MHz, $CDCl_3$, mixture, *de*=70%) spectrum (*R,S,R,S*)-**6eb** (major isomer).

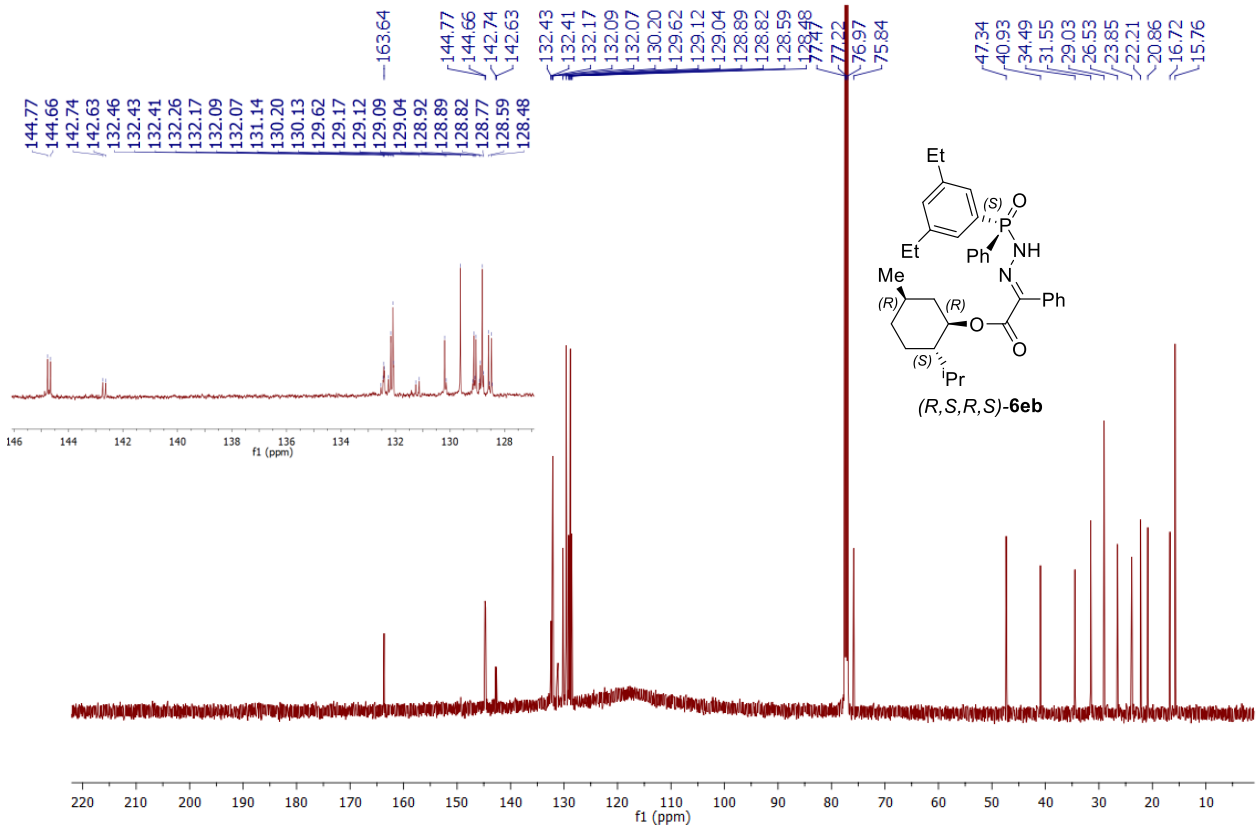

Figure S66 $^{31}P\{^{1}H\}$ NMR (162 MHz, $CDCl_3$, mixture, *de*=70%) spectrum of (*R,S,R,S*)-**6eb** (major isomer).

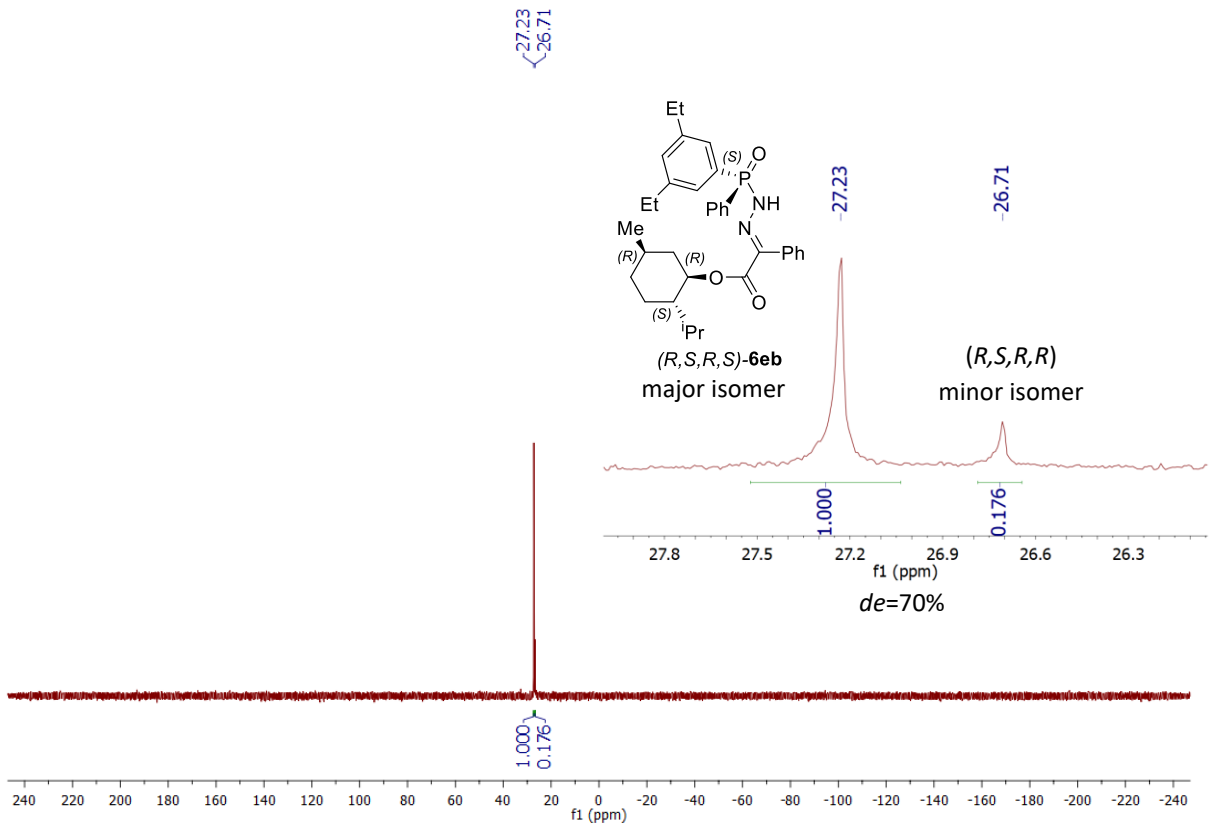

Figure S67 ^{1}H NMR (400 MHz, $CDCl_3$) spectrum of **6ai.**

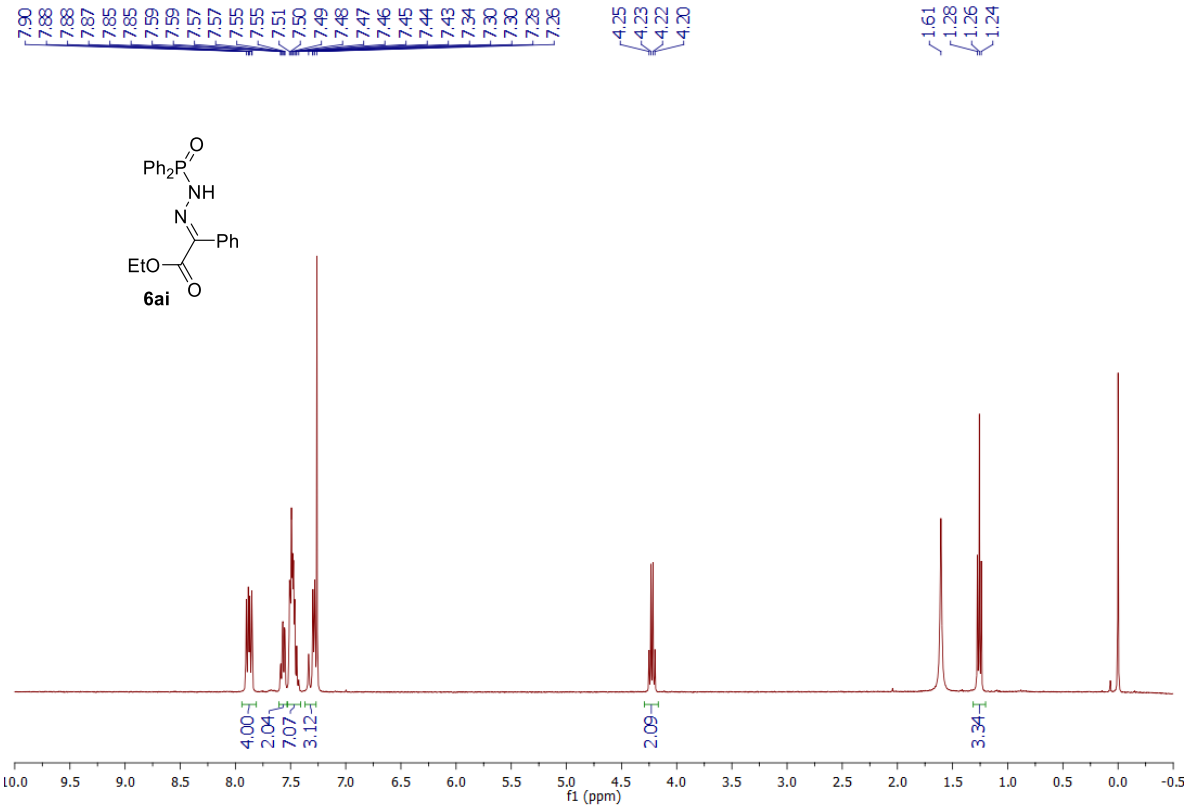

Figure S68 $^{13}C\{^{1}H\}$ NMR (126 MHz, $CDCl_3$) spectrum **6ai**.

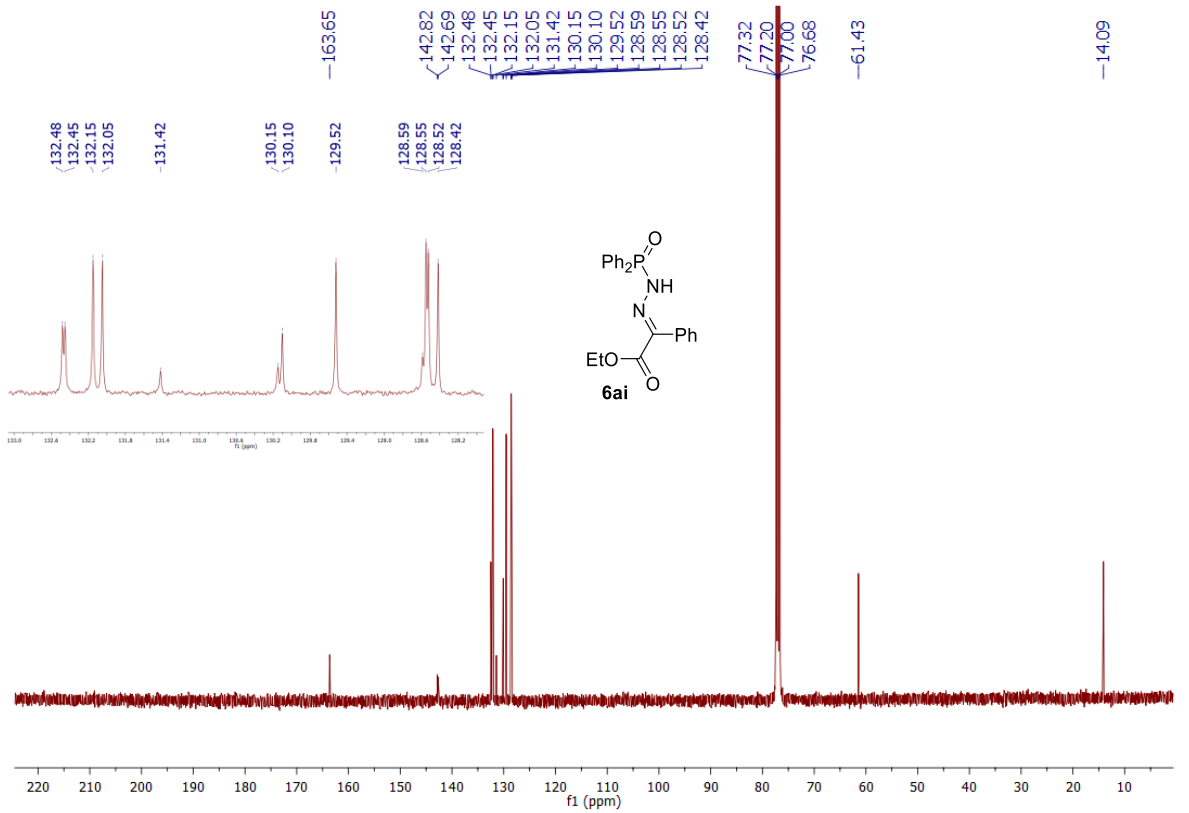

Figure S69 $^{31}P\{^{1}H\}$ NMR (162 MHz, $CDCl_3$) spectrum of **6ai.**

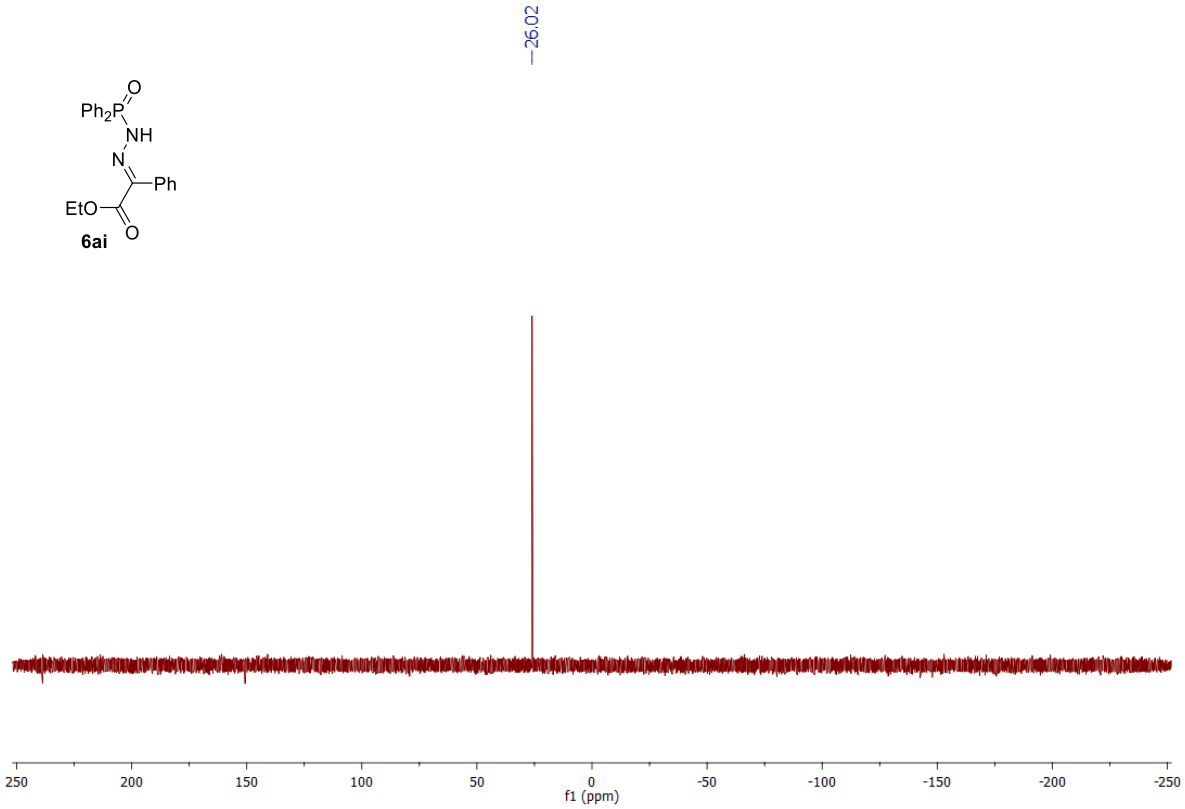

Figure S70 ^{1}H NMR (400 MHz, $CDCl_3$) spectrum of **8a.**

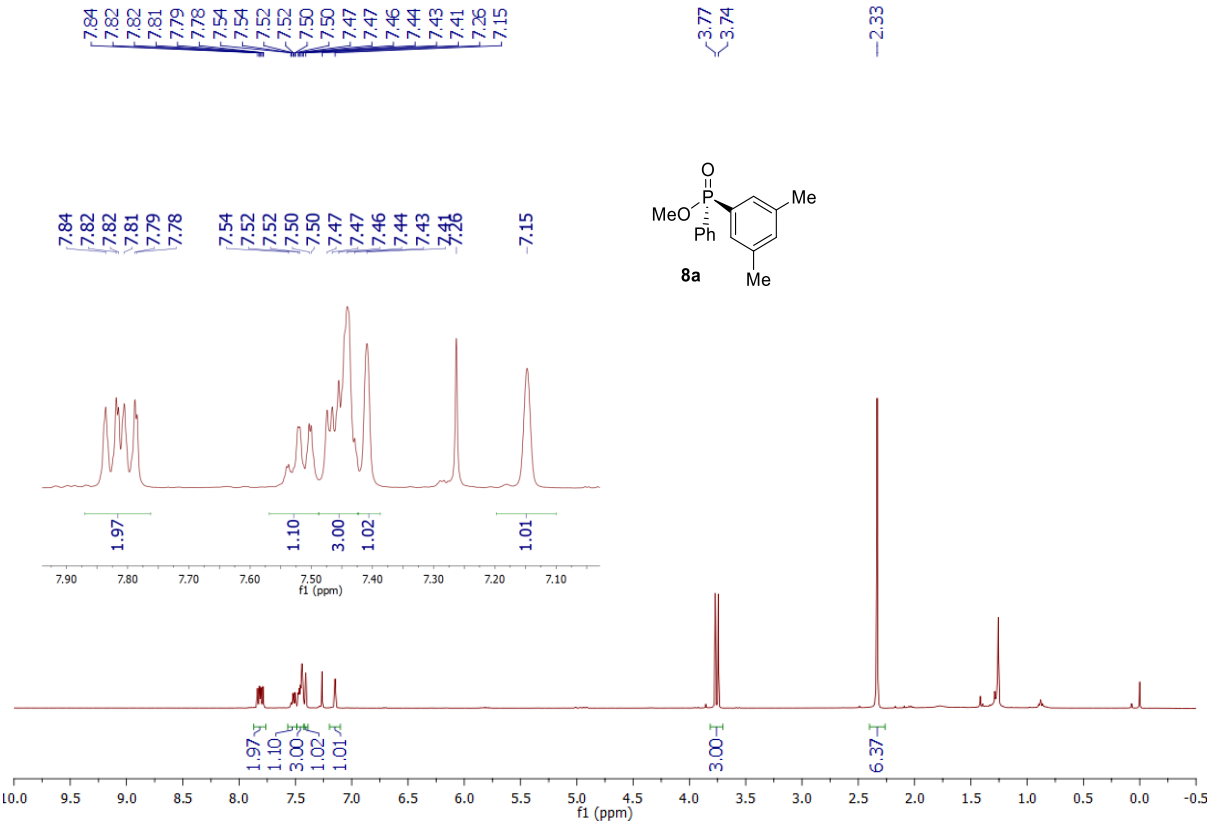

Figure S71 $^{13}C\{^{1}H\}$ NMR (101 MHz, $CDCl_3$) spectrum **8a**.

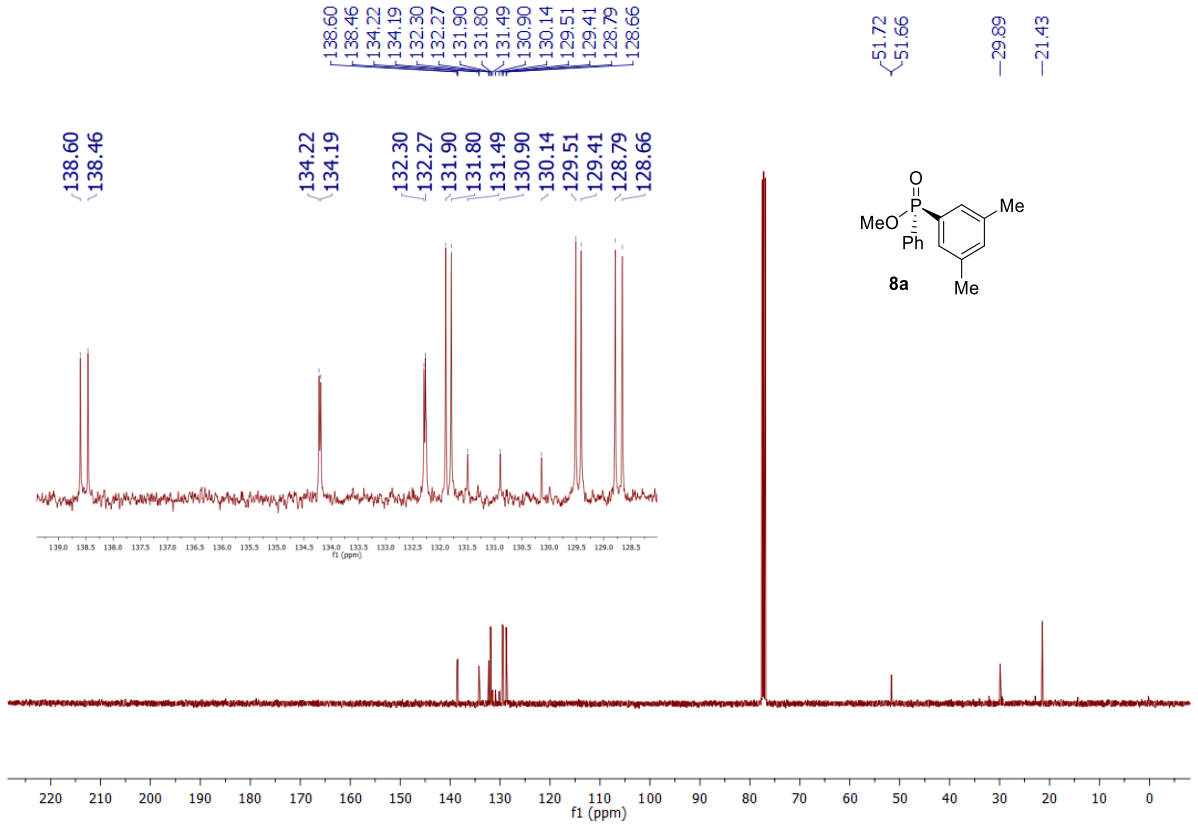

Figure S72 $^{31}P\{^{1}H\}$ NMR (162 MHz, $CDCl_3$) spectrum of **8a.**

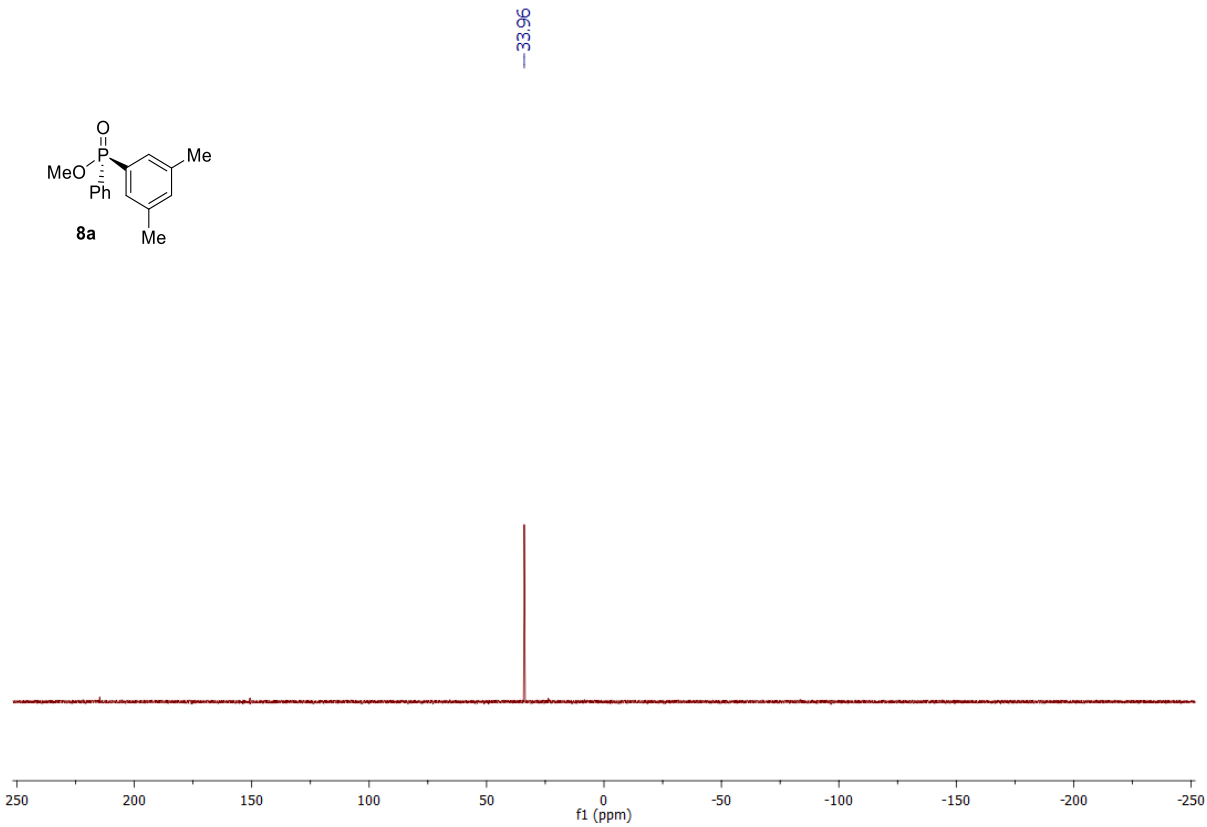

Figure S73 ^{1}H NMR (500 MHz, $CDCl_3$) spectrum of **8b.**

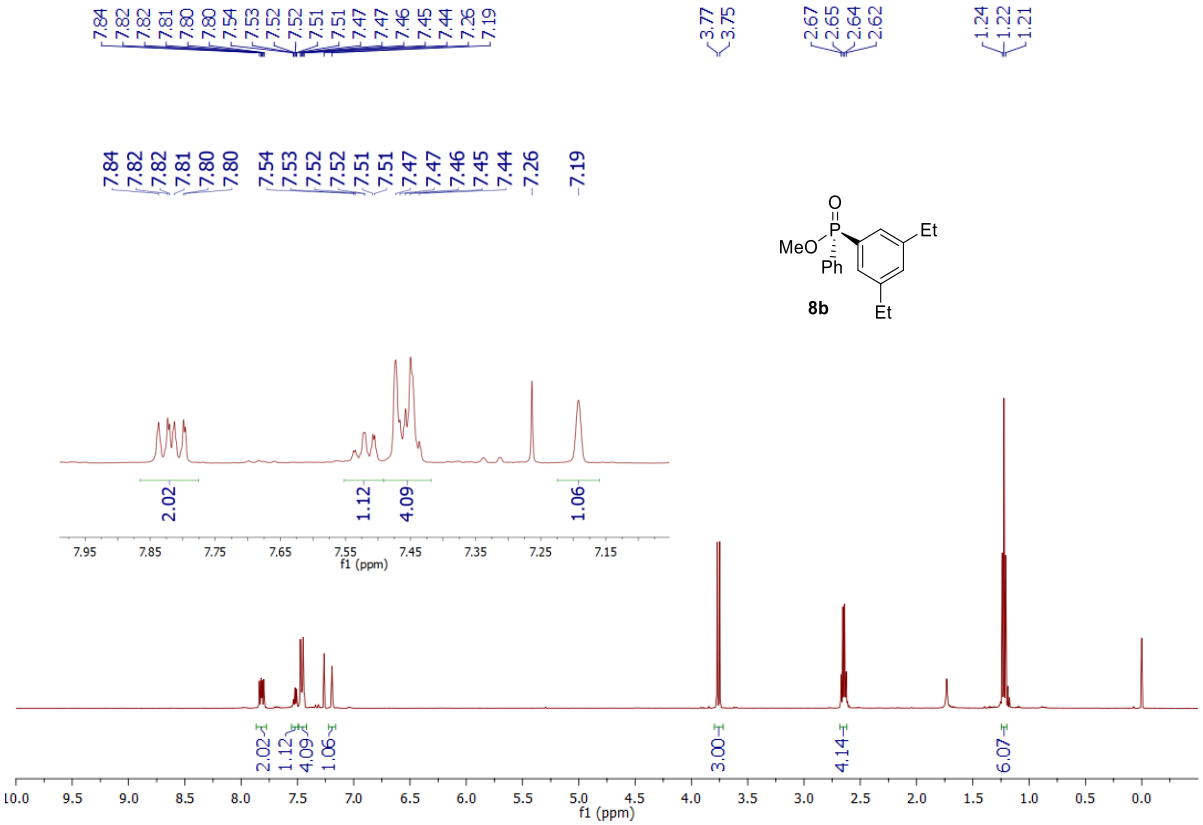

Figure S74 $^{13}C\{^{1}H\}$ NMR (126 MHz, $CDCl_3$) spectrum **8b**.

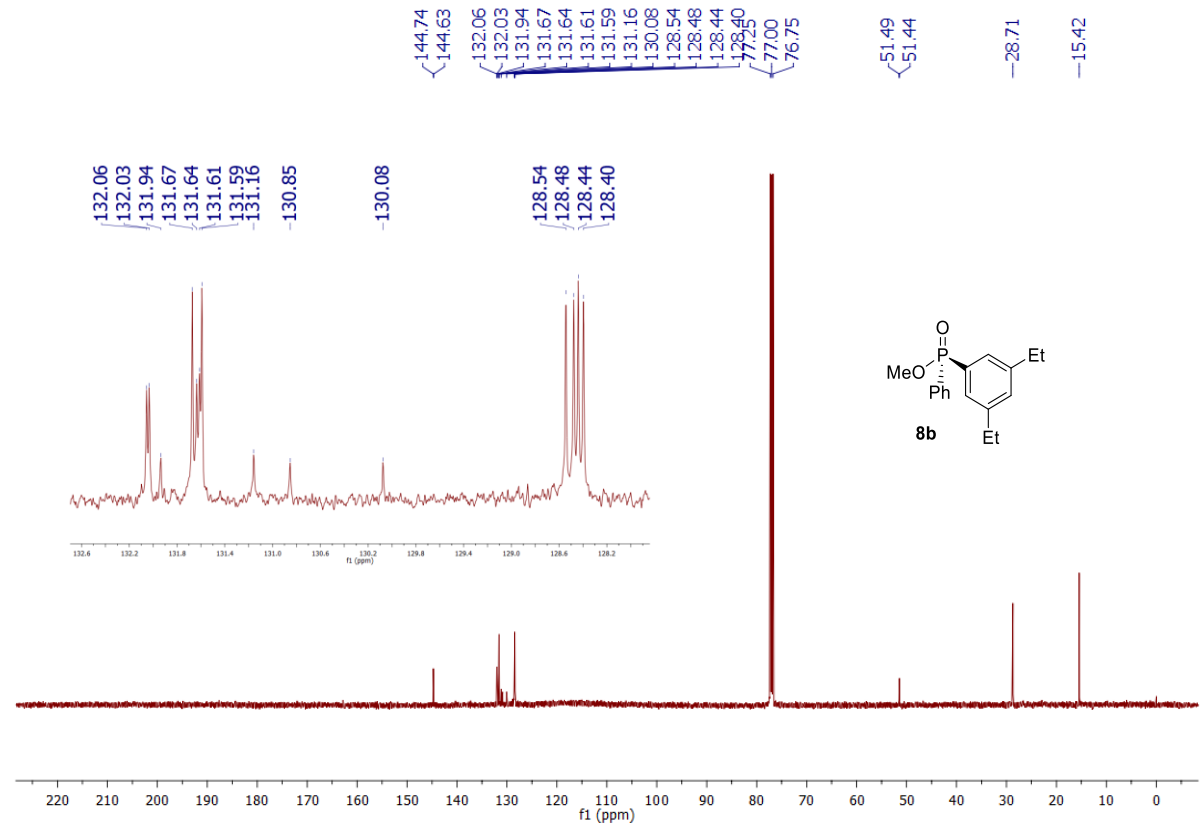

Figure S75 $^{31}P\{^{1}H\}$ NMR (162 MHz, $CDCl_3$) spectrum of **8b.**

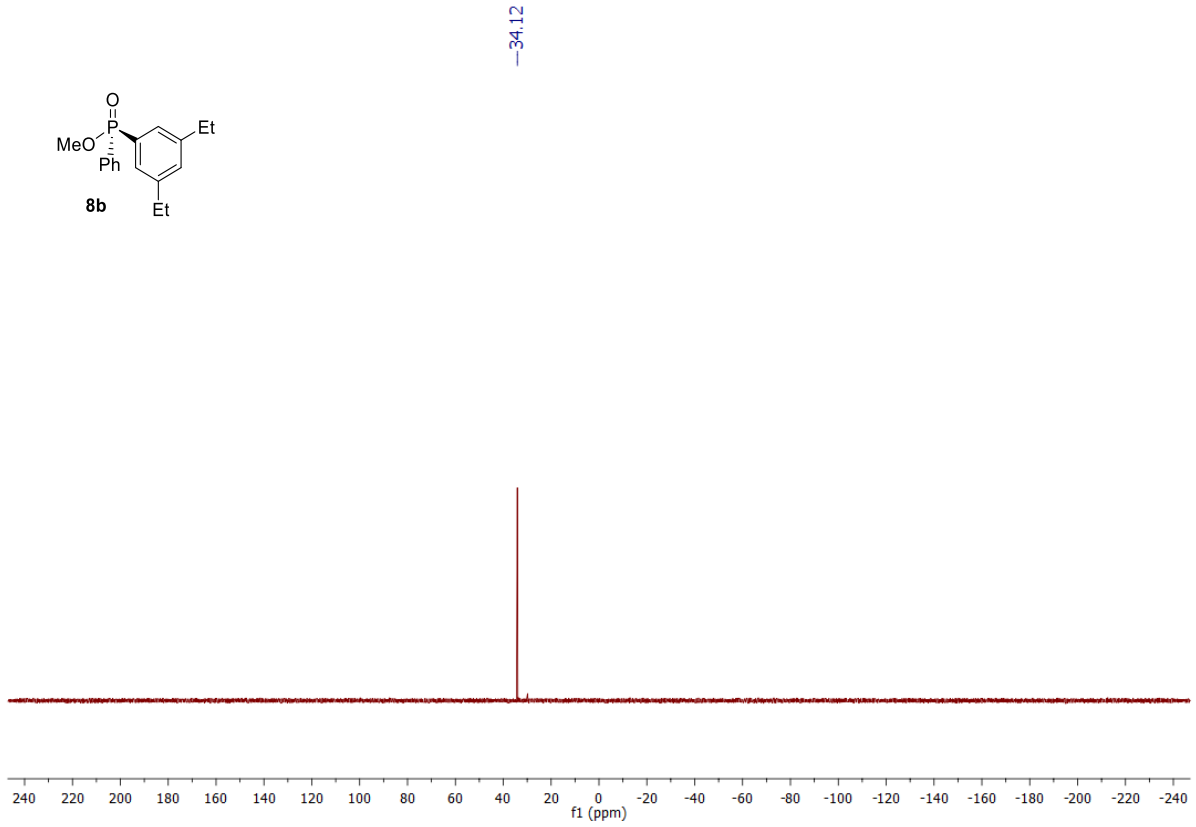

4. HPLC spectra

The enantioselectivities of the asymmetric hydrophosphination reactions were determined with Agilent 1200 Series HPLC machine fitted with specified Daicel Chiralpak columns eluted with a mixture of n-hexane/2-propanol. The samples were prepared in 2-propanol. The solvent peaks (if any) appear at the beginning of the HPLC spectra (within 6 minutes retention time).

Figure S76 Racemic HPLC spectrum of **3aa.**

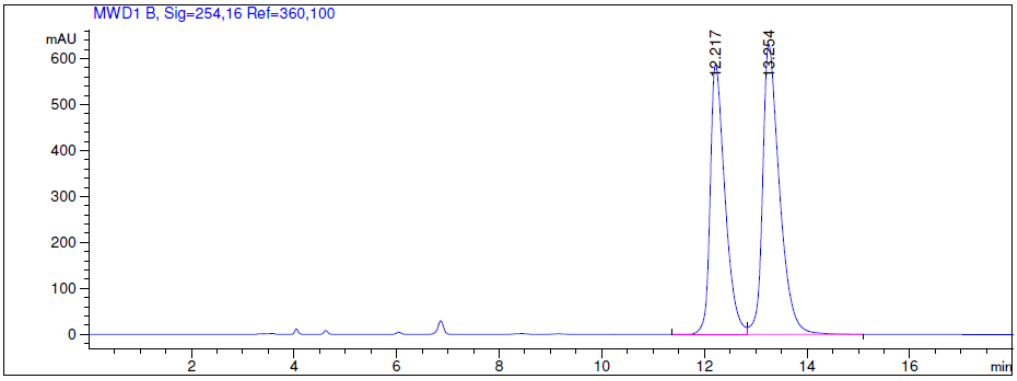

Signal 2: MWD1 B, Sig=254,16 Ref=360,100

Peak #	RetTime [min]	Type	Width [min]	Area [mAU*s]	Height [mAU]	Area %
1	12.217	BV	0.3018	1.17648e4	587.12177	45.0258
2	13.254	VB	0.3379	1.43642e4	630.23212	54.9742
Totals :				2.61290e4	1217.35388	

HPLC column: Daicel Chiralpak IE,

Temperature: 23 °C,

Flow rate: 1 ml/min.;

Eluent system: Hexane/IPA (90:10)

Figure S77 Asymmetric HPLC spectrum of **3aa.**

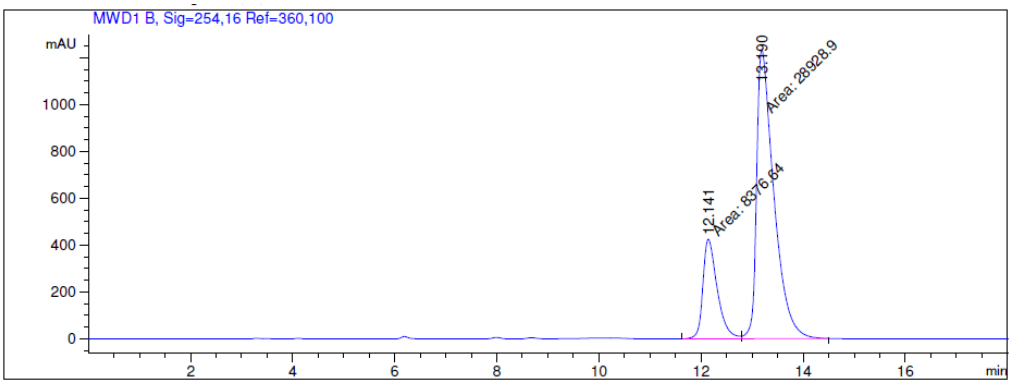

Signal 2: MWD1 B, Sig=254,16 Ref=360,100

Peak #	RetTime [min]	Type	Width [min]	Area [mAU*s]	Height [mAU]	Area %
1	12.141	MF	0.3276	8376.63672	426.15558	22.4541
2	13.190	FM	0.3903	2.89289e4	1235.31592	77.5459
Totals :				3.73055e4	1661.47150	

HPLC column: Daicel Chiralpak IE,

Temperature: 23 °C,

Flow rate: 1 ml/min.;

Eluent system: Hexane/IPA (90:10)

***ee*=55%**

Figure S78 Racemic HPLC spectrum of (±)-**6aa.**

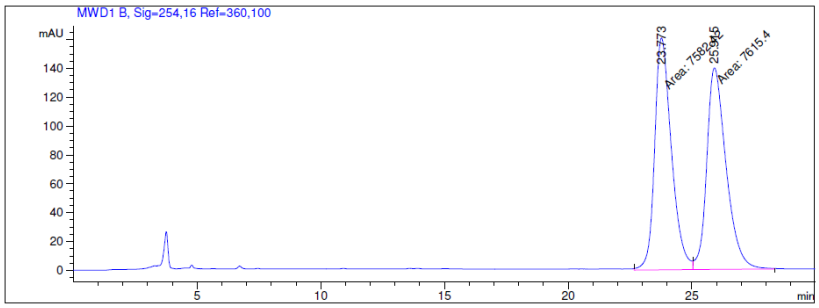


```
Signal 2: MWD1 B, Sig=254,16 Ref=360,100

Peak RetTime Type  Width     Area      Height     Area
  #   [min]        [min]   [mAU*s]     [mAU]       %
----|-------|----|-------|----------|----------|--------|
   1  23.773 MF    0.7859 7582.41943  160.80194  49.8915
   2  25.915 FM    0.9082 7615.40332  139.75473  50.1085

Totals :                  1.51978e4   300.55667
```

HPLC column: Daicel Chiralpak IE,

Temperature: 23 °C,

Flow rate: 1 ml/min.;

Eluent system: Hexane/IPA (60:40)

Figure S79 Asymmetric HPLC spectrum of *(R)*-**6aa.**

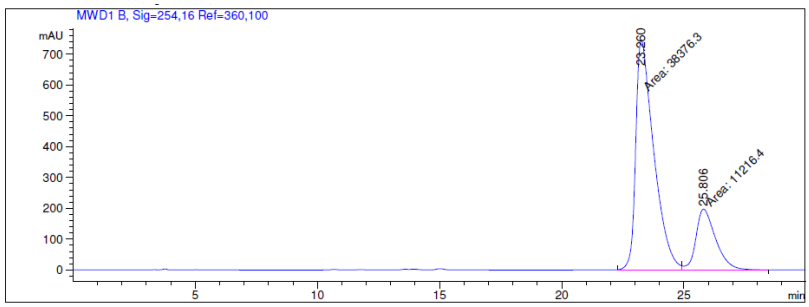


```
Signal 2: MWD1 B, Sig=254,16 Ref=360,100

Peak RetTime Type  Width     Area      Height     Area
  #   [min]        [min]   [mAU*s]     [mAU]       %
----|-------|----|-------|----------|----------|--------|
   1  23.260 MF    0.8581 3.83763e4   745.40894  77.3830
   2  25.806 FM    0.9460 1.12164e4   197.60953  22.6170

Totals :                  4.95927e4   943.01846
```

HPLC column: Daicel Chiralpak IE,

Temperature: 23 °C,

Flow rate: 1 ml/min.;

Eluent system: Hexane/IPA (60:40), ***ee*=55%**

Figure S80 Asymmetric HPLC spectrum of *(S)*-**6aa.**

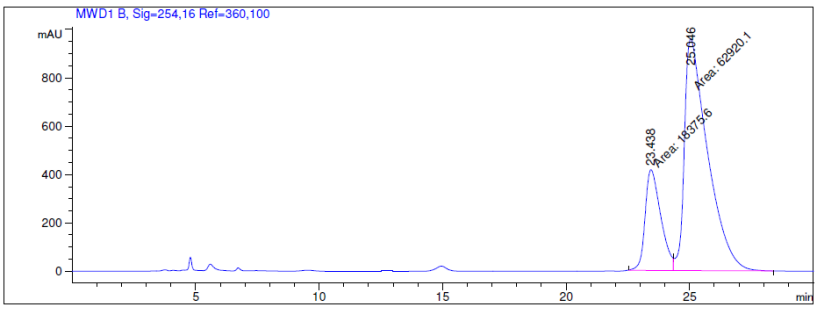


```
Signal 2: MWD1 B, Sig=254,16 Ref=360,100

Peak RetTime Type  Width     Area      Height     Area
  #   [min]        [min]   [mAU*s]     [mAU]       %
----|-------|----|-------|----------|----------|--------|
   1  23.438 MF    0.7345 1.83756e4   416.96457  22.6034
   2  25.046 FM    1.0941 6.29201e4   958.51306  77.3966

Totals :                  8.12958e4  1375.47763
```

HPLC column: Daicel Chiralpak IE,

Temperature: 23 °C,

Flow rate: 1 ml/min.;

Eluent system: Hexane/IPA (60:40), ***ee*=-55%**

(S)-**6aa** was synthesized by using *(S)*-CP (**4**) catalyst for the transformation.

Figure S81 Racemic HPLC spectrum of (±)-**6ba.**

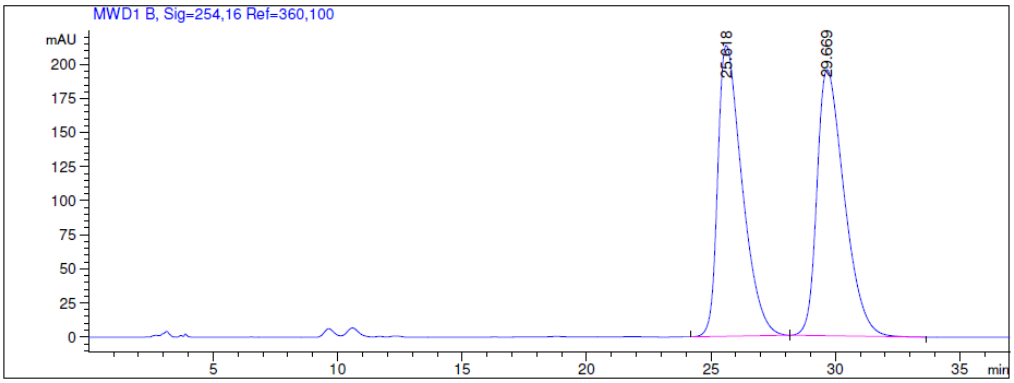

Signal 2: MWD1 B, Sig=254,16 Ref=360,100

Peak #	RetTime [min]	Type	Width [min]	Area [mAU*s]	Height [mAU]	Area %
1	25.618	BB	1.0221	1.45226e4	213.35637	49.3885
2	29.669	BB	1.1612	1.48823e4	195.25903	50.6115
Totals :				2.94049e4	408.61540	

HPLC column: Daicel Chiralpak IE,

Temperature: 23 °C,

Flow rate: 1.2 ml/min.;

Eluent system: Hexane/IPA (60:40)

Figure S82 Asymmetric HPLC spectrum of *(R)*-**6ba.**

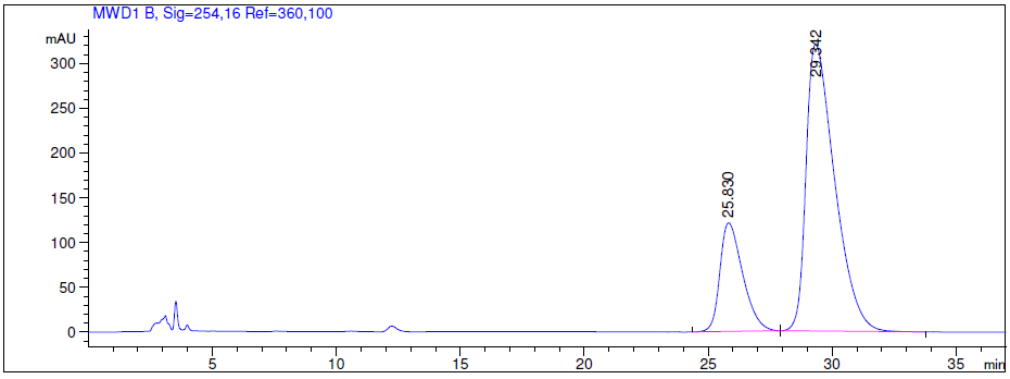

Signal 2: MWD1 B, Sig=254,16 Ref=360,100

Peak #	RetTime [min]	Type	Width [min]	Area [mAU*s]	Height [mAU]	Area %
1	25.830	BB	0.9731	7747.16357	121.29618	23.0847
2	29.342	BB	1.2283	2.58126e4	320.25778	76.9153
Totals :				3.35598e4	441.55396	

HPLC column: Daicel Chiralpak IE,

Temperature: 23 °C,

Flow rate: 1.2 ml/min.;

Eluent system: Hexane/IPA (60:40)

***ee*=54%**

Figure S83 Racemic HPLC spectrum of (±)-**6ca.**

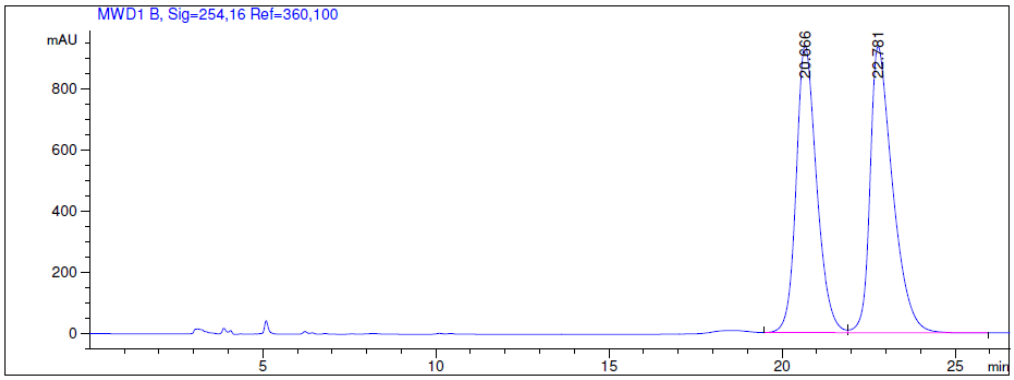

Signal 2: MWD1 B, Sig=254,16 Ref=360,100

Peak #	RetTime [min]	Type	Width [min]	Area [mAU*s]	Height [mAU]	Area %
1	20.666	BV	0.6264	3.86713e4	939.17560	47.7025
2	22.781	VB	0.6721	4.23965e4	936.62646	52.2975
Totals :				8.10678e4	1875.80206	

HPLC column: Daicel Chiralpak IE,

Temperature: 23 °C,

Flow rate: 1 ml/min.;

Eluent system: Hexane/IPA (70:30)

Figure S84 Asymmetric HPLC spectrum of *(R)*-**6ca.**

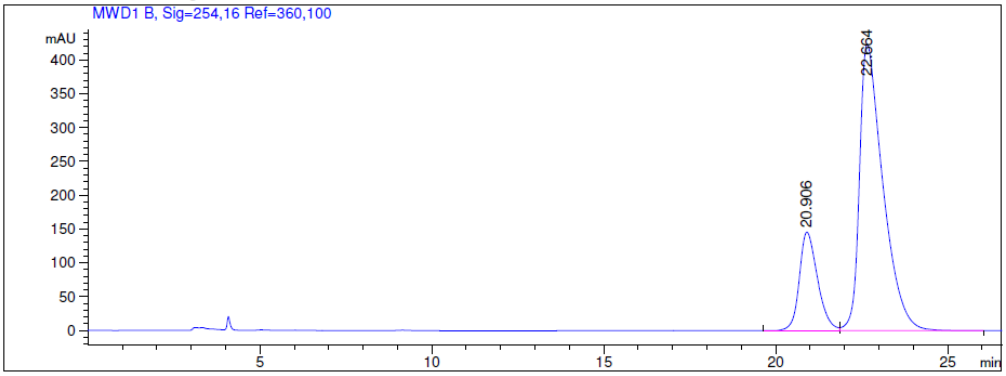

Signal 2: MWD1 B, Sig=254,16 Ref=360,100

Peak #	RetTime [min]	Type	Width [min]	Area [mAU*s]	Height [mAU]	Area %
1	20.906	BV	0.5628	5405.74219	145.71727	21.2099
2	22.664	VB	0.6971	2.00812e4	423.53925	78.7901
Totals :				2.54869e4	569.25652	

HPLC column: Daicel Chiralpak IE,

Temperature: 23 °C,

Flow rate: 1 ml/min.;

Eluent system: Hexane/IPA (70:30)

***ee*=58%**

Figure S85 Racemic HPLC spectrum of (±)-**6cb.**

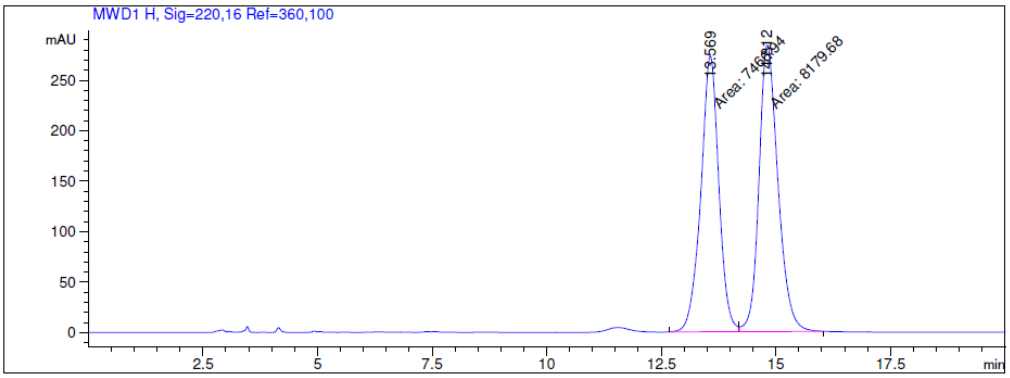


```
Signal 8: MWD1 H, Sig=220,16 Ref=360,100

Peak RetTime Type  Width     Area      Height     Area
  #   [min]        [min]   [mAU*s]     [mAU]       %
----|-------|----|-------|----------|----------|--------|
   1  13.569 MF    0.4553 7466.93555  273.31036  47.7224
   2  14.812 FM    0.4806 8179.67773  283.66522  52.2776

Totals :                 1.56466e4   556.97559
```

HPLC column: Daicel Chiralpak ID,

Temperature: 23 °C,

Flow rate: 1 ml/min.;

Eluent system: Hexane/IPA (85:15)

Figure S86 Asymmetric HPLC spectrum of *(R)*-**6cb.**

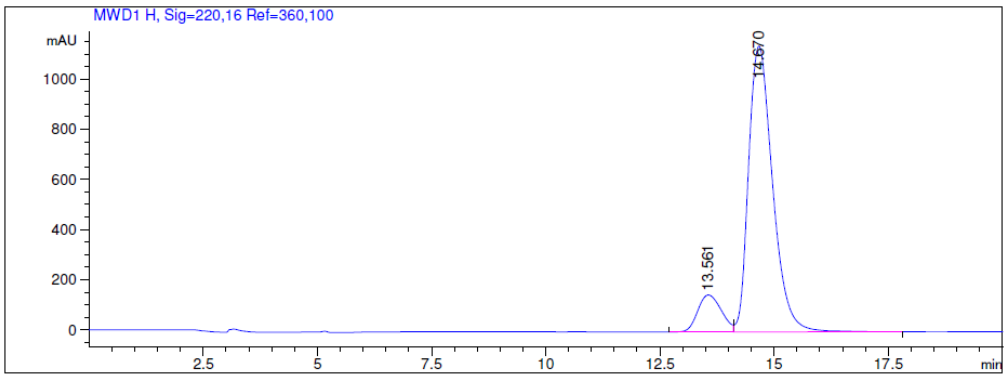


```
Signal 8: MWD1 H, Sig=220,16 Ref=360,100

Peak RetTime Type  Width     Area      Height     Area
  #   [min]        [min]   [mAU*s]     [mAU]       %
----|-------|----|-------|----------|----------|--------|
   1  13.561 BV    0.5744 5244.36475  146.94856  11.1906
   2  14.670 VB    0.5666 4.16198e4  1138.20630  88.8094

Totals :                 4.68641e4  1285.15486
```

HPLC column: Daicel Chiralpak ID,

Temperature: 23 °C,

Flow rate: 1 ml/min.;

Eluent system: Hexane/IPA (85:15)

***ee*=78%**

Figure S87 Racemic HPLC spectrum of (±)-**6db.**

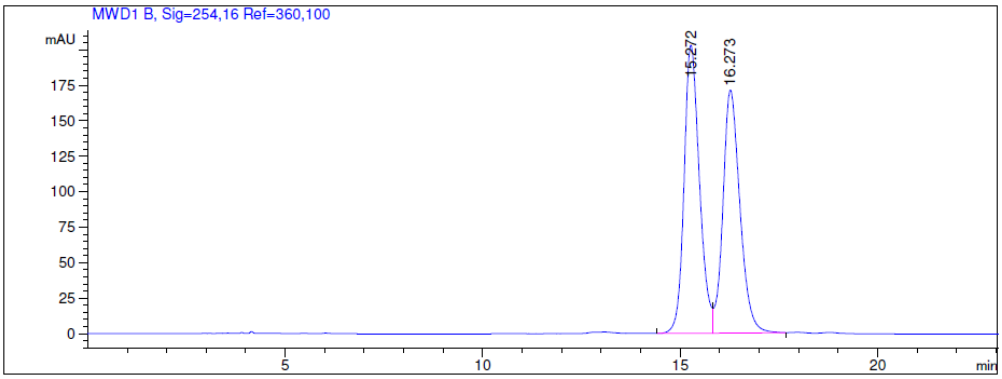

Signal 2: MWD1 B, Sig=254,16 Ref=360,100

Peak #	RetTime [min]	Type	Width [min]	Area [mAU*s]	Height [mAU]	Area %
1	15.272	BV	0.4117	5494.72266	203.07724	51.7554
2	16.273	VB	0.4529	5121.99072	171.25340	48.2446
Totals :				1.06167e4	374.33064	

HPLC column: Daicel Chiralpak ID,

Temperature: 23 °C,

Flow rate: 1 ml/min.;

Eluent system: Hexane/IPA (70:30)

Figure S88 Asymmetric HPLC spectrum of (*R*)-**6db.**

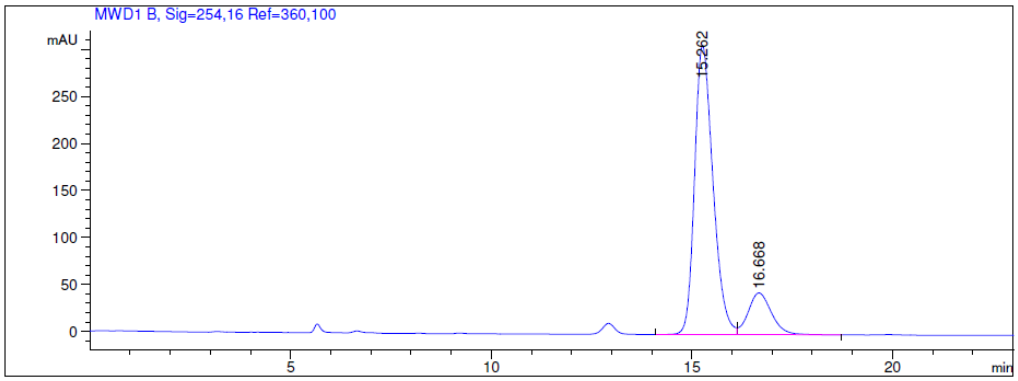

Signal 2: MWD1 B, Sig=254,16 Ref=360,100

Peak #	RetTime [min]	Type	Width [min]	Area [mAU*s]	Height [mAU]	Area %
1	15.262	BV	0.4900	9807.07129	307.53119	84.5465
2	16.668	VB	0.6190	1792.54114	44.40107	15.4535
Totals :				1.15996e4	351.93226	

HPLC column: Daicel Chiralpak ID,

Temperature: 23 °C,

Flow rate: 1 ml/min.;

Eluent system: Hexane/IPA (70:30)

***ee*=69%**

Figure S89 Racemic HPLC spectrum of (±)-**6bc.**

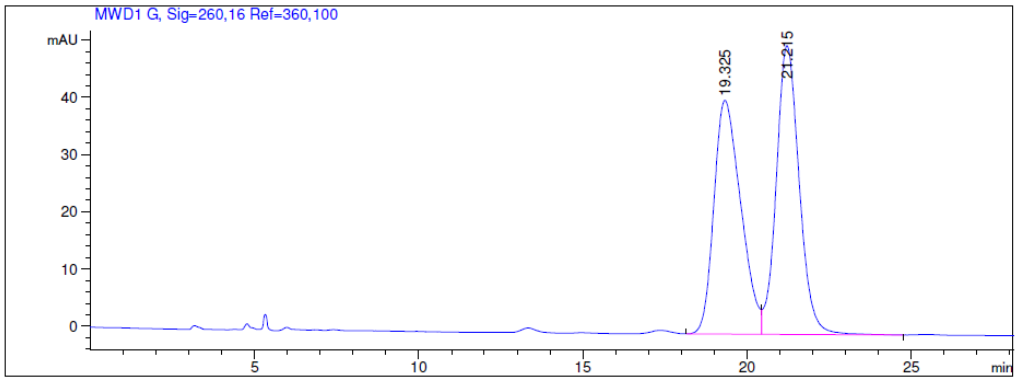

Signal 7: MWD1 G, Sig=260,16 Ref=360,100

Peak #	RetTime [min]	Type	Width [min]	Area [mAU*s]	Height [mAU]	Area %
1	19.325	BV	0.8558	2324.90698	40.86178	48.6929
2	21.215	VB	0.7443	2449.72754	50.46722	51.3071
Totals :				4774.63452	91.32900	

HPLC column: Daicel Chiralpak ID,

Temperature: 23 °C,

Flow rate: 1 ml/min.;

Eluent system: Hexane/IPA (85:15)

Figure S90 Asymmetric HPLC spectrum of *(R)*-**6bc.**

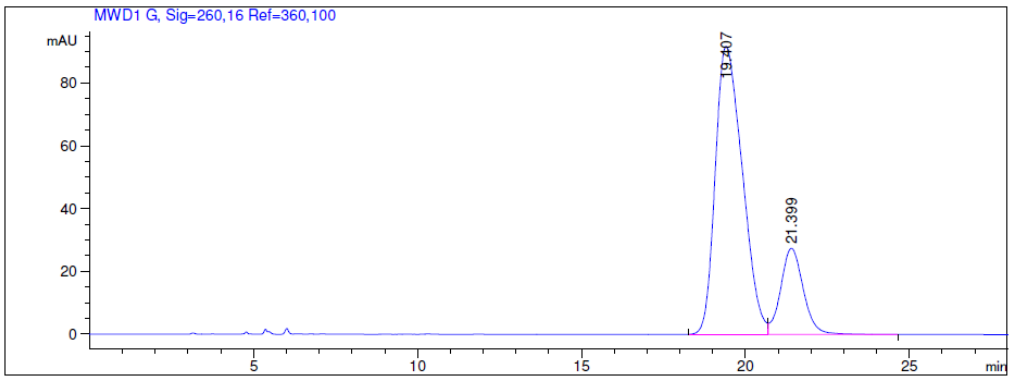

Signal 7: MWD1 G, Sig=260,16 Ref=360,100

Peak #	RetTime [min]	Type	Width [min]	Area [mAU*s]	Height [mAU]	Area %
1	19.407	BV	0.9330	5259.21338	91.72038	80.0109
2	21.399	VB	0.7311	1313.90942	27.41863	19.9891
Totals :				6573.12280	119.13901	

HPLC column: Daicel Chiralpak ID,

Temperature: 23 °C,

Flow rate: 1 ml/min.;

Eluent system: Hexane/IPA (85:15)

***ee*=60%**

Figure S91 Racemic HPLC spectrum of (±)-**6cc.**

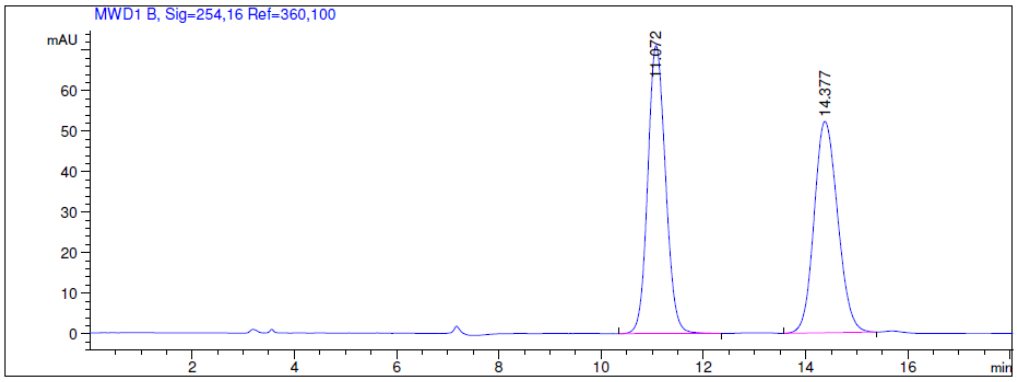

Signal 2: MWD1 B, Sig=254,16 Ref=360,100

Peak #	RetTime [min]	Type	Width [min]	Area [mAU*s]	Height [mAU]	Area %
1	11.072	BB	0.3776	1715.34119	71.07420	50.6176
2	14.377	BB	0.5001	1673.48218	52.18726	49.3824
Totals :				3388.82336	123.26146	

HPLC column: Daicel Chiralpak ID,

Temperature: 23 °C,

Flow rate: 1 ml/min.;

Eluent system: Hexane/IPA (90:10)

Figure S92 Asymmetric HPLC spectrum of *(R)*-**6cc.**

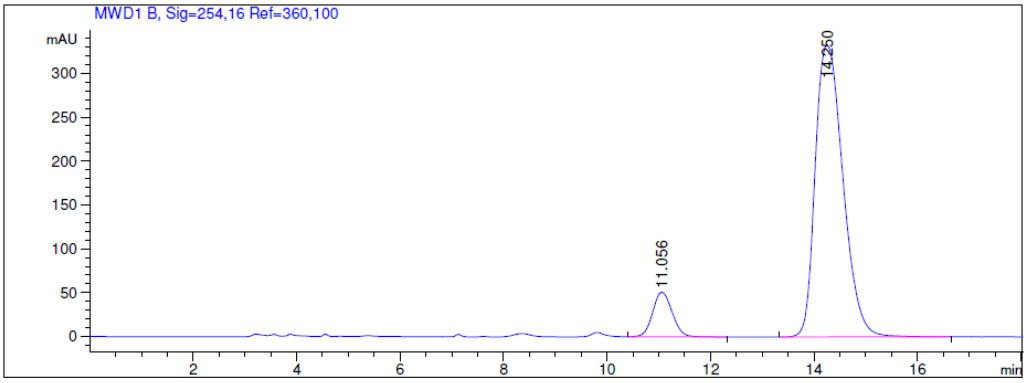

Signal 2: MWD1 B, Sig=254,16 Ref=360,100

Peak #	RetTime [min]	Type	Width [min]	Area [mAU*s]	Height [mAU]	Area %
1	11.056	BB	0.4078	1321.46460	50.75365	9.6500
2	14.250	BB	0.5858	1.23725e4	332.73782	90.3500
Totals :				1.36940e4	383.49147	

HPLC column: Daicel Chiralpak ID,

Temperature: 23 °C,

Flow rate: 1 ml/min.;

Eluent system: Hexane/IPA (90:10)

***ee*=81%**

Figure S93 Racemic HPLC spectrum of (±)-**6cd.**

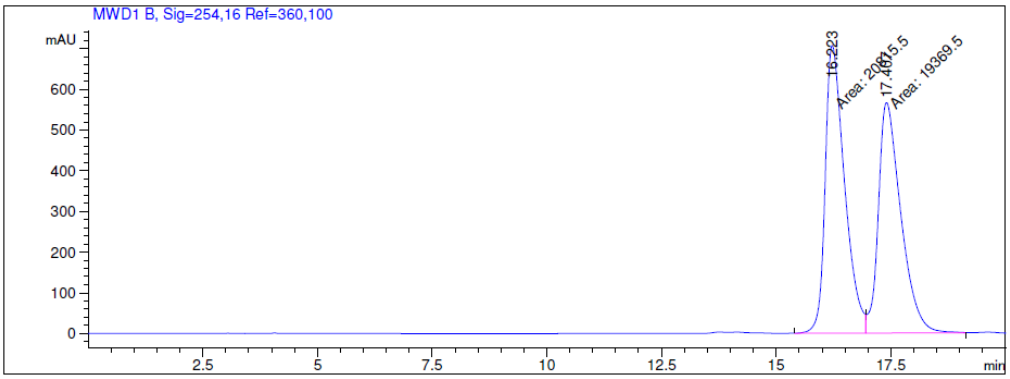


```
Signal 2: MWD1 B, Sig=254,16 Ref=360,100

Peak RetTime Type  Width     Area      Height     Area
  #   [min]        [min]   [mAU*s]     [mAU]       %
----|-------|----|-------|----------|----------|--------|
   1  16.223 MF    0.4906 2.08155e4   707.11145  51.7992
   2  17.407 FM    0.5699 1.93695e4   566.47260  48.2008

Totals :                 4.01849e4  1273.58405
```

HPLC column: Daicel Chiralpak IE,

Temperature: 23 °C,

Flow rate: 1 ml/min.;

Eluent system: Hexane/IPA (70:30)

Figure S94 Asymmetric HPLC spectrum of *(R)*-**6cd.**

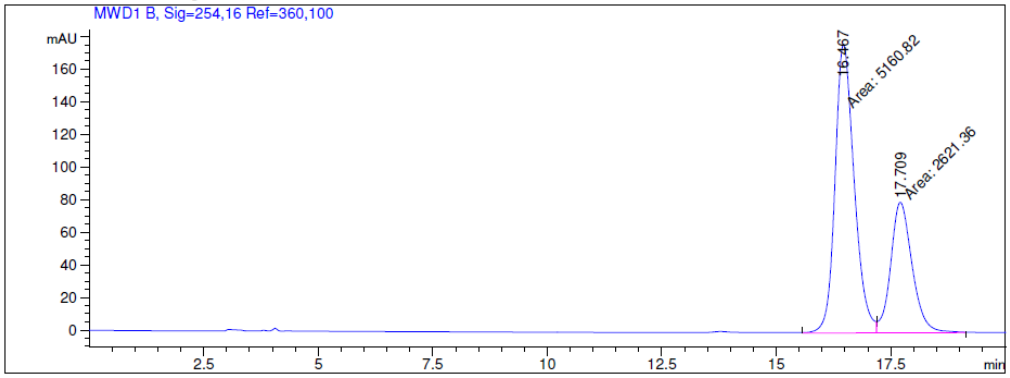


```
Signal 2: MWD1 B, Sig=254,16 Ref=360,100

Peak RetTime Type  Width     Area      Height     Area
  #   [min]        [min]   [mAU*s]     [mAU]       %
----|-------|----|-------|----------|----------|--------|
   1  16.467 MF    0.4861 5160.81934  176.96373  66.3159
   2  17.709 FM    0.5454 2621.35669   80.10585  33.6841

Totals :                 7782.17603  257.06958
```

HPLC column: Daicel Chiralpak IE,

Temperature: 23 °C,

Flow rate: 1 ml/min.;

Eluent system: Hexane/IPA (70:30)

***ee*=33%**

Figure S95 Racemic HPLC spectrum of (±)-**6ce.**

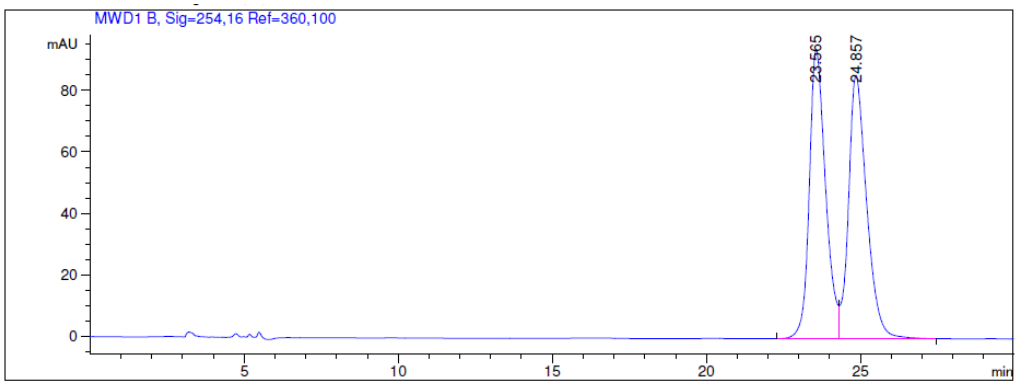

Signal 2: MWD1 B, Sig=254,16 Ref=360,100

Peak #	RetTime [min]	Type	Width [min]	Area [mAU*s]	Height [mAU]	Area %
1	23.565	BV	0.5544	3449.41113	93.93780	49.6534
2	24.857	VB	0.6107	3497.56641	85.60771	50.3466
Totals :				6946.97754	179.54551	

HPLC column: Daicel Chiralpak IE,

Temperature: 23 °C,

Flow rate: 1 ml/min.;

Eluent system: Hexane/IPA (85:15)

Figure S96 Asymmetric HPLC spectrum of *(S)*-**6ce.**

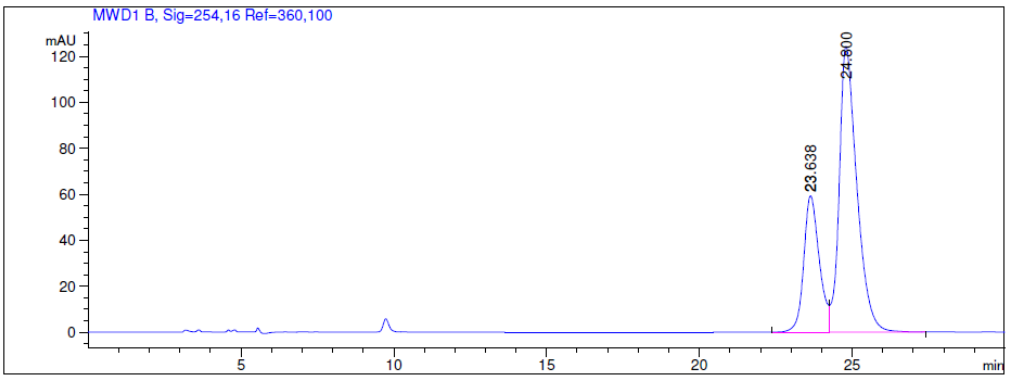

Signal 2: MWD1 B, Sig=254,16 Ref=360,100

Peak #	RetTime [min]	Type	Width [min]	Area [mAU*s]	Height [mAU]	Area %
1	23.638	BV	0.5345	2097.96777	59.33110	29.6196
2	24.800	VB	0.5957	4985.08008	124.35921	70.3804
Totals :				7083.04785	183.69032	

HPLC column: Daicel Chiralpak IE,

Temperature: 23 °C,

Flow rate: 1 ml/min.;

Eluent system: Hexane/IPA (85:15)

***ee*=41%**

Figure S97 Racemic HPLC spectrum of (±)-**8a.**

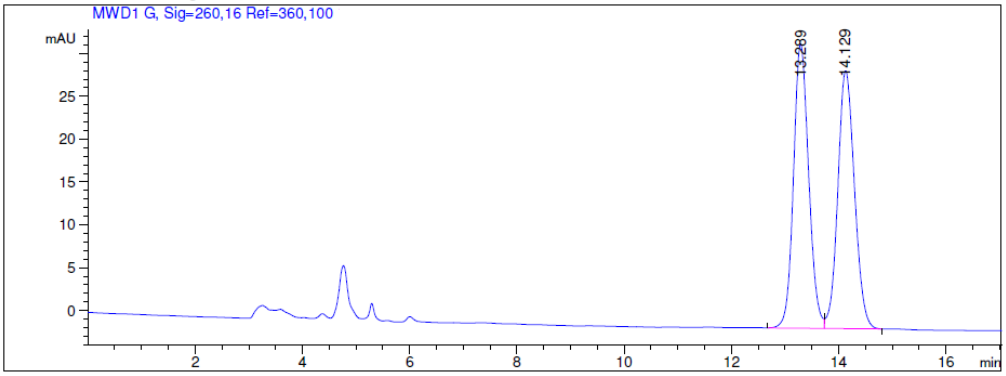

Signal 7: MWD1 G, Sig=260,16 Ref=360,100

Peak #	RetTime [min]	Type	Width [min]	Area [mAU*s]	Height [mAU]	Area %
1	13.289	BV	0.3039	653.49774	33.16544	50.0957
2	14.129	VB	0.3361	651.00208	30.12320	49.9043
Totals :				1304.49982	63.28863	

HPLC column: Daicel Chiralpak ID,

Temperature: 23 °C,

Flow rate: 1 ml/min.;

Eluent system: Hexane/IPA (85:15)

Figure S98 Asymmetric HPLC spectrum of *(R)*-**8a.**

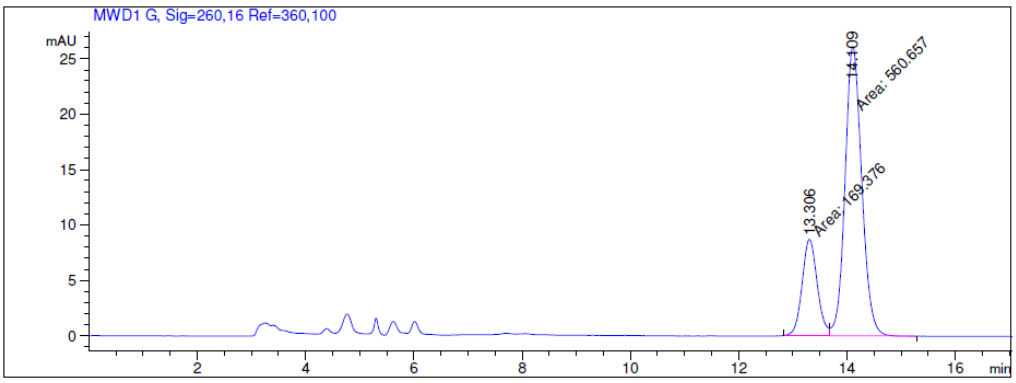

Signal 7: MWD1 G, Sig=260,16 Ref=360,100

Peak #	RetTime [min]	Type	Width [min]	Area [mAU*s]	Height [mAU]	Area %
1	13.306	MF	0.3243	169.37553	8.70529	23.2011
2	14.109	FM	0.3577	560.65686	26.12079	76.7989
Totals :				730.03239	34.82608	

HPLC column: Daicel Chiralpak ID,

Temperature: 23 °C,

Flow rate: 1 ml/min.;

Eluent system: Hexane/IPA (85:15)

***ee*=54%**

Figure S99 Racemic HPLC spectrum of (±)-**8b.**

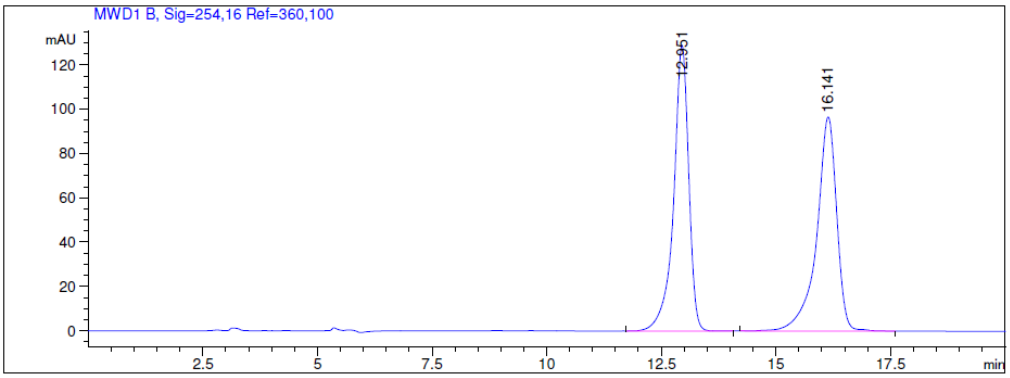


```
Signal 2: MWD1 B, Sig=254,16 Ref=360,100

Peak RetTime Type  Width     Area      Height     Area
  #   [min]        [min]   [mAU*s]     [mAU]       %
----|-------|----|-------|----------|----------|--------|
   1  12.951 BB    0.3441 2964.41333  129.00148  50.1043
   2  16.141 BB    0.4523 2952.06616   96.66156  49.8957

Totals :                  5916.47949  225.66304
```

HPLC column: Daicel Chiralpak IC,

Temperature: 23 ^{o}C,

Flow rate: 1 ml/min.;

Eluent system: Hexane/IPA (80:20)

Figure S100 Asymmetric HPLC spectrum of *(R)*-**8b.**

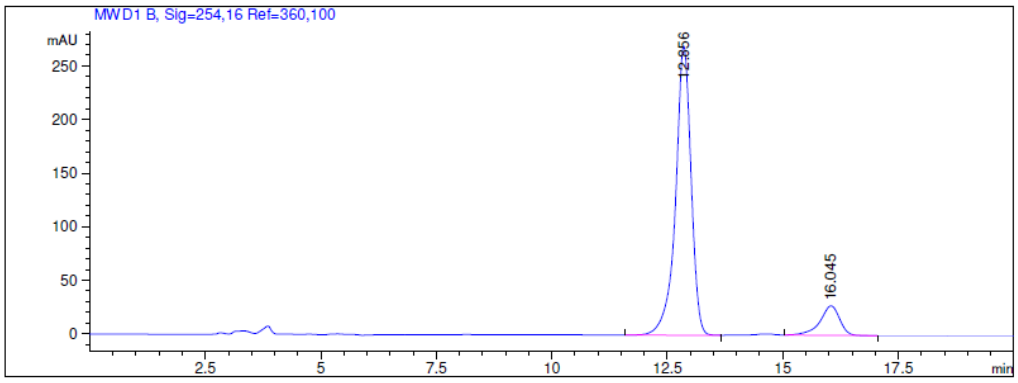


```
Signal 2: MWD1 B, Sig=254,16 Ref=360,100

Peak RetTime Type  Width     Area      Height     Area
  #   [min]        [min]   [mAU*s]     [mAU]       %
----|-------|----|-------|----------|----------|--------|
   1  12.856 BB    0.3536 6324.26270  269.68747  88.5531
   2  16.045 BB    0.4460  817.51233   27.56480  11.4469

Totals :                  7141.77502  297.25227
```

HPLC column: Daicel Chiralpak IC,

Temperature: 23 ^{o}C,

Flow rate: 1 ml/min.;

Eluent system: Hexane/IPA (80:20)

***ee*=77%**

5. Stereochemical investigation on 6eb.

Experiment 1:

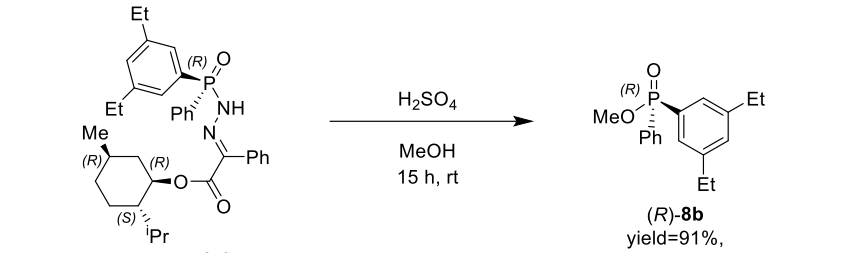

(*R,S,R,R*)-**6eb**
de=68% (determined by $^{31}P\{^{1}H\}$ NMR)

(*R*)-**8b**
yield=91%,
ee=67% (determined by chiral HPLC)

To identify the stereochemistry of the generated **6eb** diastereomers at the first place, the isolated compounds were transformed to diarylphosphinates via acidic methanolysis. The enantiomeric excess of the generated enantioenriched diarylphosphinates were measured via chiral HPLC and the results were compared with the previous measurements (Figure S97 and S98). According to the investigation, (*R*)-**4** catalyst generated (*R,S,R,R*)-**6eb**, which was further derivatized to (*R*)-**8b**.

Figure S101 Asymmetric HPLC spectrum of (*R*)-**8b** generated from (*R,S,R,R*)-**6eb**.

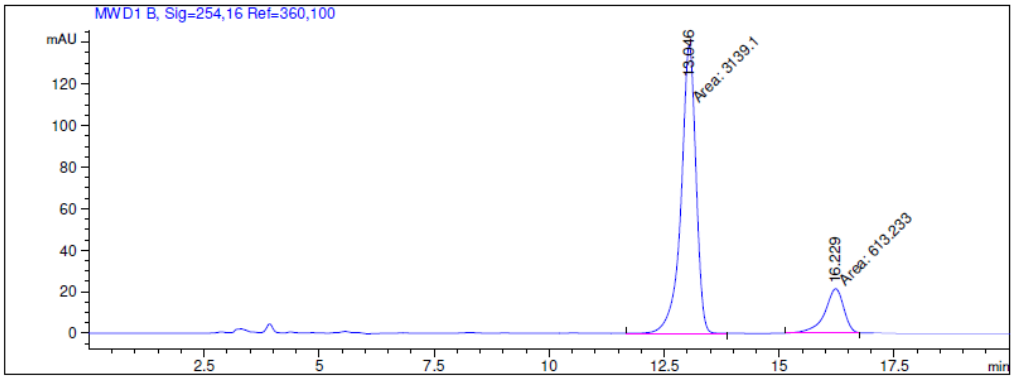


```
Signal 2: MWD1 B, Sig=254,16 Ref=360,100

Peak RetTime Type  Width     Area      Height     Area
  #   [min]        [min]   [mAU*s]     [mAU]       %
----|-------|----|-------|----------|----------|--------|
   1  13.046 MM    0.3768 3139.10376  138.86555  83.6573
   2  16.229 MM    0.4811  613.23328   21.24221  16.3427

Totals :                  3752.33704  160.10776
```

HPLC column: Daicel Chiralpak IC,

Temperature: 23 °C,

Flow rate: 1 ml/min.;

Eluent system: Hexane/IPA (80:20)

***ee*=67%**

Experiment 2:

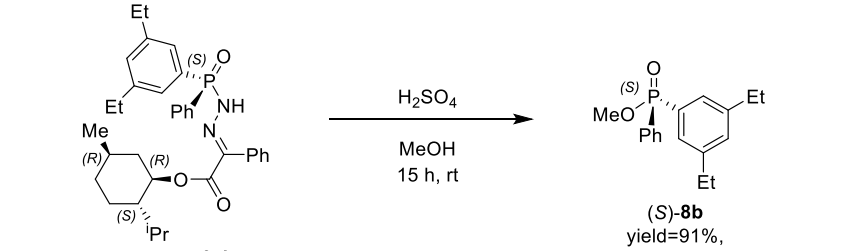

(*R,S,R,S*)-**6eb**
de=70% (determined by $^{31}P\{^{1}H\}$ NMR)

(*S*)-**8b**
yield=91%,
ee=72% (determined by chiral HPLC)

Figure S102 Asymmetric HPLC spectrum of (*R*)-**8b** generated from (*R,S,R,R*)-**6eb**.

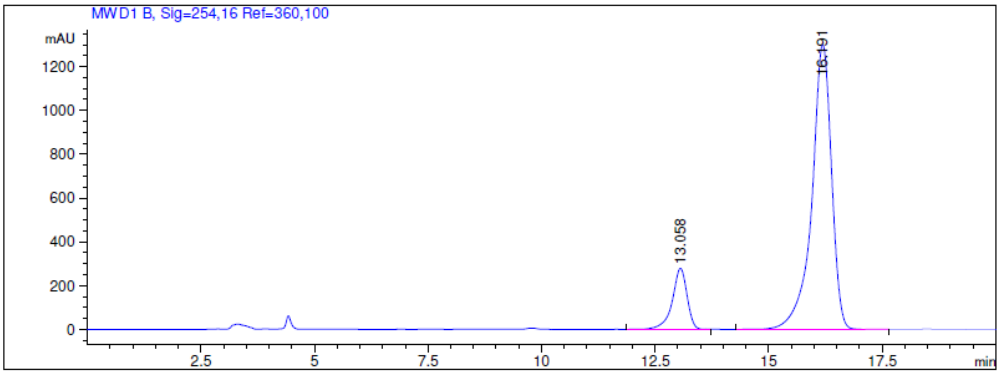

Signal 2: MWD1 B, Sig=254,16 Ref=360,100

Peak #	RetTime [min]	Type	Width [min]	Area [mAU*s]	Height [mAU]	Area %
1	13.058	BB	0.3429	6332.87012	278.85968	13.8680
2	16.191	BB	0.4548	3.93326e4	1300.71960	86.1320
Totals :				4.56654e4	1579.57928	

HPLC column: Daicel Chiralpak IC,

Temperature: 23 ^{o}C,

Flow rate: 1 ml/min.;

Eluent system: Hexane/IPA (80:20)

***ee*=72%**

6. X-Ray measurement data

Crystallographic data of *(R)*-3aa.

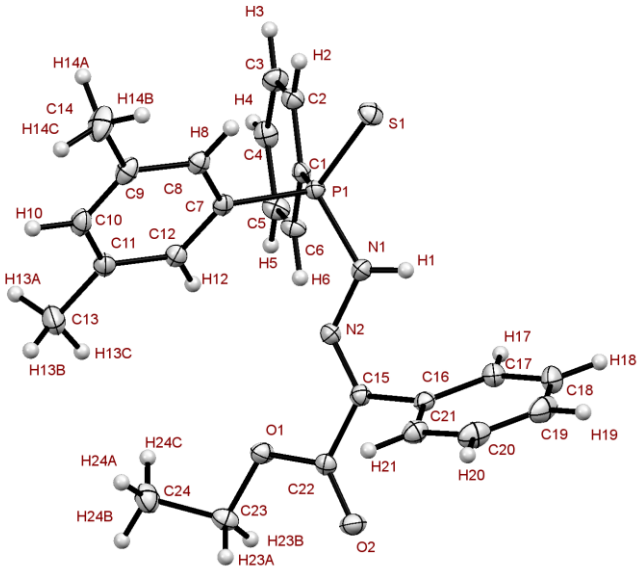

Figure S103 ORTEP structure of compound (*R*)-**3aa** with ellipsoids at 50% probability.

A colorless block-like specimen of $C_{24}H_{25}N_2O_2PS$, approximate dimensions 0.140 mm x 0.180 mm x 0.210 mm, was used for the X-ray crystallographic analysis. The X-ray intensity data were measured (λ = 0.71073 Å).

The total exposure time was 0.21 hours. The frames were integrated with the Bruker SAINT software package using a narrow-frame algorithm. The integration of the data using an orthorhombic unit cell yielded a total of 26681 reflections to a maximum θ angle of 35.63° (0.61 Å resolution), of which 10359 were independent (average redundancy 2.576, completeness = 99.5%, R_{int} = 5.44%, R_{sig} = 8.64%) and 7687 (74.21%) were greater than $2\sigma(F^2)$. The final cell constants of a = 8.3139(2) Å, b = 16.3794(3) Å, c = 16.6172(4) Å, volume = 2262.88(9) $Å^3$, are based upon the refinement of the XYZ-centroids of 6880 reflections above 20 σ(I) with 5.479° < 2θ < 69.38°. Data were corrected for absorption effects using the Multi-Scan method (SADABS). The ratio of minimum to maximum apparent transmission was 0.841. The calculated minimum and maximum transmission coefficients (based on crystal size) are 0.9520 and 0.9680.

The structure was solved and refined using the Bruker SHELXTL Software Package, using the space group P 21 21 21, with Z = 4 for the formula unit, $C_{24}H_{25}N_2O_2PS$. The final anisotropic full-matrix least-squares refinement on F^2 with 274 variables converged at R1 = 5.14%, for the observed data and wR2 = 11.01% for all data. The goodness-of-fit was 1.027. The largest peak in the final difference electron density synthesis was 0.525 $e^-/Å^3$ and the largest hole was -0.479 $e^-/Å^3$ with an RMS deviation of 0.079 $e^-/Å^3$. On the basis of the final model, the calculated density was 1.281 g/cm^3 and F(000), 920 e^-.

Crystallization method: concentrated solution of pure (*R*)-**3aa** was prepared in DCM (20 mg compound in 2 mL solvent), followed by the slow addition Hexanes in small portions, over a period of one week.

Table S3. Sample and crystal data for *(R)*-3aa.

Identification code	CCDC 1965254
Crystallization solvent	DCM/ Hexanes
Chemical formula	$C_{24}H_{25}N_2O_2PS$
Formula weight	436.49 g/mol
Temperature	100(2) K
Wavelength	0.71073 Å

Crystal size	0.140 x 0.180 x 0.210 mm	
Crystal habit	colorless block	
Crystal system	orthorhombic	
Space group	P 21 21 21	
Unit cell dimensions	a = 8.3139(2) Å	α = 90°
	b = 16.3794(3) Å	β = 90°
	c = 16.6172(4) Å	γ = 90°
Volume	2262.88(9) $Å^3$	
Z	4	
Density (calculated)	1.281 g/cm^3	
Absorption coefficient	0.236 mm^{-1}	
F(000)	920	

Table S4. Data collection and structure refinement for *(R)*-3aa.

Theta range for data collection	2.74 to 35.63°
Index ranges	-13<=h<=11, -26<=k<=21, -27<=l<=24
Reflections collected	26681
Independent reflections	10359 [R(int) = 0.0544]
Coverage of independent reflections	99.5%
Absorption correction	Multi-Scan
Max. and min. transmission	0.9680 and 0.9520
Structure solution technique	direct methods
Structure solution program	XT, VERSION 2014/5
Refinement method	Full-matrix least-squares on F^2
Refinement program	SHELXL-2017/1 (Sheldrick, 2017)
Function minimized	$\Sigma\, w(F_o^2 - F_c^2)^2$
Data / restraints / parameters	10359 / 0 / 274
Goodness-of-fit on F^2	1.027
Δ/σ_{max}	0.001
Final R indices	7687 data; I>2σ(I) R1 = 0.0514, wR2 = 0.0919
	all data R1 = 0.0843, wR2 = 0.1101
Weighting scheme	$w=1/[\sigma^2(F_o^2)+(0.0346P)^2+0.5814P]$ where $P=(F_o^2+2F_c^2)/3$
Absolute structure parameter	0.06(3)
Largest diff. peak and hole	0.525 and -0.479 $eÅ^{-3}$
R.M.S. deviation from mean	0.079 $eÅ^{-3}$

Crystallographic data of *(R)*-6ca.

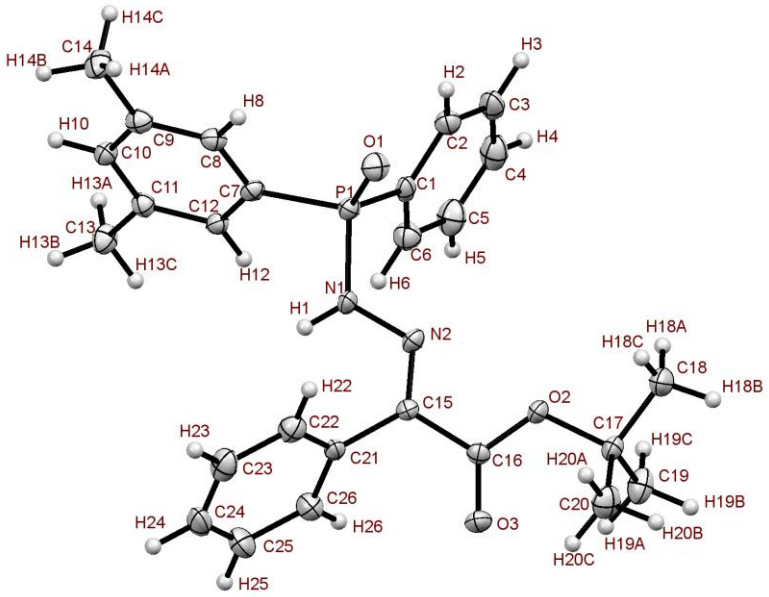

Figure S104 ORTEP structure of compound (*R*)-**6ca** with ellipsoids at 50% probability.

A colorless block-like specimen of $C_{26}H_{29}N_2O_3P$, approximate dimensions 0.080 mm x 0.120 mm x 0.200 mm, was used for the X-ray crystallographic analysis. The X-ray intensity data were measured (λ = 0.71073 Å).

A total of 174 frames were collected. The total exposure time was 0.19 hours. The frames were integrated with the Bruker SAINT software package using a narrow-frame algorithm. The integration of the data using an orthorhombic unit cell yielded a total of 25200 reflections to a maximum θ angle of 29.60° (0.72 Å resolution), of which 6637 were independent (average redundancy 3.797, completeness = 99.6%, R_{int} = 8.45%, R_{sig} = 8.00%) and 5168 (77.87%) were greater than $2\sigma(F^2)$. The final cell constants of a = 8.9507(3) Å, b = 11.6512(5) Å, c = 22.9288(9) Å, volume = 2391.16(16) $Å^3$, are based upon the refinement of the XYZ-centroids of 3997 reflections above 20 σ(I) with 4.984° < 2θ < 55.26°. Data were corrected for absorption effects using the Multi-Scan method (SADABS). The ratio of minimum to maximum apparent transmission was 0.828. The calculated minimum and maximum transmission coefficients (based on crystal size) are 0.9720 and 0.9890.

The structure was solved and refined using the Bruker SHELXTL Software Package, using the space group P 21 21 21, with Z = 4 for the formula unit, $C_{26}H_{29}N_2O_3P$. The final anisotropic full-matrix least-squares refinement on F^2 with 295 variables converged at R1 = 5.89%, for the observed data and wR2 = 13.93% for all data. The goodness-of-fit was 1.057. The largest peak in the final difference electron density synthesis was 0.819 $e^-/Å^3$ and the largest hole was -0.414 $e^-/Å^3$ with an RMS deviation of 0.070 $e^-/Å^3$. On the basis of the final model, the calculated density was 1.246 g/cm^3 and F(000), 952 e^-.

Crystallization method: concentrated solution of pure (*R*)-**6ca** was prepared in DCM (20 mg compound in 2 mL solvent), followed by the slow addition Hexanes in small portions, over a period of one week.

Table S5. Sample and crystal data for *(R)*-6ca.

Identification code	CCDC 1965253
Crystallization solvent	DCM/ Hexanes
Chemical formula	$C_{26}H_{29}N_2O_3P$
Formula weight	448.48 g/mol
Temperature	100(2) K
Wavelength	0.71073 Å
Crystal size	0.080 x 0.120 x 0.200 mm

Crystal habit	colorless block	
Crystal system	orthorhombic	
Space group	P 21 21 21	
Unit cell dimensions	a = 8.9507(3) Å	α = 90°
	b = 11.6512(5) Å	β = 90°
	c = 22.9288(9) Å	γ = 90°
Volume	2391.16(16) $Å^3$	
Z	4	
Density (calculated)	1.246 g/cm^3	
Absorption coefficient	0.144 mm^{-1}	
F(000)	952	

Table S6. Data collection and structure refinement for *(R)*-6ca.

Theta range for data collection	2.87 to 29.60°
Index ranges	-12<=h<=9, -15<=k<=16, -30<=l<=31
Reflections collected	25200
Independent reflections	6637 [R(int) = 0.0845]
Coverage of independent reflections	99.6%
Absorption correction	Multi-Scan
Max. and min. transmission	0.9890 and 0.9720
Structure solution technique	direct methods
Structure solution program	XT, VERSION 2014/5
Refinement method	Full-matrix least-squares on F^2
Refinement program	SHELXL-2018/3 (Sheldrick, 2018)
Function minimized	$\Sigma\ w(F_o^2 - F_c^2)^2$
Data / restraints / parameters	6637 / 0 / 295
Goodness-of-fit on F^2	1.057
Δ/σ_{max}	0.001
Final R indices	5168 data; I>2σ(I) R1 = 0.0589, wR2 = 0.1233
	all data R1 = 0.0874, wR2 = 0.1393
Weighting scheme	$w=1/[\sigma^2(F_o^2)+(0.0573P)^2+0.7719P]$ where $P=(F_o^2+2F_c^2)/3$
Absolute structure parameter	0.25(16)
Largest diff. peak and hole	0.819 and -0.414 $eÅ^{-3}$
R.M.S. deviation from mean	0.070 $eÅ^{-3}$

Crystallographic data of 6ai.

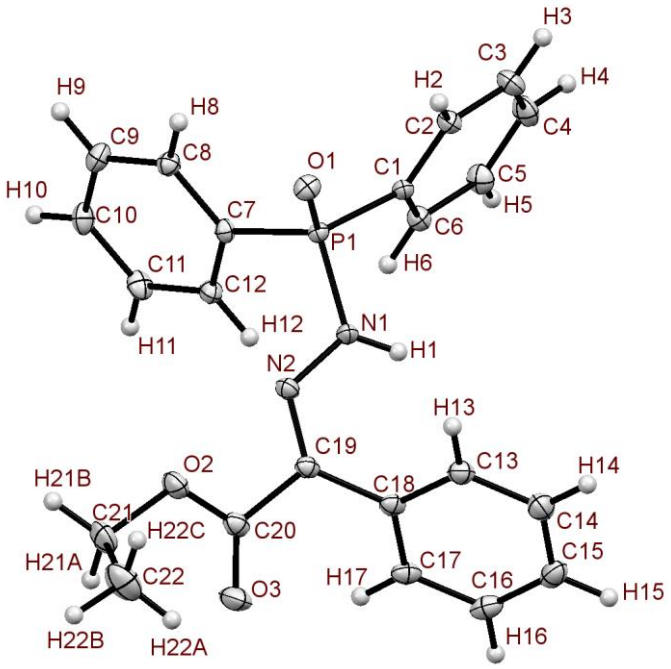

Figure S105 ORTEP structure of compound **6ai** with ellipsoids at 50% probability.

A colorless needle-like specimen of $C_{22}H_{21}N_2O_3P$, approximate dimensions 0.020 mm x 0.040 mm x 0.220 mm, was used for the X-ray crystallographic analysis. The X-ray intensity data were measured (λ = 0.71073 Å).

A total of 301 frames were collected. The total exposure time was 0.33 hours. The frames were integrated with the Bruker SAINT software package using a narrow-frame algorithm. The integration of the data using an orthorhombic unit cell yielded a total of 27042 reflections to a maximum θ angle of 32.57° (0.66 Å resolution), of which 7052 were independent (average redundancy 3.835, completeness = 99.7%, R_{int} = 5.52%, R_{sig} = 5.83%) and 6059 (85.92%) were greater than $2\sigma(F^2)$. The final cell constants of a = 8.4671(2) Å, b = 10.4320(2) Å, c = 22.0317(4) Å, volume = 1946.03(7) $Å^3$, are based upon the refinement of the XYZ-centroids of 7853 reflections above 20 σ(I) with 5.154° < 2θ < 64.81°. Data were corrected for absorption effects using the Multi-Scan method (SADABS). The ratio of minimum to maximum apparent transmission was 0.832. The calculated minimum and maximum transmission coefficients (based on crystal size) are 0.9640 and 0.9970.

The structure was solved and refined using the Bruker SHELXTL Software Package, using the space group P 21 21 21, with Z = 4 for the formula unit, $C_{22}H_{21}N_2O_3P$. The final anisotropic full-matrix least-squares refinement on F^2 with 254 variables converged at R1 = 4.38%, for the observed data and wR2 = 9.55% for all data. The goodness-of-fit was 1.066. The largest peak in the final difference electron density synthesis was 0.354 $e^-/Å^3$ and the largest hole was -0.343 $e^-/Å^3$ with an RMS deviation of 0.059 $e^-/Å^3$. On the basis of the final model, the calculated density was 1.339 g/cm^3 and F(000), 824 e^-.

Crystallization method: concentrated solution of pure **6ai** was prepared in DCM (20 mg compound in 2 mL solvent), followed by the slow addition Hexanes in small portions, over a period of one week.

Table S7. Sample and crystal data for 6ai.

Identification code	CCDC 1965252
Crystallization solvent	DCM/ Hexanes
Chemical formula	$C_{22}H_{21}N_2O_3P$
Formula weight	392.38 g/mol
Temperature	100(2) K

Wavelength	0.71073 Å	
Crystal size	0.020 x 0.040 x 0.220 mm	
Crystal habit	colorless needle	
Crystal system	orthorhombic	
Space group	P 21 21 21	
Unit cell dimensions	a = 8.4671(2) Å	α = 90°
	b = 10.4320(2) Å	β = 90°
	c = 22.0317(4) Å	γ = 90°
Volume	1946.03(7) $Å^3$	
Z	4	
Density (calculated)	1.339 g/cm^3	
Absorption coefficient	0.167 mm^{-1}	
F(000)	824	

Table S8. Data collection and structure refinement for 6ai.

Theta range for data collection	2.69 to 32.57°
Index ranges	-9<=h<=12, -14<=k<=15, -32<=l<=33
Reflections collected	27042
Independent reflections	7052 [R(int) = 0.0552]
Coverage of independent reflections	99.7%
Absorption correction	Multi-Scan
Max. and min. transmission	0.9970 and 0.9640
Structure solution technique	direct methods
Structure solution program	XT, VERSION 2014/5
Refinement method	Full-matrix least-squares on F^2
Refinement program	SHELXL-2018/3 (Sheldrick, 2018)
Function minimized	$\Sigma\, w(F_o^2 - F_c^2)^2$
Data / restraints / parameters	7052 / 0 / 254
Goodness-of-fit on F^2	1.066
Final R indices	6059 data; I>2σ(I) R1 = 0.0438, wR2 = 0.0881
	all data R1 = 0.0580, wR2 = 0.0955
Weighting scheme	$w=1/[\sigma^2(F_o^2)+(0.0371P)^2+0.3454P]$ where $P=(F_o^2+2F_c^2)/3$
Absolute structure parameter	0.03(4)
Largest diff. peak and hole	0.354 and -0.343 $eÅ^{-3}$
R.M.S. deviation from mean	0.059 $eÅ^{-3}$

Crystallographic data of (±)-6bc.

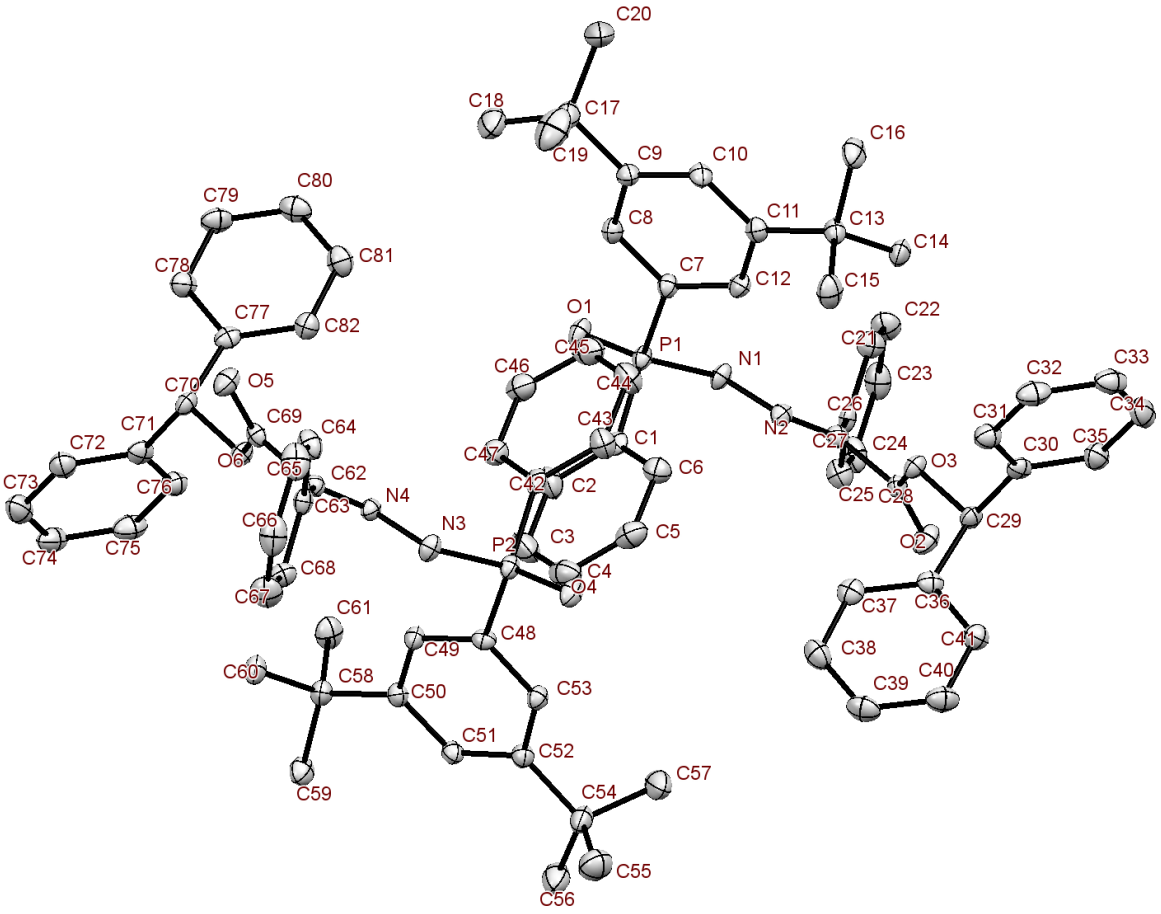

Figure S106 ORTEP structure of compound **(±)-6bc** with ellipsoids at 50% probability.

A colorless block-like specimen of $C_{41}H_{43}N_2O_3P$, approximate dimensions 0.140 mm x 0.200 mm x 0.220 mm, was used for the X-ray crystallographic analysis. The X-ray intensity data were measured (λ = 0.71073 Å).

A total of 635 frames were collected. The total exposure time was 0.18 hours. The frames were integrated with the Bruker SAINT software package using a narrow-frame algorithm. The integration of the data using a triclinic unit cell yielded a total of 72111 reflections to a maximum θ angle of 29.58° (0.72 Å resolution), of which 19085 were independent (average redundancy 3.778, completeness = 99.6%, R_{int} = 11.31%, R_{sig} = 11.50%) and 9211 (48.26%) were greater than $2\sigma(F^2)$. The final cell constants of a = 11.2032(6) Å, b = 11.6162(6) Å, c = 27.3632(15) Å, α = 79.7546(18)°, β = 79.3863(19)°, γ = 80.302(2)°, volume = 3410.2(3) $Å^3$, are based upon the refinement of the XYZ-centroids of 7188 reflections above 20 σ(I) with 4.810° < 2θ < 59.06°. Data were corrected for absorption effects using the Multi-Scan method (SADABS). The ratio of minimum to maximum apparent transmission was 0.885. The calculated minimum and maximum transmission coefficients (based on crystal size) are 0.9740 and 0.9830.

The structure was solved and refined using the Bruker SHELXTL Software Package, using the space group P -1, with Z = 4 for the formula unit, $C_{41}H_{43}N_2O_3P$. The final anisotropic full-matrix least-squares refinement on F^2 with 859 variables converged at R1 = 7.35%, for the observed data and wR2 = 20.41% for all data. The goodness-of-fit was 1.033. The largest peak in the final difference electron density synthesis was 0.978 $e^-/Å^3$ and the largest hole was -0.543 $e^-/Å^3$ with an RMS deviation of 0.076 $e^-/Å^3$. On the basis of the final model, the calculated density was 1.252 g/cm^3 and F(000), 1368 e^-.

Crystallization method: concentrated solution of pure **6ai** was prepared in DCM (20 mg compound in 2 mL solvent), followed by the slow addition Hexanes in small portions, over a period of one week.

Table S9. Sample and crystal data for (±)-6bc.

Identification code	CCDC 1965255	
Crystallization solvent	DCM/ Hexanes	
Chemical formula	$C_{41}H_{43}N_2O_3P$	
Formula weight	642.74 g/mol	
Temperature	100(2) K	
Wavelength	0.71073 Å	
Crystal size	0.140 x 0.200 x 0.220 mm	
Crystal habit	colorless block	
Crystal system	triclinic	
Space group	P -1	
Unit cell dimensions	a = 11.2032(6) Å	α = 79.7546(18)°
	b = 11.6162(6) Å	β = 79.3863(19)°
	c = 27.3632(15) Å	γ = 80.302(2)°
Volume	3410.2(3) $Å^3$	
Z	4	
Density (calculated)	1.252 g/cm^3	
Absorption coefficient	0.123 mm^{-1}	
F(000)	1368	

Table S10. Data collection and structure refinement for (±)-6bc.

Theta range for data collection	2.30 to 29.58°
Index ranges	-15<=h<=15, -16<=k<=14, -37<=l<=37
Reflections collected	72111
Independent reflections	19085 [R(int) = 0.1131]
Coverage of independent reflections	99.6%
Absorption correction	Multi-Scan
Max. and min. transmission	0.9830 and 0.9740
Structure solution technique	direct methods
Structure solution program	XT, VERSION 2014/5
Refinement method	Full-matrix least-squares on F^2
Refinement program	SHELXL-2018/3 (Sheldrick, 2018)
Function minimized	$\Sigma\, w(F_o^2 - F_c^2)^2$
Data / restraints / parameters	19085 / 0 / 859
Goodness-of-fit on F^2	1.033
Final R indices	9211 data; I>2σ(I) R1 = 0.0735, wR2 = 0.1574
	all data R1 = 0.1657, wR2 = 0.2041
Weighting scheme	$w=1/[\sigma^2(F_o^2)+(0.0621P)^2+2.3549P]$ where $P=(F_o^2+2F_c^2)/3$
Largest diff. peak and hole	0.978 and -0.543 $eÅ^{-3}$
R.M.S. deviation from mean	0.076 $eÅ^{-3}$

5. References

1. Huang, Y.; Pullarkat, S. A.; Li, Y.; Leung, P.-H., Palladium(ii)-catalyzed asymmetric hydrophosphination of enones: efficient access to chiral tertiary phosphines. *Chem. Comm.* **2010,** *46* (37), 6950-6952.
2. Huang, Y.; Pullarkat, S. A.; Li, Y.; Leung, P.-H., Palladacycle-Catalyzed Asymmetric Hydrophosphination of Enones for Synthesis of C*- and P*-Chiral Tertiary Phosphines. *Inorg. Chem.* **2012,** *51* (4), 2533-2540.
3. Yang, X.-Y.; Gan, J. H.; Li, Y.; Pullarkat, S. A.; Leung, P.-H., Palladium catalyzed asymmetric hydrophosphination of α,β- and α,β,γ,δ-unsaturated malonate esters – efficient control of reactivity, stereo- and regio-selectivity. *Dalton Trans.* **2015,** *44* (3), 1258-1263.
4. Messerle, L.; Curtis, M. D., Reaction of diaryldiazomethanes with a metal-metal triple bond: synthesis, structural characterizations, and reactivity of novel bridging diazoalkane and alkylidene complexes. *J. Am. Chem. Soc.* **1980,** *102* (26), 7789-7791.
5. Maxwell, J. L.; Brown, K. C.; Bartley, D. W.; Kodadek, T., Mechanism of the Rhodium Porphyrin-Catalyzed Cyclopropanation of Alkenes. *Science* **1992,** *256* (5063), 1544-1547.
6. Straub, B. F.; Rominger, F.; Hofmann, P., Transition metal α-carbonyl diazoalkane coordination chemistry: structures derived from a side-on diazomalonate platinum complex. *Inorg. Chem. Comm.* **2000,** *3* (5), 214-217.
7. Straub, B. F., Pd(0) Mechanism of Palladium-Catalyzed Cyclopropanation of Alkenes by CH2N2: A DFT Study. *J. Am. Chem. Soc.* **2002,** *124* (47), 14195-14201.
8. Harrold, N. D.; Corcos, A. R.; Hillhouse, G. L., Synthesis, structures, and catalytic reactivity of bis(N-heterocyclic carbene) supported diphenyldiazomethane and 1-azidoadamantane complexes of nickel. *J. Org. Chem.* **2016,** *813*, 46-54.
9. Rull, S. G.; Álvarez, E.; Fructos, M. R.; Belderrain, T. R.; Pérez, P. J., The Elusive Palladium-Diazo Adduct Captured: Synthesis, Isolation and Structural Characterization of [(ArNHC-PPh2)Pd(η2-N2C(Ph)CO2Et)]. *Chem. Eur. J.* **2017,** *23* (32), 7667-7671.
10. Wong, F. M.; Wang, J.; Hengge, A. C.; Wu, W., Mechanism of Rhodium-Catalyzed Carbene Formation from Diazo Compounds. *Org. Lett.* **2007,** *9* (9), 1663-1665.
11. de Frémont, P.; Marion, N.; Nolan, S. P., Carbenes: Synthesis, properties, and organometallic chemistry. *Coord. Chem. Rev.* **2009,** *253* (7), 862-892.
12. Xia, Y.; Qiu, D.; Wang, J., Transition-Metal-Catalyzed Cross-Couplings through Carbene Migratory Insertion. *Chem. Rev.* **2017,** *117* (23), 13810-13889.
13. Jia, Y.-X.; Li, B.-B.; Li, Y.; Pullarkat, S. A.; Xu, K.; Hirao, H.; Leung, P.-H., Stereoelectronic and Catalytic Properties of Chiral Cyclometalated Phospha-palladium and -platinum Complexes. *Organometallics* **2014,** *33* (21), 6053-6058.